



**STRUCTURAL SYSTEMS  
RESEARCH PROJECT**

Report No.  
SSRP-2000/08

**PRESSS PHASE 3:  
THE FIVE-STORY PRECAST  
TEST BUILDING  
VOL. 3-4**

**FRAME DIRECTION RESPONSE**

By

**STEFANO PAMPANIN  
M.J.N. PRIESTLEY  
SRI SRITHARAN**

Report Submitted to the Precast Concrete Institute

November 2000

Department of Structural Engineering  
University of California, San Diego  
La Jolla, California 92093-0085

University of California, San Diego  
Department of Structural Engineering  
Structural Systems Research Project

Report No. SSRP-2000/08

**PRESSS Phase 3: The Five-Story Precast  
Test Building  
Vol. 3-4  
Frame Direction Response**

By

**Stefano Pampanin**  
*Graduate Student*

**M.J.N. Priestley**  
*Professor of Structural Engineering*

**Sri Sritharan**  
*Research Scientist*

Report Submitted to the Precast Concrete Institute

Department of Structural Engineering  
University of California, San Diego  
La Jolla, California 92093-0085

November 2000

# TABLE OF CONTENTS

TABLE OF CONTENTS .....	ii
Table of Figures.....	v
List of tables.....	vii
ABSTRACT .....	viii
ACKNOWLEDGMENTS .....	ix
CHAPTER 1 .....	1
<b>Introduction</b> .....	<b>1</b>
1.1. Current Code Provisions and Recommendations.....	1
1.2. The PRESSS Research Program .....	4
1.1.2. Basic Conceptual Connections.....	5
1.2. Non-Linear elastic (NLE) .....	5
1.3. Objective and Scope of the Present Research.....	7
1.4. Organization of the Report.....	8
CHAPTER 2 .....	10
<b>“Unbonded” Concept: Structural Significance and Research Background .....</b>	<b>10</b>
3.1. Experimental Tests at NIST: Preliminary Phases .....	10
3.2. Original Development of Unbonded Tendons .....	12
3.3. Experimental Tests at UCSD .....	14
3.4. Analytical Studies .....	15
3.4.1. Dynamic Analyses .....	15
3.4.2. Moment Rotation Behavior: Trilinear Idealization.....	16
3.4.2.1. Limits of the Procedure.....	21
3.4.3. Alternative Approach: Fiber Element Analysis .....	22

3.4.3.1.	The Analytical Model using Fiber Elements.....	22
3.4.3.2.	Experimental Validation of the Fiber Model .....	24
2.4.3.3	Considerations.....	26
3.5.	Hybrid Connections: Experimental and Analytical Studies.....	27
3.5.1.	Experimental Tests.....	28
2.5.2.	Analytical Modeling of Hybrid Connections .....	31
<b>CHAPTER 3</b>	.....	<b>32</b>
<b>PROPOSED PROCEDURE FOR MOMENT-ROTATION ANALYSIS OF DUCTILE CONNECTIONS</b>	.....	<b>32</b>
3.1.	Motivations .....	32
4.1.	Main Scheme of the Procedure .....	33
3.2.	Member Compatibility Condition: the “Monolithic Beam Analogy” .....	38
3.3.	Alternative Approximate Procedure .....	42
3.4.	Preliminary Validation of the Procedure .....	45
3.5.1.	Specimen Description, Details and Test Procedure (NIST Phase IVb) .....	46
3.5.2.	Steel Behavior Modeling .....	50
3.5.3.	Concrete Behavior Modeling .....	51
3.5.4.	Experimental-Analytical Comparison.....	51
3.6.	Conclusions.....	54
<b>CHAPTER 4</b>	.....	<b>56</b>
<b>Analytical Modeling of Frame Systems:</b>	.....	<b>56</b>
4.1.	The PRESSS Test-Building .....	56
4.2.	The Frame Systems.....	58
Pretensioned connection .....	59	
TCY connection.....	59	
Hybrid Connection.....	59	
TCY-Gap Connection .....	60	
4.3.	Design Philosophy .....	60

4.3.1.	DBD Procedure.....	61
4.4.	Modeling of the Monotonic Behavior.....	65
4.4.1.	The TCY-Gap Connection Physical Model.....	67
4.4.2.	The Frame Finite Element Model.....	69
4.4.3.	Pushover Analysis.....	70
4.5.	Modeling of the Cyclic behavior.....	74
4.5.1.	Quasi-static Cyclic Analysis.....	77
<b>CHAPTER 5.....</b>		<b>78</b>
<b>Experimental Results and Preliminary Analytical-Experimental Comparison .....</b>		<b>78</b>
5.1.	Test Plan.....	78
5.1.1.	Pseudo-dynamic Procedure.....	78
5.1.2.	Input Ground Motions.....	79
5.1.3.	Flexibility Test and Inverse Triangular Test.....	81
5.2.	Experimental Results.....	82
5.2.1.	Damage Level Observations.....	82
5.2.2.	Force-Displacement Characteristics.....	87
5.3.	Experimental-Analytical Comparison.....	102
5.3.1.	Validation of the Displacement-Based Design (DBD) Method.....	118
5.3.1.1.	DBD Back-Calculations.....	119
<b>CHAPTER 6.....</b>		<b>121</b>
<b>Conclusions.....</b>		<b>121</b>
6.1.	Brief Summary of the Research Results.....	121
6.2.	Further Investigations and Possible Applications.....	122
<b>REFERENCES.....</b>		<b>124</b>
<b>APPENDIX A PHOTO DOCUMENTATION.....</b>		<b>129</b>

## TABLE OF FIGURES

Figure 1– Commonly Used Arrangements of Precast Members and Cast in Place Concrete in New Zealand (from Restrepo, 1993) .....	2
Figure 1. 2 - Erection of precast connections typical in New Zealand .....	3
Figure 1. 3 -Typical Arrangement of Precast Framed Construction in the ex-U.S.S.R.....	4
Figure 1. 4 - Hysteretic behavior of the basic conceptual connection systems.....	7
Figure 2.1a. Hysteretic behavior for NIST phase I specimens .....	11
Figure 2. 2 – Prestress loss due to inelastic response.....	13
Figure 2. 3 – Shear transfer mechanism in the joint region with unbonded tendons .....	14
Figure 2. 4 – Possible strut and tie mechanism for interior subassembly .....	15
Figure 2. 5– Discrete moment-rotation relationship for unbonded post-tensioned.....	17
Figure 2. 6 – Trilinear idealization.....	18
Figure 2. 7 –Partially Unbonded post-tensioned beam-column subassembly .....	23
Figure 2. 8 – Fiber element model .....	23
Figure 2. 9 – Hysteretic behavior for NIST specimen GPZ4:.....	25
Figure 2. 10 – Experimental analytical comparison for NIST specimen GPZ4 .....	25
Figure 2. 11 –Hysteretic energy dissipation for NIST specimen GPZ4.....	26
Figure 2. 12 –Hybrid connection - PRESSS 5-storey building.....	28
Figure 2. 13 –Hysteretic behavior of hybrid connection – NIST Phase IV b .....	29
Figure 2. 14 –Hysteretic behavior of hybrid connections – NIST Phase IV b.....	30
Figure 3.1 – Frame and beam rotations relationship .....	34
Figure 3.2 – Gap opening mechanism .....	35
Figure 3.3 – Elastic and plastic steel strain components.....	36
Figure 3.4 – Monolithic beam analogy .....	40
Figure 3.5 – Beam-column connection in the prototype building .....	47
Figure 3.6 – Bonding of PT steel in Model Connections.....	47
Figure 3.7 – Test set-up .....	48
Figure 3.8 – Beam section reinforcement .....	49
Figure 3.9 – Imposed Displacement History for NIST Phase IVb specimens.....	50
Figure 3.10 – Validation of the analytical procedure: NIST hybrid specimen M-P-Z4 .....	52
Figure 3. 11 – Validation of the analytical procedure: NIST hybrid specimen O-P-Z4 .....	52
Figure 3.12 – “Monolithic beam analogy” and approximate procedures: cross-comparison .....	53

Figure 3.13 – “Monolithic beam analogy” and approximate procedures: comparison with test results.....	54
Figure A.1 – Hybrid connections (average drift 1.7 %).....	130
Figure. A.2 – TCY-Gap connections EQ2 Excitation (average drift 1.7 %).....	131
Figure. A.3 – TCY connection EQ II Excitation (average drift 1.7 %).....	132
Figure. A.4 – Pretensioned connections EQ2 Excitation (average drift 1.7 %).....	133
Figure. A.5 – Hybrid connections EQ3 Excitation (average drift 2.2 %).....	134
Figure. A.6 – TCY-Gap connections EQ3 Excitation (average drift 2.2 %).....	135
Figure. A.7 – TCY connections EQ3 Excitation (average drift 2.2 %).....	136
Figure. A.8 – TCY connections EQ3 Excitation (average drift 2.2 %).....	137
Figure A.9 – Pretensioned connections EQ3 Excitation(average drift 2.2 %).....	138
Figure. A.10 – Hybrid connections End of Test(average drift 4.5 %).....	139
Figure. A.11 – TCY-Gap connection End of Test (average drift 4.5 %).....	140
Figure. A.12 – Pretensioned connections – End of Test (average drift 4.5 %).....	141
Figure A.13 – TCY connections – End of Test (average drift 4.5 %).....	142
Figure. A.14 – Torsional rotation in hybrid beams: welding intervention (EQ-III level).....	143
Figure. A.15 – Floor damage (EQ-III level).....	144
Figure. A.16 – Welded X-plate (EQ-III level).....	145
Figure. A.17 – Seismic columns base- connection to the foundation:.....	146
Figure A.18 – Gravity column and first floor slab (End of Test).....	147
Figure A.19 – Out-of plane damage in the wall :.....	148

## LIST OF TABLES

Table 3.1 - Reinforcement details of test specimens (Stanton et al., 1997).....	47
Table 4.1 – Distribution of the different type of connections in the test-building.....	57
Table 4.2 – Design parameters according to the DBD procedure .....	61
Table 4.3 - Lateral force distribution from DBD design.....	62
Table 4.4– Imposed column base moments.....	63
Table 4.5 – Internal design forces: beam and column moments.....	63
Table 4.6 – Design vs. actual estimated capacities: prestressed frame .....	72
Table 4.7 – Design vs. actual estimated capacities: non-prestressed (TCY) frame .....	72

## ABSTRACT

The structural response of the five-story PRESSSS precast test building is described in the frame direction of response. Floor forces, moments, and story shears are presented as time-histories of response at different levels of excitation up to twice the design seismic intensity. An extensive photographic record of condition of the frame elements at different stages of testing is also presented.

Structural response in the frame direction was very good. The prestressed frame showed little damage under seismic intensity equal to twice the design level, while exhibiting excellent re-centering characteristics, which reduced residual displacements to negligible amount. Although the TC-Y frame (non-prestressed) displayed increased damping compared with the prestressed frame. Damage was more extensive, particularly at seismic intensities exceeding the design level, and residual displacements were larger.

The report also describes the development of an analytical procedure to describe the moment-rotation characteristics of the beam/column connections, including the strain incompatibility at the critical sections caused by use of unbonded tendons. The procedure is capable of describing all four connection types: Hybrid (post-tensioned), prestensional, TCY-gap, and TCY. Calibration against beam/column subassemblages tested in Phase II of the PRESSSS program indicates excellent agreement behavior between theory and experiment.

The analytical models were assembled into a global model of the full building, which was analyzed under the pseudo-dynamic seismic input applied to the test structure. Predictions from this analytical model agreed well with experimental results, though experimental displacements exceeded predicted values by about 10%. Boek analyses of the results indicated that the prime reason for this small discrepancy was an overestimation of the hysteretic damping model.

Finally, the test provided excellent validation of the direct displacement-based design procedure used to design the test building.

## ACKNOWLEDGMENTS

The project described in this report has involved a large number of individuals and organizations, all of whom deserve individual thanks and acknowledgment. A full list would be impossibly long. Of particular importance are Dr. Chris Latham (UCSD) and Professor Akira Igarashi (Kyoto University) whose efforts in solving the extremely difficult problems of controlling the pseudo-dynamic tests were essential to the test success.

The efforts of the building designers, Professor John Stanton (plus University of Washington graduate students), Ms Suzanne Nakaki, who not only did a superb job of the building design, as evidenced by its excellent performance, but also were present during most of the long-night testing sessions, are particularly acknowledged.

Primary financial support for the PRESSS research program was provided by the PCI (Precast/Prestressed Concrete Institute), the NSF (National Science Foundation), and the PCMAC (Precast/Prestressed Concrete Manufacturers Association of California). The extent of industry support, in terms of financial assistance, material donation, technical advice, and provision of precast products is unparalleled in major United States structural research projects.

Special thanks are due Mario J. Dertolini, chairman of ATLASS and PRESSS Ad Hoc Committee, and Thomas D'Arcy, chairman of the PRESSS Phase III Advisory Group.

In addition, contributors to the testing program include A.T. Curd Structures, Inc., BauTech, Co.; California Field Iron Workers Administrative Trust; Charles Pankow Builders, Ltd.; Clark Pacific; Coreslab Structures, L.A.; Dayton Superior; Dywidag Systems International; ERICO; Florida Wire & Cable, Inc.; Fontana Steel; Gillies Trucking; Headed Reinforcement Corporation; Horizon High Reach; JVI, Inc.; LG Design; Master Builders, Inc.; NMB Splice Sleeve ; Pomeroy Corporation; Precision Imagery; Spancrete of California; Sumiden Wire; and White Cap.

# CHAPTER 1

## INTRODUCTION

The use and development of precast concrete structures in seismic areas have been limited, to date, by the lack of confidence and knowledge about their performance in seismic regions as well as by the absence of rational seismic design provisions in major model building codes.

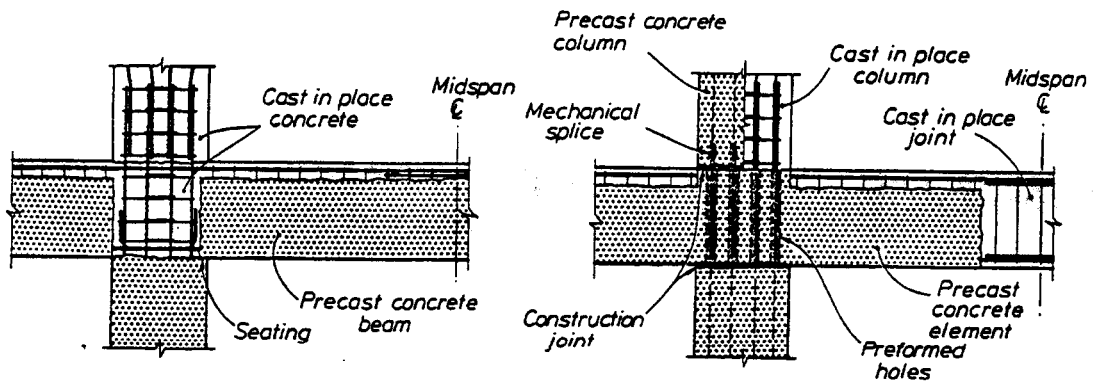
Due to these uncertainties, the recognized advantages of precast concrete construction over cast-in place methods commonly refer only to construction aspects (quality control, velocity of erection), while its structural efficiency is overlooked.

The poor performance of several precast parking structures in the 1994 Northridge Earthquake (Priestley 1995), due to incorrect design detailing rather than intrinsic limits of the structural systems, has probably increased the lack of confidence on such structural systems, contributing to result in further restrictions on precast usage in seismic zones.

### 1.1. Current Code Provisions and Recommendations

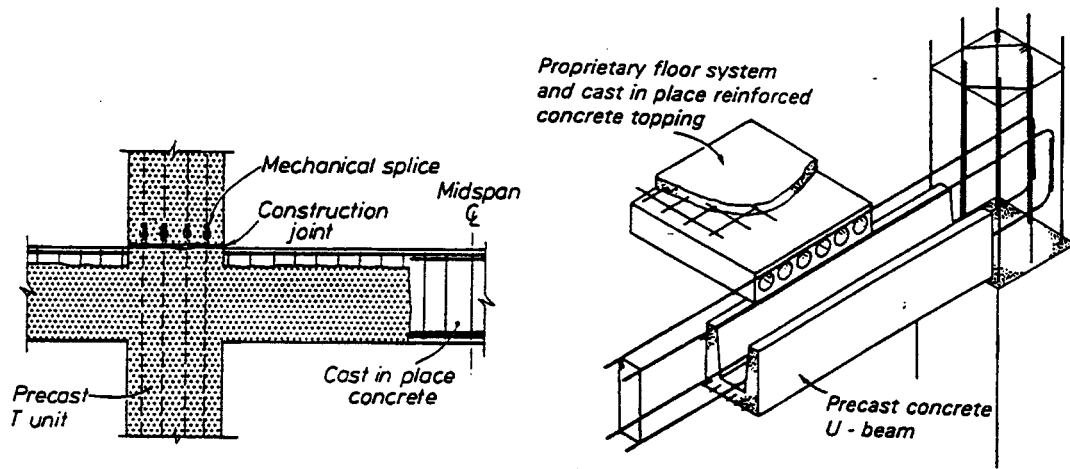
Common trends in the current design codes require the behavior of precast systems to be either analogous to equivalent cast-in-place solutions or to be validated by extensive experimental and analytical evidences. In the former approach, typically referred to as “emulation” of cast in place concrete, precast member elements are thus joined using cast-in-place techniques, greatly reducing the well recognized advantages of precast constructions, namely construction speed and cost. The connection can either be localized within the beam-column joint or in the middle of a structural member, which does not necessarily correspond to a unique prefabricated segment, as typical of cruciform prefabricated beam-column joints.

Extensive analytical and experimental studies have been performed in New Zealand (Park 1990, Restrepo et al. 1992) proposing different various arrangements of precast concrete members for ductile moment resisting frames according to the “emulation” of cast-in-place solutions philosophy (Figs 1.1, 1.2), later also adopted in the construction practice in Japan.



(a) System 1 - Precast Beam Units between Columns

(b) System 2 - Precast Beam Units through Columns



(c) System 3 - Precast T or Cruciform Units

(d) Precast Concrete System Involving Shell Beams

Figure 1 – Commonly Used Arrangements of Precast Members and Cast in Place Concrete in New Zealand (from Restrepo, 1993)

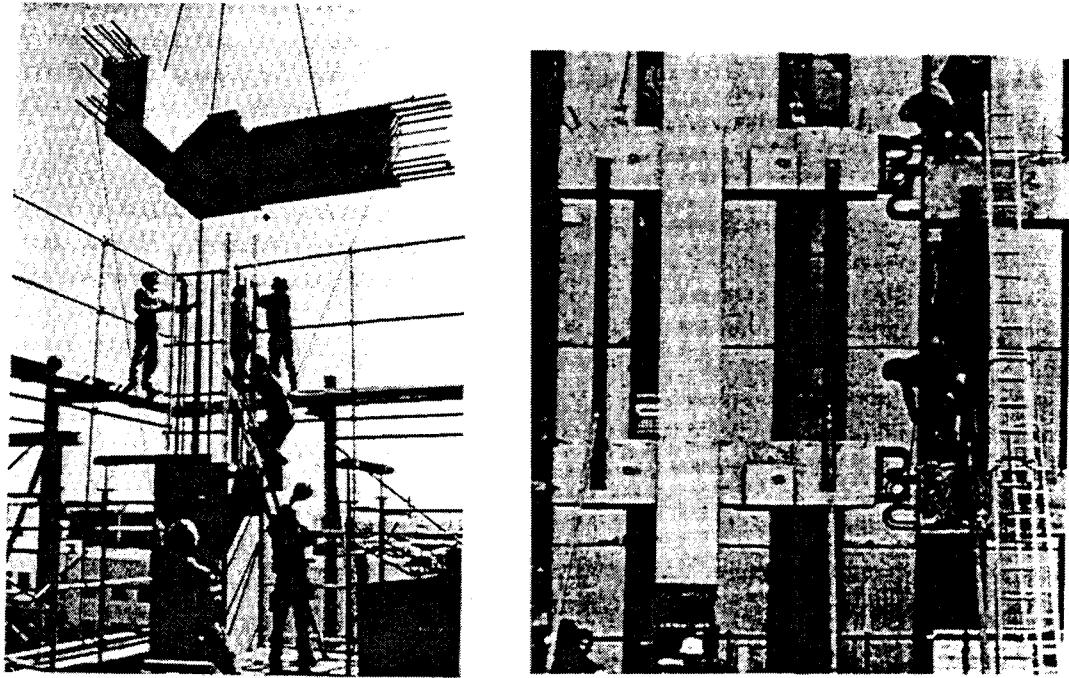


Figure 2 - Erection of precast connections typical in New Zealand  
(from Restrepo, 1993)

In the United States the UBC 97 (Uniform Building Code) describes how the required analogy with a monolithic solution can be reached :

- *wet connection*: as previously described, precast concrete elements are connected with partial or total casting-in-place of the connection;
- *strong connection*: the connection is required to remain elastic, while the inelastic response is assigned to regions localized outside the joint.

The Eurocode 8 simply provides an informative appendix on seismic design of precast concrete structures, accepting the feasibility of a connection with dissipation capability in the critical region. The behavior factor  $q$ , suggested for systems observing the design provisions of the appendix, is modified, in comparison to cast-in-place solutions, by a reduction factor which depends on the energy dissipation capacity of the adopted connections. In any case, unless special studies are undertaken, ductility class “high”, (which implies special requirements in the detailing to assure development of a stable mechanism associated with large dissipation of hysteretic energy) is not suggested for the design of precast structures.

A scheme of a typical arrangement of precast frame connection adopted in Europe according to the emulation of cast in place approach is shown in Figure 1.3.

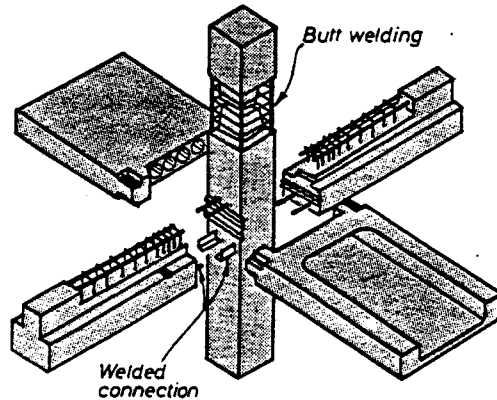


Figure 1.3 -Typical Arrangement of Precast Framed Construction in the ex-U.S.S.R  
(Bychenkov, 1978)

## 1.2. The PRESSS Research Program

As the fourth phase of a coordinated U.S-Japan analytical and large scale testing program for seismic response of buildings, the U.S. PRESSS Program (Priestley 1991,1992) was initiated in 1990 to:

1. develop practical and efficient solutions for precast systems in seismic areas, as alternatives to the “emulation” of cast-in-place reinforced concrete;
2. provide rational design recommendations for the codes.

“Dry” connection solutions, not relying on the use of cast-in-place concrete, as well as “ductile” connections, which imply concentration of the inelastic demand in the critical regions, have been adopted and developed in the PRESSS program, as alternatives to “wet” and “strong” concepts respectively.

Precast elements are therefore maintained, following a Capacity Design approach, in the elastic range, while the inelastic demand is accommodated within the connection itself. Reduced level of damage in the precast beams, compared with cast-in-place RC structure, is therefore expected.

In the first two phases of the program, intensive analytical and experimental studies were carried out by numerous U.S. Universities and Research Institutes (Priestley 1996). A variety of ductile connection details were developed in cooperation with industry representatives, tested in beam-

column subassemblies and modeled with an analytical platform based on modifications to the fiber-element program DRAIN-2X.

### 1.1.2. Basic Conceptual Connections

Most of the several frame connections developed and investigated during these phases of the PRESS Program, can be reduced to four main basic conceptual categories (Fig. 1.4), briefly outlined below:

### 1.2. Non-Linear elastic (NLE)

The precast beams and columns are generally connected through some forms of unbonded post-tensioned (PT) reinforcing bars.

The loss of strain compatibility between the concrete and the PT steel becomes the basic concept to develop a non-linear-elastic behavior: instead of *section* strain compatibility it's more appropriate to refer to member strain compatibility.

As cracking develops at the beam-column interface section, the strain in the concrete is increased due to the curvature demand, while the post-tensioned unbonded steel only suffers a slow increase in strain (which is constantly developed along all the unbonded length), remaining in the elastic range.

A clamping elastic force will thus be developed by the PT steel, ideally reducing to zero the inelastic residual displacement and defining a non-linear elastic characteristic of the hysteretic behavior. While an ideal NLE behavior doesn't provide any energy dissipation, the actual hysteretic behavior of a beam-column subassembly with unbonded tendons can result in a value of the equivalent viscous damping  $\xi$  around 10%, which is slightly larger than that provided by a purely linear elastic system ( $\xi=2-5\%$ ), but remains much smaller than typical values for an equivalent cast-in place concrete connection.

### **Tension-Compression Yield (TCY)**

Similar to a monolithic connection, designed according to the “emulation of cast-in place concrete approach”, the TCY connection behavior is characterized by yielding in tension and in compression, under reverse seismic loading, of the mild steel reinforcement.

Reasonable energy dissipation can thus be guaranteed ( $\xi=25-35\%$ ), while significant residual displacements are expected.

The peculiar properties of the NLE and TCY conceptual systems can be combined in a hybrid solution in which appreciable energy dissipation is provided by the yielding of the mild steel and a clamping force, with consequent minimum residual displacement, can be developed by unbonded PT steel. The behavior of this type of connections, utilized in the frame system of the test building is further discussed in Chapter 3.

### **Shear Yield (SY) Connection System**

Typically located at midspan of beams with the use of precast beams for the connection, this system performs inelastic shear response at the connection, with a hysteretic behavior very similar to the TCY system.

### **Energy Dissipating/Coulomb Friction (CF) Connection Systems**

An approximate rigid perfectly plastic hysteretic behavior is achieved by using a friction sliding damping device which provides inelastic action.

Steel plate assembly, connecting the top of the beam to the column, embedded in the beam and bolted onto the side of the column (Palmieri et al. 1997) can be referred to as an example of an efficient friction device. Slotted holes in the plate assemblies permit sliding along the vertical plate surface on the sides of the beam.

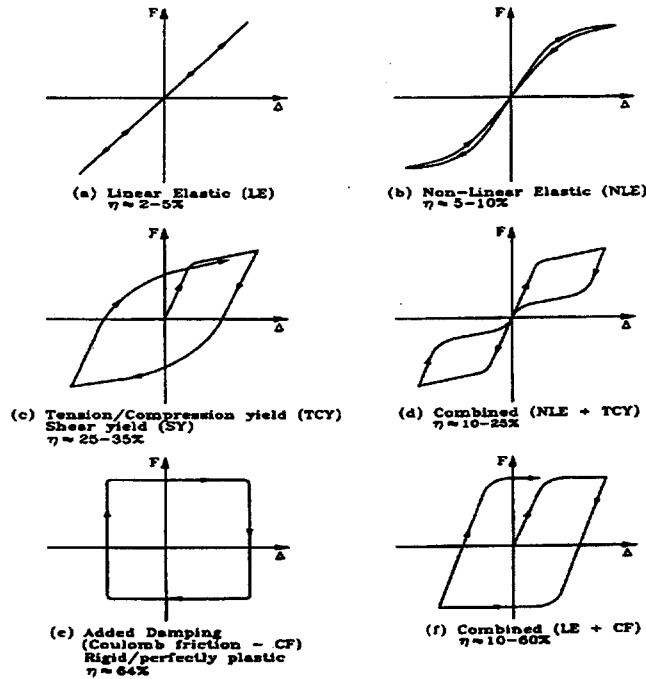


Figure 1. 4 - Hysteretic behavior of the basic conceptual connection systems  
(From Priestley, 1996)

### 1.3. Objective and Scope of the Present Research

As will be later presented in more details, four different connections, based on the direct or combined application of the NLE and TCY conceptual schemes, have been selected and adopted in the third and final phase of the PRESSS Program, consisting in the seismic design, construction and test at the University of California at San Diego of a 60 % scale five-story precast concrete building.

The necessity of developing a reliable model for the analytical prediction of the response of the test-building lead to an extensive review of the literature concerning the analytical modeling of such kind of ductile connections. Commonly recognized difficulties had been so far encountered in the prediction of a moment-curvature (or moment-rotation) behavior of connections in presence of partially or totally unbonded tendons, due to the lack of strain compatibility in the sections and the uncertainties in the definition of a correspondence between the deformation in the concrete and in the steel at a local level (section). Global relationship, based on the whole member behavior, should better be investigated and studied.

Simplified approaches have been proposed in literature, based either on section or fiber element analysis. While in the former case only a discrete bilinear or trilinear idealization of a moment curvature behavior have been developed, in the latter the appreciable results obtained can't be translated in a simple procedure analogous to a section analysis typical of cast-in-place reinforced concrete connections.

In this report a simple and rigorous step-by-step general procedure for the section analysis of connections with partially or totally debonded tendons\bars is presented and illustrated in detail in Chapter 3. Validation of the procedure is achieved through comparison with results from tests on beam-column subassemblies conducted at NIST (National Institute of Standard and Technology) and at the University of Minnesota in the previous phases of the research program. The four different connections adopted in the 5-storey test-building have been analyzed and utilized as a platform for the finite element model used for the prediction of the response of the whole building in the frame direction. Analytical predictions (Pushover and Dynamic non-linear analyses) as well as preliminary comparisons with the experimental global behavior of the test-structure, are presented to further confirm the reliability of the proposed analytical procedure.

#### **1.4. Organization of the Report**

A brief introduction on the current code provisions, construction practice and research approaches is presented in Chapter 1

The structural implications on the use of "unbonded" concepts in dry ductile connections are presented in Chapter 2, as well as previous analytical and experimental studies developed on these alternative precast connections. Different analytical methods, adopted to date in literature to describe the behavior of connections in presence of unbonded tendons, are summarized, underlining the strong and weak aspects.

The section analysis procedure proposed in this contribution to solve the problem of strain compatibility is introduced in Chapter 3, in its general scheme first, and, subsequently, in details, showing the results of the validation with experimental tests on beam-column subassemblies.

The proposed procedure is therefore adopted as a basis to develop an analytical model of a complete frame structure and predict the behavior of the 5-story precast concrete PRESSS test-

building. Focusing on the frame direction, summary of design concepts, structural features and test procedures are presented in Chapter 4, and the main assumptions in the modeling of the monotonic and cyclic behavior of the connections described.

Chapter 5 describes and discusses the experimental results in the frame direction. Photographic report of the damage level as well as force displacement characteristics from the test data are presented as well as preliminary analytical-experimental comparison of the response. Conclusions and suggestions for possible further investigations are finally given.

## CHAPTER 2

### **“UNBONDED” CONCEPT: STRUCTURAL SIGNIFICANCE AND RESEARCH BACKGROUND**

In this chapter an overview of previous research regarding connections which utilize the concept of “unbonded” Post-Tensioned (PT) tendons/bar or unbonded length in ordinary longitudinal reinforcement, is given. The influences of the unbonding on the structural behavior are underlined and the conceptual moment-rotation behavior is described. Previous proposals for the analytical modeling of such typology of connections are reviewed, illustrating basic assumptions, affinity with experimental results and limits.

#### **2.1. Experimental Tests at NIST: Preliminary Phases**

An extensive series of tests conducted at the National Institute of Standard and Technology (NIST) has investigated the seismic performance of ductile precast beam-column connections and compared with monolithic equivalent systems.

Started in 1987 with the aim of developing preliminary guidelines for the design of precast concrete frame connections in regions of high seismic activity, the research program consisted in the testing of twenty-two 1/3 scale model interior connections designed in accordance to the Uniform Building Code (UBC 1985).

The experimental program comprised four phases: in the preliminary phase of the research program, the viability of post-tensioning as a connecting methodology was analyzed, and the behavior of monolithic RC connections compared with the performance of similar bonded post-tensioned PC connection (Cheok and Lew, 1990). Experimental hysteretic behavior of Phase I specimens are shown in Figures 2.1a.

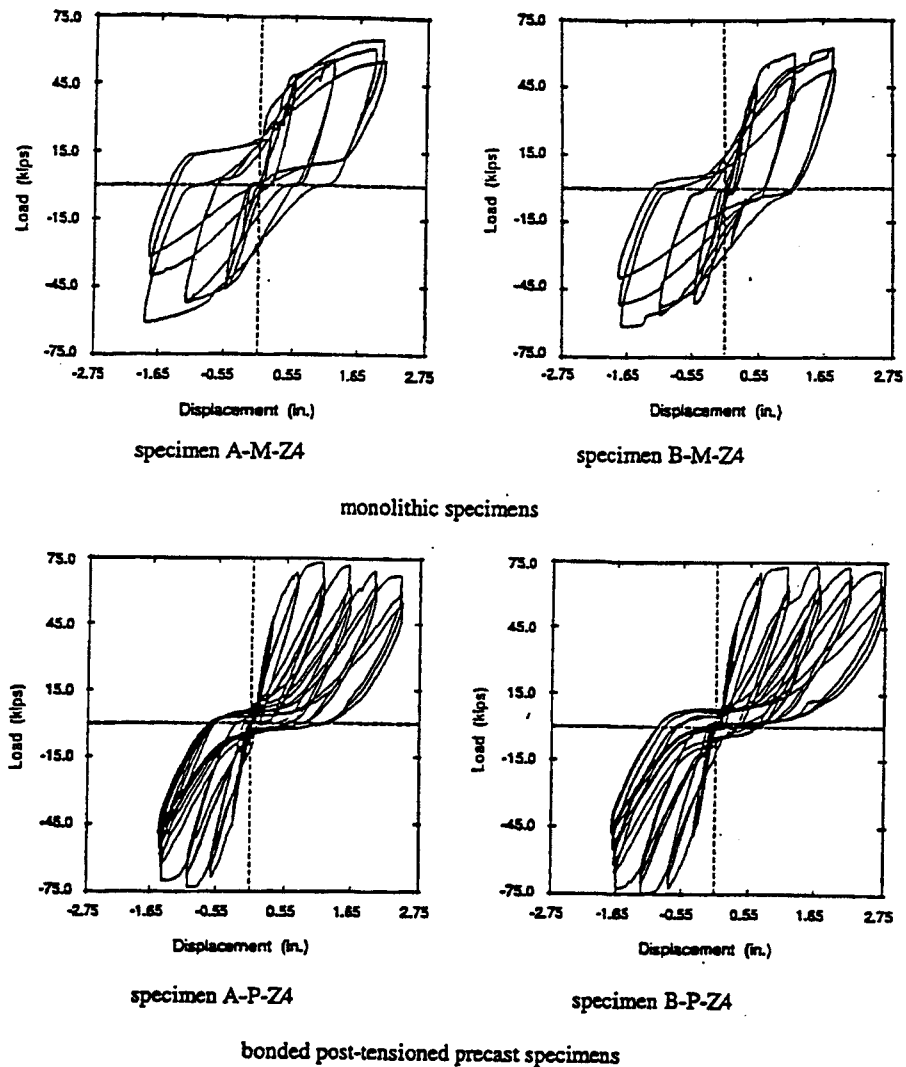
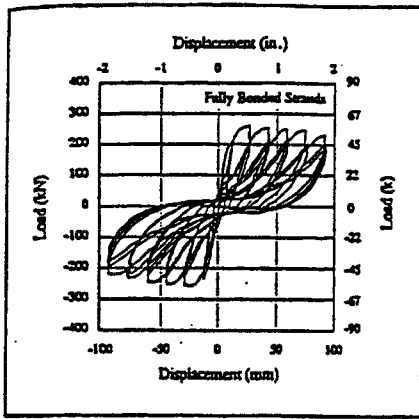


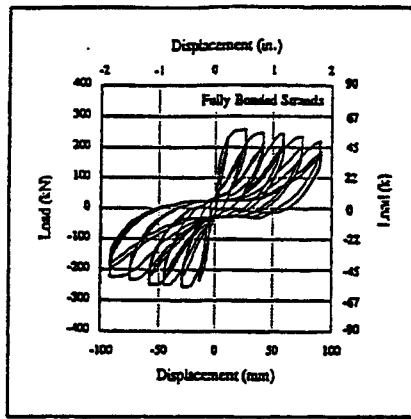
Figure 2.1a. Hysteretic behavior for NIST phase I specimens  
(from Cheek and Lew 1990)

While general satisfactory results in terms of ductility, strength and initial stiffness were observed, significant stiffness degradation in the unloading phases at high drift levels as well as limited energy dissipation capacity when compared to the monolithic solutions were reported during the Phase I.

The choice of the material, as well as positioning of the PT steel, were examined during the Phase II as parameters to offset such weaknesses (Cheek and Lew, 1991). Relocating the PT steel from the top or bottom of the section to the centroid of the cross-section, reduces the strain level experienced by the PT steel, maintaining the clamping force at higher drift levels. The excessive pinching of the force-deflection hysteretic loops, with an unloading branch with zero-slope stiffness at loads near zero was not affected (Fig. 2.1b). No particular effects were noted in the use of bars or tendons.

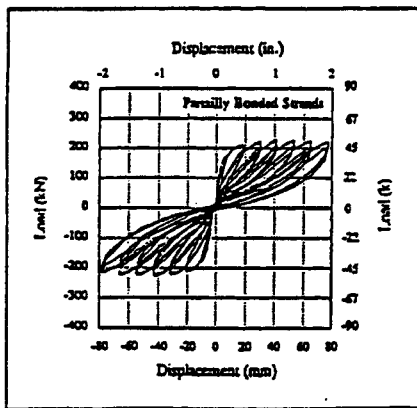


specimen E-P-Z4

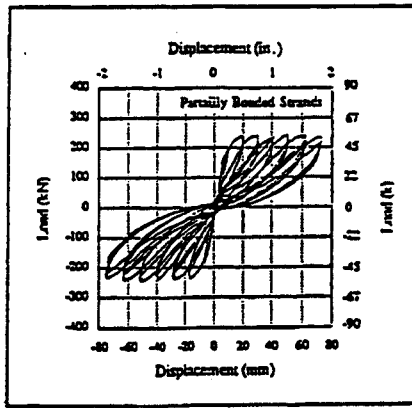


specimen F-P-Z4

Figure 2.1b. Hysteretic behavior for NIST phase II specimens (from Cheek and Lew 1991)



specimen G-P-Z4



specimen H-P-Z4

Figure 2.1c Hysteretic behavior for NIST Phase III specimens (from Cheek and Lew, 1993)

## 2.2. Original Development of Unbonded Tendons

The use of unbonded tendons, partially debonded through the joint and for some distance on either side, was first conceived and proposed by Priestley and Tao [1993] as a viable solution for precast concrete ductile connections.

It was recognized (Priestley and Tao, 1993) that the stiffness degradation phenomenon, previously described, is caused by a reduction of the effective prestressed clamping force through the column, resulting from inelastic strain of the prestressing steel at the critical section. Referring to Figure 2.2 where  $f_{s_i}$  indicates the initial steel stress after prestressed losses, it appears that low-level of deformation demand will not cause loss of prestress as long as it remains in the elastic range. On unloading from higher levels of deformations in the inelastic range, the prestress may partially ( $f_{s2}$ ) or entirely ( $f_{s3}$ ) be lost, with undesirable consequences when, as typical in these kind of connections, the shear resistance relies on a friction mechanism at the beam column interface.

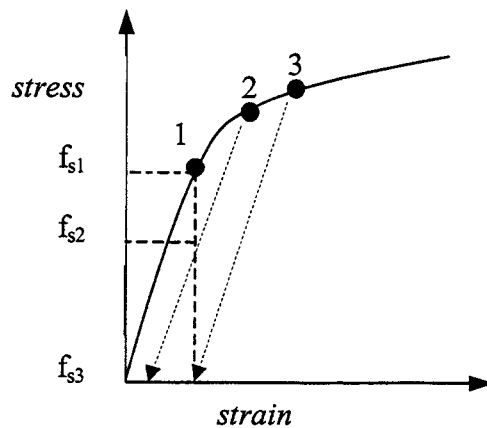


Figure 2.2 – Prestress loss due to inelastic response  
(from Priestley and Tao, 1993)

The use of partially debonded tendons was suggested as a convenient solution and analytically investigated, as is described in Paragraph 2.4.1.

Main advantages can be indicated as follows:

- An accurate design of the unbonded length can guarantee that the limit of proportionality of the PT steel is not exceeded at the maximum predicted level of displacement, avoiding any loss of prestress and thus maintaining shear friction at the interface.
- Due to the clamping elastic forces from the PT steel, a significant self-centering property, with reduction of the residual displacement, is provided. The hysteretic behavior is essentially nonlinear elastic, with the shortcoming of reduced energy dissipation capacity.

- When the tendons are located at the top and bottom of the section, the beam-column joint reinforcement could be greatly simplified since the entire horizontal shear force is transferred by a diagonal compression strut (Fig. 2.3).

The prestress tensile force on either side of the joint would be in fact equal for each tendon, debonded through the joint. No special vertical joint shear reinforcement would thus be needed, in addition to an essentially nominal transverse hoops.

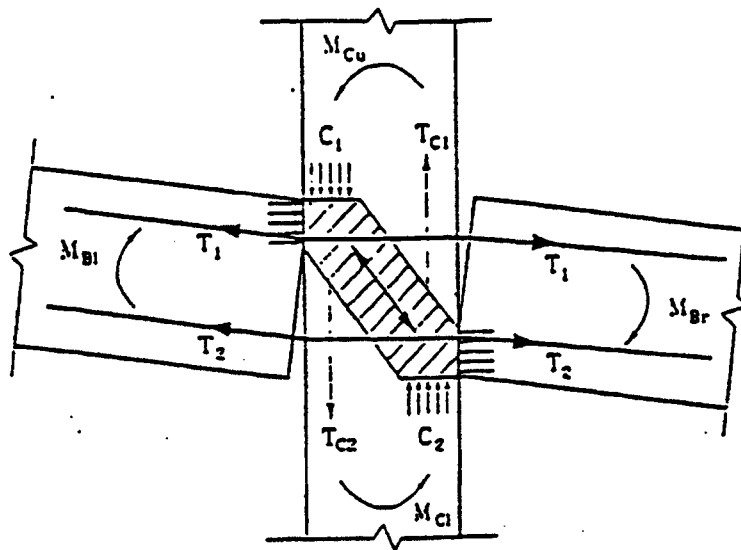


Figure 2.3 – Shear transfer mechanism in the joint region with unbonded tendons  
(from Priestley and Tao, 1993)

### 2.3. Experimental Tests at UCSD

Experimental studies were conducted at the University of California at San Diego on full-scale exterior and interior unbonded post-tensioned precast beam-column subassemblies to investigate the seismic performance of this typology of connections, resulting in expected satisfactory confirmations (MacRae and Priestley 1994).

A more refined strut and tie mechanism for the shear joint transfer in an interior connection was proposed, based on the observed yielding of the transverse reinforcement (Fig. 2.4).

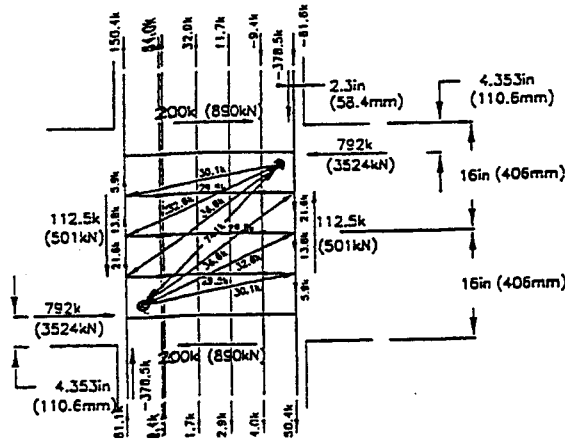


Figure 2. 4 – Possible strut and tie mechanism for interior subassembly  
(from MacRae and Priestley, 1994)

It was clearly shown that the compressive action of the PT bars results in increased performance of the joint, when compared to an equivalent cast-in-place solution both in terms of strength and ductility. Consequently, limited level of cracking and damage has been generally observed in the joint region, as well as in the beam elements, most of the inelastic demand being concentrated in a single flexural crack at beam-column interface.

The “unbonding” concept was also applied in the Phase III of the NIST experimental program to improve the hysteretic behavior of the precast concrete specimens (Cheok and Lew, 1993).

Figure 2.1c shows the load-lateral displacement relationship for the two specimens tested, which were identical to those of Phase II illustrated in Fig. 2.1b, except that the strands were unbonded through the joint. The improvements in terms of zero-slope stiffness degradation and reduction of residual displacement is evident.

## 2.4. Analytical Studies

### 2.4.1. Dynamic Analyses

Promising efficiency of these categories of connections has been shown from referenced past research. On the other hand potentially undesirable characteristics can result from a debonded design, such as a limited energy dissipation capacity (once the PT steel is designed to remain in the elastic range) which could result in increased lateral displacements.

Extensive dynamic inelastic analyses investigated the theoretical seismic response of precast-prestressed concrete frames with partially unbonded tendons and compared the results with fully bonded or monolithic solutions, by means of time-history analyses (Priestley and Tao, 1993) of S.D.O.F. oscillators with different initial periods and ideal hysteretic rules: linear elastic, bilinear elastic (unbonded tendons), bilinear elastoplastic (monolithic), bilinear degrading (fully bonded).

Analytical results indicated that, “despite the total lack of hysteretic energy absorption in the bilinear elastic model, displacement for medium to long period structures with such force-displacement response would be less than 35 percent larger than elasto-plastic systems of the same period”. Furthermore, in a real situation reinforced concrete (monolithic case) would exhibit a less ideal hysteretic response than the elasto-plastic, and the actual bilinear elastic response is likely to have higher equivalent viscous damping than the 5% assumed in the analyses. Consequently, it’s reasonable to predict closer level of displacements between basically different damped models.

Effects on the whole response of frame systems including different kind of connections were investigated with dynamic time-history analyses (Brewer, 1993) on 5-story and 15-story frame structures. Bilinear elastic, bilinear degrading and bilinear elasto-plastic, once again were utilized as hysteretic models to represent unbonded, bonded post-tensioned and cast-in-place solutions respectively. In the 15-story building case, similar maximum roof drift were reached regardless the connection model adopted, while more significant inconsistencies characterized the 5-story case.

#### **2.4.2. Moment Rotation Behavior: Trilinear Idealization**

The high level (ideally infinite) of curvature at the beam-column interface makes it more rational to describe the behavior of a beam-column connection referring either to the relative rotation concentrated at the interface or to global parameters of a beam-column subassembly (lateral force - top displacement). In the former case the characteristic particular mechanism of the connection, in terms of opening and closing of a concentrated gap, can be directly captured. In the latter approach, elastic flexural behavior of the precast members converging into the connection, as well as shear deformation of the panel zone are implicitly included in the general relationship, and should be therefore computed and subtracted in order to investigate the behavior of the connection at the beam-column interface.

Having proposed a preliminary distinction in under-reinforced and over-reinforced connection, a few key points can be identified and assumed as limit states related to the PT steel or concrete behavior (Fig. 2.5):

1. Decompression limit state ( $M_{cr}, \theta_{cr}$ )  
 Defines the beginning of the crack opening, when the concrete at the extreme fiber of the beam connection reaches zero stress, after the imposed compression due to the initial post-tension stress in the strands.
  
2. Linear limit state ( $M_l, \theta_l$ )  
 Defines the end of the elastic range, which does not correspond to a clear stress-strain state in the section, as typical in a bonded connection after the yielding of the steel.

Significant conceptual consequences derive from this peculiarity. Although a clear deviation from the linear behavior can be noted, a rigorous definition of ductility can not be adopted. In fact, while a common definition of such parameter is assumed to be the ratio between the actual displacement and yielding displacement, it originally derives from energy concepts, which are invalidated by the non-dissipative characteristics of a non-linear elastic hysteretic behavior.

Abandoning the rigor of the definition, in the presence of unbonded tendons connections, the term ductility will thus only describe the post-linear behavior of the connection.

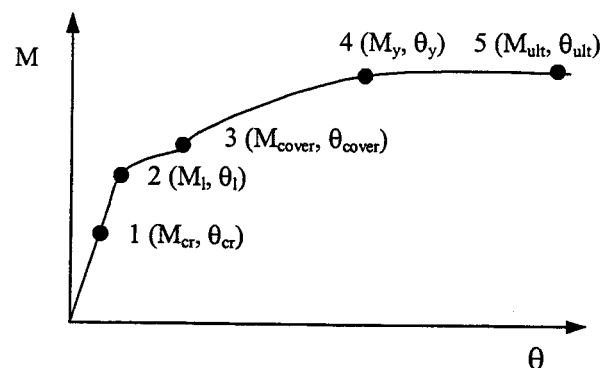


Figure 2. 5– Discrete moment-rotation relationship for unbonded post-tensioned under-reinforced beam connections (from Lehigh PRESSS Report, 1998)

3. Cover spalling limit state ( $M_{cover}, \theta_{cover}$ )  
It corresponds to the spalling of the unconfined concrete.
4. Yield limit state ( $M_y, \theta_y$ ).  
This point is only defined for under-reinforced connections, when the PT yields before achieving the ultimate strength of the section.
5. Ultimate limit states ( $M_{ult}, \theta_{ult}$ )  
The failure occurs due to the crushing of the confined concrete.

A simplified trilinear idealization (Fig 2.6) force-deflection or moment rotation behavior has been proposed (Priestley and Tao, 1993), based on the evaluation of the key points already mentioned above.

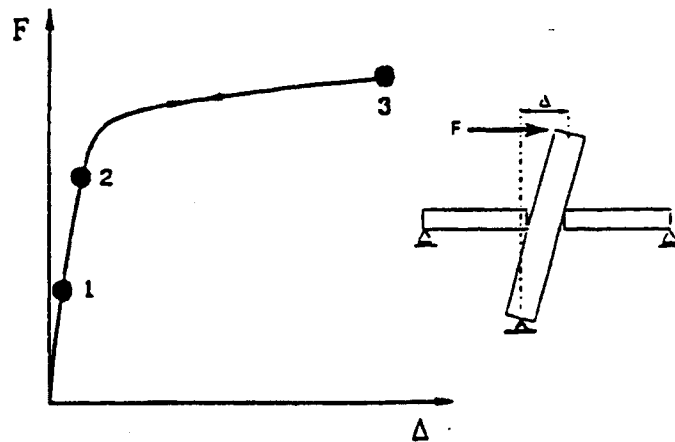


Figure 2. 6 – Trilinear idealization  
(From Priestley and Tao, 1993)

#### 1. Decompression limit states

From a linear distribution of stress in the concrete corresponding to a decompression point at the extreme fiber of the section, the moment  $M_{cr}$  can be simply evaluated as:

$$M_{cr} = \frac{P_i h_b}{6}$$

where  $P_i$  is the initial prestressing force (acting at the beam mid-height) and  $h_b$  is the beam depth.

The corresponding rotation  $\theta_{cr}$  can be evaluated as:

$$\theta_{cr} = \frac{1}{2} \frac{M}{EI_g} \frac{L_b}{2}$$

where  $I_g$  is the gross moment of inertia referred to the uncracked section.

$L_b$  is the beam length, thus  $L_b/2$  represent the equivalent cantilever scheme, i.e. distance from the interface to the point of contraflexure in the beam.

## 2. Linear limit states

Since deviation from the linear elastic behavior is negligible until the crack has propagated at least to the centroidal axis of the beam, the evaluation of the parameter at this limit states results in:

$$M_l = \frac{P_i h_b}{3} \Rightarrow M_l = 2M_{cr}$$

As will be later discussed, experimental validation of this approach showed a general underestimation in this term. Assuming that the neutral axis position is moved beyond the centroid of the cross-section, an upper bound can be estimated (Lehigh PRESSS Report, 1998) when the gap is opened over the entire height of the section:

$$M_l = \frac{P_i h_b}{2} \Rightarrow M_l = 3M_{cr}$$

A reasonable upper bound has been set as  $M_l < 2.5 M_{cr}$ .

Above this point, the evaluation of a step-by-step moment-rotation curve is difficult, due to the lack of strain compatibility in the section which invalidates the commonly utilized linear relationship between steel and concrete strains.

### 3. Yielding and ultimate limit states

In the case of under-reinforced beams, in which by definition the limit of proportionality of the PT steel is reached, it's reasonable to assume that, at the yielding point, the concrete ultimate conditions are approached. An equivalent ultimate compression stress-block, can be thus be utilized, resulting in a moment of the equivalent compression stress block around the neutral axis as indicated in the following expression:

$$M_c = \alpha\beta\left(1 - \frac{\beta}{2}\right)bc^2 f'_c$$

where  $\alpha$  and  $\beta$  are the stress-block parameters as suggested from Popovics (1973) depending on the strain level.

When approaching the ultimate conditions, these parameters are quite insensitive to the variation of the deformation level and thus result in negligible errors on the moment capacity, even when they are crudely estimated

The term  $\alpha\beta(1-\beta/2)$  may in fact change from 0.33 to 0.415. The neutral axis depth  $c$  is given by:

$$c = \frac{A_{ps} f_{slp}}{\beta b \alpha f'_{cc}}$$

with

$f'_{cc}$  compressive strength of the concrete, assumed to be confined

$f_{slp}$  the steel stress at the limit of proportionality

$A_{ps}$  the total area of prestressing steel

The ultimate moment capacity is hence:

$$M_u = A_{ps} f_{slp} \cdot \left( \frac{h_b}{2} - \frac{\beta c}{2} \right)$$

The corresponding rotation is evaluated taking into account the extension of the prestressing tendon from the column centerline to the end of the debonded region:

$$\Delta l = \Delta \varepsilon_s \left( \frac{h_c}{2} + x \right)$$

where  $x$  is the unbonded length of the tendons on either side of the column.

At the limit of proportionality of the prestressing stress-strain curve, the increase in steel strain is:

$$\Delta \varepsilon_s = \frac{(f_{slp} - f_{si})}{E_s}$$

$f_{si}$  being the initial steel stress after losses

Hence:

$$\theta_y = \frac{\Delta l}{\left( \frac{h_b}{2} - c \right)}$$

In the case of under-reinforced connection, it was shown that the beam ultimate moment capacity ( $M_{ult}$ ) is approximately equal to the yield moment ( $M_y$ ). The ultimate conditions in terms of rotation can be based (Lehigh PRESSS Report, 1998) on the ultimate concrete strain ( $\varepsilon_{cu}$ ) and the confined concrete crushing length of the beam connection ( $L_{cr}$ ):

$$\theta_{ult} = \phi_{ult} L_{cr} = \frac{\varepsilon_{cu}}{c} L_{cr}$$

#### 2.4.2.1. Limits of the Procedure

Such an approach is reliable for under-reinforced connections which are expected to experience yielding of the PT steel at small levels of displacements. In the over-reinforced case, serious difficulties have been so far encountered in the development of approximate formulas for the definition of a discrete moment-rotation behavior.

Crushing of the concrete at small rotations or late yielding of the PT steel (i.e. occurring after large rotations) are considered two possible conditions which characterize an over-reinforced beam-connection.

While the decompression and the linear limit state parameters can be evaluated with the formulas described above regardless of the characteristic (under or over-reinforced) of the connection, the evaluation of moments and rotations beyond the limit point is considerably more difficult because of the following aspects:

- 1) the estimation of the strain in the steel can no longer be based on yielding condition assumptions;
- 2) the neutral axis position cannot be estimated with a close-form equation, since a stable value is not available;
- 3) a trial and error procedure, able to satisfy both equilibrium and member compatibility, must be utilized

#### **2.4.3. Alternative Approach: Fiber Element Analysis**

An alternative approach for the characterization of the behavior of connections which are utilizing the concept of unbonding can rely on a finite element analysis, which can better take into account global relationships (equilibrium, compatibility) involving single members or the whole specimen, and thus predict a more realistic behavior of the critical section at the connection interface. It's necessary to remember that such an approach, alternative to a typical section analysis, represents a higher level of complexity.

Accurate analytical modeling of unbonded post-tensioned beam-column subassemblies using fiber elements has been performed at the University of Lehigh (Lehigh PRESSS Report, 1998). In the following paragraph a brief summary of those studies is presented.

##### **2.4.3.1. The Analytical Model using Fiber Elements**

A typical interior beam-column subassembly and the corresponding fiber model are illustrated in Figures 2.7-2.8. The unbonded length of the beam, where the inelastic deformation is expected to occur, is modeled with a fiber beam-column element, while elastic beam-column elements are

utilized to model the elastic regions of the beam, where only elastic deformations are expected. Truss elements model the PT steel.

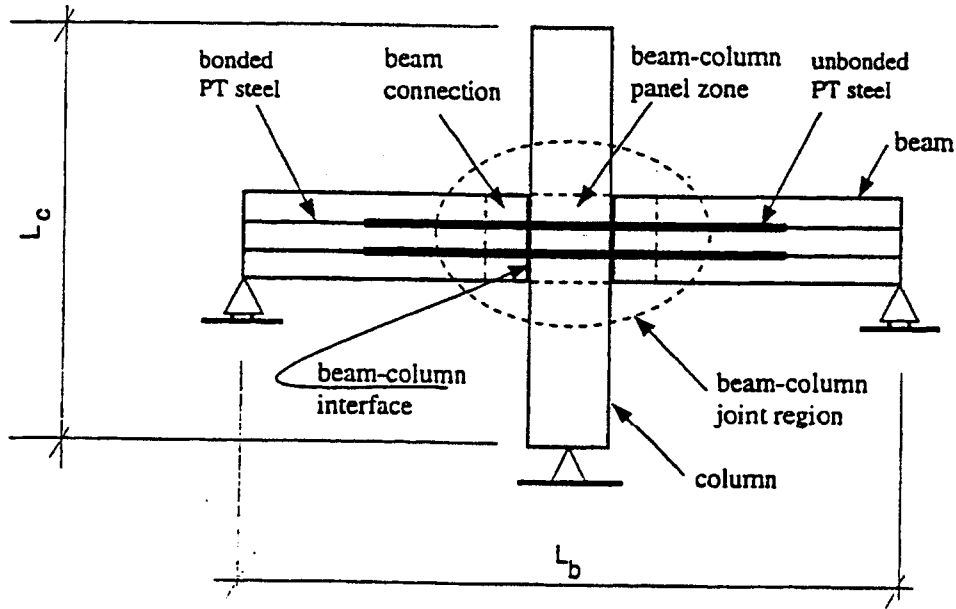


Figure 2.7 –Partially Unbonded post-tensioned beam-column subassembly (from Lehigh PRESSS Report, 1998)

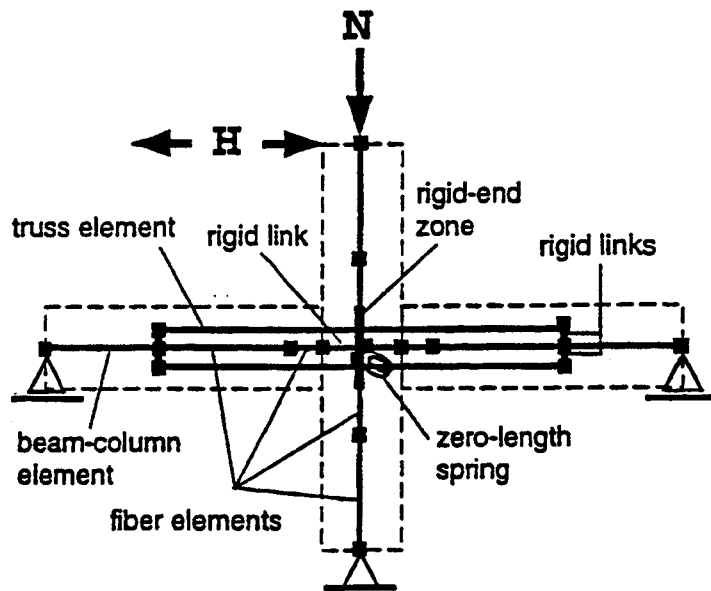


Figure 2.8 – Fiber element model (from Lehigh PRESSS Report, 1998)

Panel zone shear deformations are modeled by a zero-length spring element, while rigid links and rigid ends are used to model the panel zone flexural deformations. Furthermore rigid links connect the truss element end zones to the adjacent fiber nodes at the locations of the PT steel anchorages.

The fiber element discretization of the unbonded region is realized through a number of fiber element segments whose behavior is monitored at the midsection (slice). Each slice is divided in fibers with a defined stress-strain relationship, representing bonded steel or concrete behavior. The Post-tensioned steel tendons/bars are modeled with truss elements whose end nodes are slaved to the adjacent concrete nodes through rigid links. This solution seems to guarantee member compatibility between the concrete and the steel deformations, pending correct assumptions on the behavior of the opening and closing of the gap at the beam-column interface. It seems, however, that the hypothesis of "plane sections remain plane" could no longer be valid in the region close to the interface section. This local behavior can not be taken into account by the fiber model, which assumes a linear strain variation over the cross-section height. On the other hand, the opening of the gap can be captured as an accumulation of tensile deformations over a certain length of the beam. By integrating, at each level of the section, the concrete fiber tensile strains over the unbonded length, the width of the gap can be evaluated.

Furthermore, the variation in the number of fibers subjected to tension in the loading or unloading phase, can represent the softening and re-stiffening effects in the connection.

#### **2.4.3.2. Experimental Validation of the Fiber Model**

In order to validate the efficiency of the fiber model described above, the experimental results from subassemblies tested at NIST during the Phase III were utilized for the verification. In particular, the NIST-specimen GPZ4 was selected for the analytical-experimental comparison. Description of the subassembly geometric and mechanical properties, as well as test setup and displacement pattern utilized for the quasi-static cyclic test can be found in (Cheok and Lew, 1993).

As illustrated in Figures 2.9 to 2.11, the fiber model provides a good estimate of the elastic behavior of the test specimen, especially in terms of initial stiffness and strength. On the other

hand, inaccuracies in the prediction of ultimate deflection, yielding point, and hysteretic energy dissipation, underline the necessity of further refining the model parameters, which should be defined according to a logical and general global relationship, rather than geared to match the experimental results.

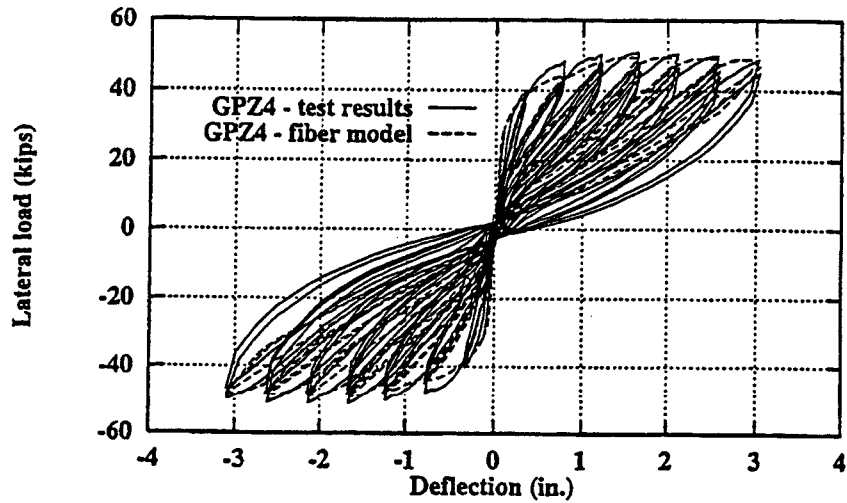


Figure 2.9 – Hysteretic behavior for NIST specimen GPZ4:  
a) test result b) Lehigh fiber model  
(from Lehigh PRESSS Report, 1998)

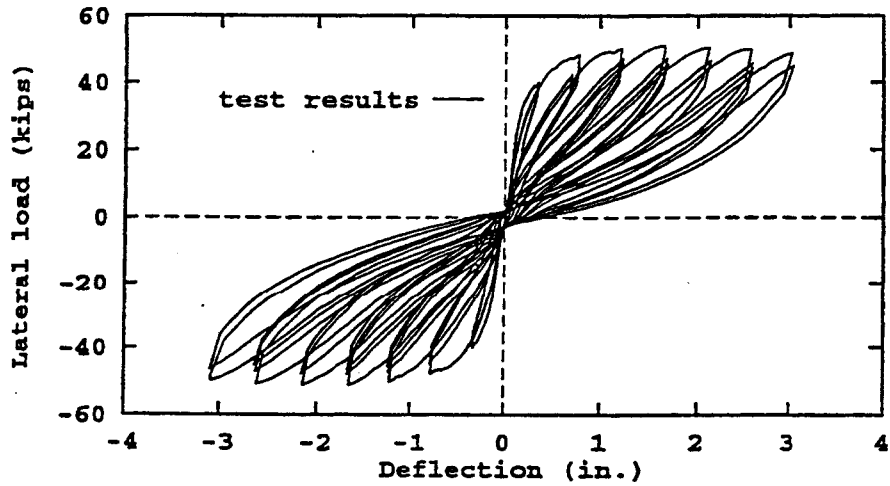


Figure 2.10 – Experimental analytical comparison for NIST specimen GPZ4  
(from Lehigh PRESSS Report, 1998)

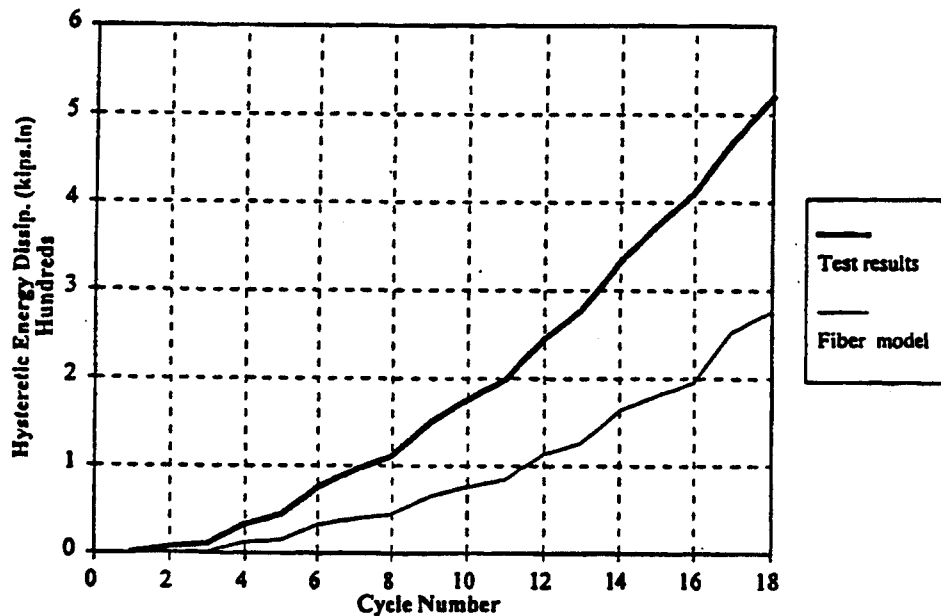


Figure 2. 11 –Hysteretic energy dissipation for NIST specimen GPZ4  
(from Lehigh PRESSS Report, 1998)

A significant increase (close to 30%) in the value of a critical parameter such as the unbonded length was, for instance, adopted in the analytical predictions of Lehigh to account for a suspected bond deterioration which might have been occurred during the test, gradually extending the initial unbonded length as the level of deflection was increasing.

### 2.4.3.3 Considerations

Although a fiber element approach, substantially more complex than a section analysis, should naturally be more adequate to take into account global relations of equilibrium or compatibility valid over the entire structural member, refinements and calibration of the parameters seems to be still necessary to fully and correctly describe the behavior of connections with unbonded tendons/bars.

While the number of points that can be evaluated in the moment-rotation curve of the connection is clearly increased, such an approach is considerably more complex than a simple “hand-calculation” section analysis, as commonly utilized for cast-in-place reinforced concrete

structures. Since the predictions for inelastic deformation capacity depend critically on the length of fibers in the end region, it is not clear that accurate predictions of capacity will result.

In the following chapter the proposed procedure for a step-by-step section analysis in which the member compatibility, thus global property, can rationally be taken into account as an additional condition to the steel-concrete strain relationship, is presented in detail.

## **2.5. Hybrid Connections: Experimental and Analytical Studies**

As previously underlined, unbonded tendon connections can guarantee optimum self-centering capability with a typical non-linear elastic behavior. On the other side, very low energy dissipation capability can be provided from these kind of connections. Although past studies, as described in previous paragraphs, in the form of dynamic analysis of S.D.O.F, realistically assess the importance (sometimes over-emphasized) of hysteretic energy absorption in the response of medium-to-long period systems with debonded tendons (Priestley and Tao 1993), this parameter still plays a significant role in the response of a structure, as typically recognized by the codes, which define elastic design spectra for different value of viscous damping coefficient  $\xi$ .

In the first chapter the basic conceptual characteristics of precast beam-column connections developed during the preliminary phases of the PRESS program have been introduced.

As briefly anticipated, the Hybrid system (Fig. 2.12) was conceived to combine and optimize the main advantages of the conceptual NLE (Non Linear Elastic) and TCY (Tension-Compression-Yielding). Both mild steel and unbonded post-tensioned tendons are adopted as longitudinal reinforcement. The unbonded tendons, placed in ducts located in the middle of the section to reduce the deformations, are designed to remain in the elastic range and provide an elastic clamping moment, thus self-centering properties to the connection. Mild steel at the top and at the bottom of the section are used as longitudinal reinforcement with high dissipation characteristics.

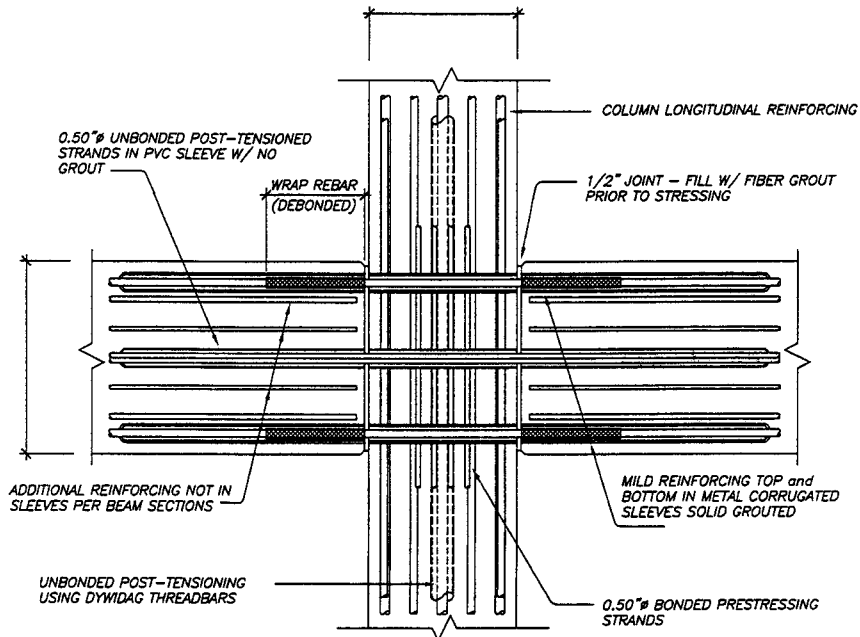


Figure 2. 12 –Hybrid connection - PRESSS 5-storey building  
(from Sritharan, Priestley et al., 2000)

Shear is carried across the interface by friction provided by the action of the PT tendons. Most of the rotational inelastic demand is concentrated at the beam-column interface, where a neat flexural crack is supposed to open and close, strongly reducing the damage in the precast elements, as opposed to a cast-in-place monolithic solution with distributed flexural cracks along the beam.

In order to reduce the strain level in the mild steel and avoid fracture, they can be unbonded for a short length (few inches) in the beam-column interface region.

### 2.5.1. Experimental Tests

The hybrid solution showed extremely promising behavior since the first experimental tests on subassemblies performed at NIST during the last phase IV of the extensive program mentioned above (Cheok and Stone 1994, Stone et al. 1995).

In Phase IVa different configurations were tested, varying the position of the PT steel from the top and bottom (replaceable positions) to the center (reduction of strain), the use of PT steel- high

strength bar or strands, and other variables. The results of this phase were utilized to select the specimen details to be adopted in the following stage.

Phase IVb consists of four-beam column connections. Having established that the most efficient solution, both in term of costs and performance, was to place unbonded tendons in the center of the section and mild steel at the top and bottom, the effect of different combinations (ratios) of mild and PT steel and alternate types of mild steel, as a means of improving the energy dissipation properties, were investigated.

Basic reinforcement properties as well as geometric dimensions of the test specimens can be found in (Stanton et al., 1997). The hysteretic behaviors of the different connections are shown in Figures 2.13-2.14.

Each specimen was subjected to an increasing displacement pattern until failure, arbitrarily defined as the point at which the strength dropped to 80 percent of the peak resistance. Results were compared with experimental behavior of equivalent monolithic connections.

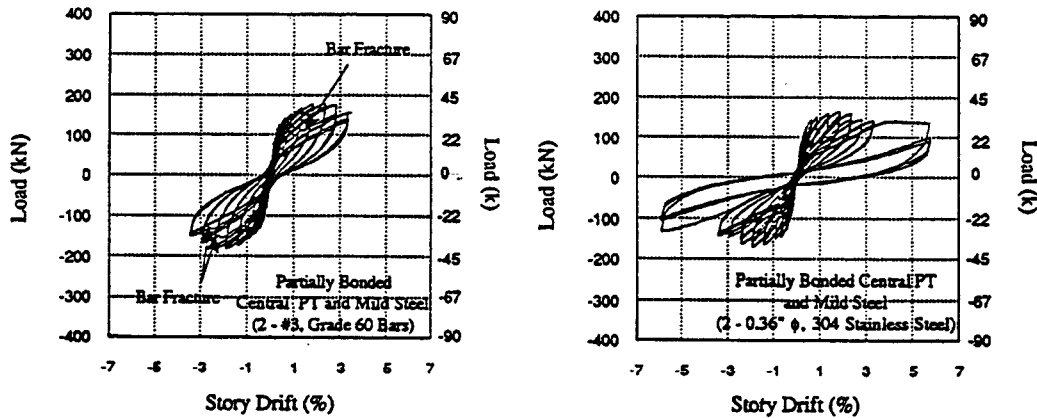


Figure 2. 13 –Hysteretic behavior of hybrid connection – NIST Phase IV b specimens O-P-Z4 and P-P-Z4 (from Cheek and Stone, 1994)

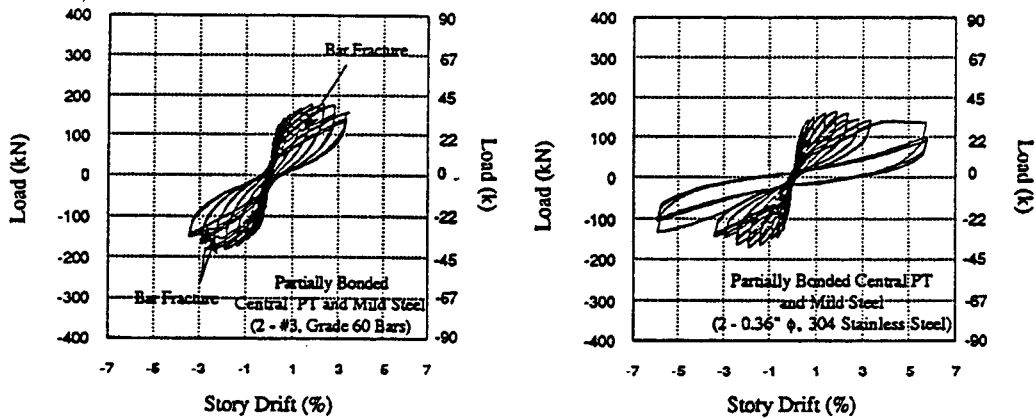


Figure 2. 14 –Hysteretic behavior of hybrid connections – NIST Phase IV b specimens M-P-Z4 and N-P-Z4 (from Cheok and Stone, 1994)

The level of damage in the precast elements, both beams and columns, was minimal in the precast connections even at high levels of drift (above 3%), as opposite to severe cracking pattern shown by the monolithic specimens. As expected, all the inelastic demand was concentrated at the interface through the opening and closing of a gap. Limited joint shear damage was also observed, when compared with cast-in-place solution at same levels of displacement. The reason can be found in a different strut and tie mechanism of shear transferring through the joint, which can result in significant lower shear reinforcement requirements in both the beam and the beam-column joint.

The energy dissipated by the precast specimens was comparable to (if not superior to) that provided by the monolithic specimens, up to a drift of 1.5%. At higher drift levels the energy dissipated was on average 75% of that dissipated by the monolithic specimens.

Such properties appear to be even more important when considering that the relative design drift corresponding to a UBC Zone IV loading on the specimen varied between 1% and 1.5%. Furthermore, self-centering properties with essentially no residual drift following large inelastic deformation were confirmed. In addition, the failure of longitudinal bars, did not cause a sudden strength degradation, as in the cast-in place solution. At the assumed conventional failure level, the precast specimens retained an average of 55 percent of the maximum strength, thanks to the undamaged prestressing strands.

### 2.5.2. Analytical Modeling of Hybrid Connections

Extensive parametric studies to investigate the performance of moment-resisting precast concrete frames with hybrid connections under seismic loads were conducted by (Cheok et al. 1998), utilizing an “a posteriori” approach for the development of the hysteretic model of the connections.

Based on the observed hysteretic behavior from experimental tests, a versatile hysteretic model was developed and defined by means of seven parameters to incorporate the particular characteristics of the experimental force-deformation loop: stiffness and strength degradations, pinching. The identification of the seven parameters were obtained observing similitude requirements with the experimental scaled tests and minimizing the error between the predicted and experimental energy dissipation per cycle.

During the parametric analyses on frame structures, the resultant moment-curvature envelope was characterized by a trilinear curve with an initial stiffness based on the prototype beam dimensions, and a yielding moment set equal to the design beam moment. The remaining parameters to complete the  $M-\phi$  envelope were obtained by maintaining similitude between the experimental specimen and the design prototype.

Such an approach is clearly opposite to the “a priori” procedures described in the previous paragraphs, namely section analysis or fiber element analysis. Although an optimum analogy can be obtained when the similitude is done based on experimental tests on a section with same characteristics, significant unpredictable errors can be introduced when the characteristic parameters of the section are varied, in terms of geometry, reinforcement ratio, PT-mild steel ratio, location of the bars, steel or concrete mechanical properties etc.

It clearly appears that such an empirical procedure for the definition of the moment-curvature/rotation behavior of hybrid or, more generally, unbonded-type connections can not be suggested as a viable reliable approach.

## CHAPTER 3

### PROPOSED PROCEDURE FOR MOMENT-ROTATION ANALYSIS OF DUCTILE CONNECTIONS

#### 3.1. Motivations

Characteristics and limits of different approaches to define a moment-rotation behavior of precast beam column connections have been discussed in the previous chapter.

Simplified section analysis based on a trilinear idealization, fiber element analysis as well as an empirical procedure have been proposed. Discrete coherence with experimental test results can be obtained with different levels of complexity in the analyses, without nevertheless achieving the aim of providing a simple procedure based on a typical section analysis which can account for global conditions (member compatibility).

As previously discussed the main difficulty related to the behavior of unbonded tendons, which violate the strain compatibility between steel and concrete in the section, are due to the impossibility of defining the neutral axis position with a closed-form equation, since a stable value is not available. A trial and error procedure, able to satisfy both equilibrium and member compatibility, should therefore be utilized.

While the equilibrium equation can still be formulated at the critical section level, the deformation compatibility relationship must consider the global behavior of the connection, including beam and column elements as well as panel zones.

The following procedure is designed to be valid for any typology of connection characterized by “unbonding” concepts:

- Partially bonded or unbonded tendons/bars
- Unbonded length in mild steel
- Hybrid (combination of the above) connection

The general scheme will refer to a hybrid connection with presence of unbonded tendons (assumed to be at mid-height of the section) and mild steel unbonded for a short length in proximity to the beam-column interface. Simple modifications can easily adapt the general case to a particular one.

#### **4.1.Main Scheme of the Procedure**

In a first stage the gross trial and error procedure are presented, assuming simplified hypotheses on the stress-strain distribution of the concrete, in order to focus and become familiar with the global scheme.

Subsequently the member compatibility condition will be introduced, under the concept of “monolithic beam analogy”, and described.

##### **1. Fix the rotation $\theta$**

The effective rotation  $\theta_b$  developed at the beam-column interface due to the opening of the crack, can be related to the drift of the frame system with simple geometric considerations (Fig. 3.1):

$$\theta_b = \frac{\theta}{\left(1 - \frac{h_c}{l}\right)}$$

$h_c$ = column depth

$\theta$ = column rotation (average of the story drifts above and below that floor level)

$l$ = beam ideal length (from center to center of the joint)

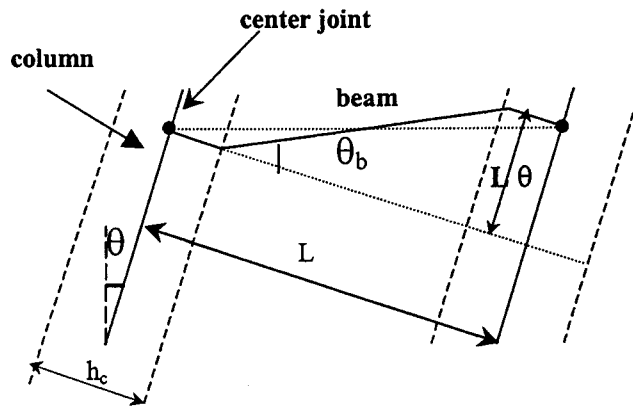


Figure 3.1 – Frame and beam rotations relationship

2. **Guess initial neutral axis depth c**

3. **Evaluation of strain in the post-tensioned tendons (unbonded)**

The increase in the strain in the post-tensioned tendons due to the beam deformation is taken into account and evaluated.

$$\varepsilon_{pt} = \frac{n \cdot \Delta_{pt}}{l_{ub}}$$

where:

- n = number of total openings along the beam (at beam-column interfaces)
- $\Delta_{pt}$  = total displacement (elastic + plastic) at the level of the post-tensioned tendon

$$\Delta_{pt} = \theta \cdot \left( \frac{h}{2} - c \right)$$

$h/2 - c$  is the relative position of the PT tendons (assumed to be at mid-height of the section)

$h$  = beam section height

$l_{ub}$  = unbonded length of the tendons

In the case, later discussed, of a two bay frame systems with tendons unbonded along the total length of the 2-bays beam, the average deformation should take into account all the effective analogous openings at the column-beam interface. A multiplied factor  $n=4$  of the total displacement  $\Delta_{pt}$ , in the evaluation of the strain  $\varepsilon_{pt}$  should thus be adopted.

#### 4. Determination of the strain in the mild steel and concrete

As previously discussed, a section strain compatibility in the section cannot be adopted in order to relate the strain in the mild steel and in the PT steel, which should be separately evaluated referring to the deformation of all the beam members (member compatibility). In this case the concentration of the rotation at the beam-column interface due to the opening of the crack (Fig. 3.2) simplifies the procedure.

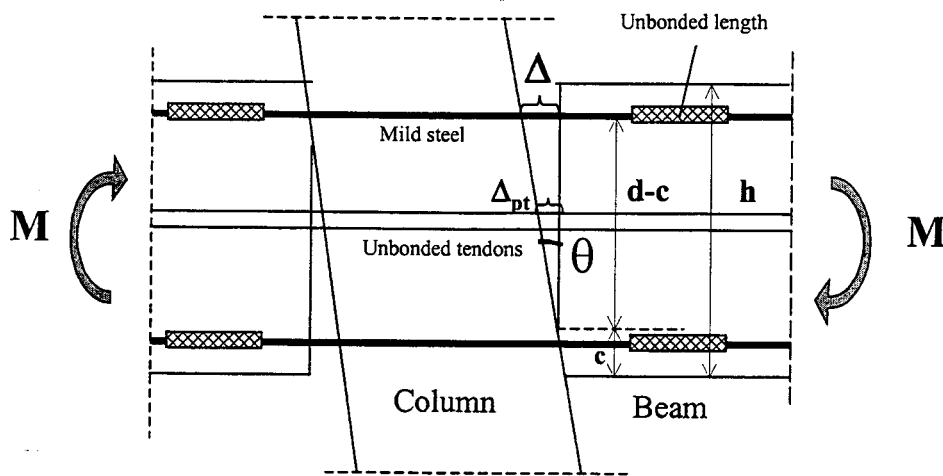


Figure 3.2 – Gap opening mechanism

The strain in the steel can be estimated as:

$$\varepsilon_s = \frac{(\Delta - 2\Delta_{sp})}{l_{ub}}$$

where:

- $\Delta$  = total displacement at the level of the mild steel, due to the opening of the crack
- $\Delta_{sp}$  = displacement due to strain penetration. It's assumed that in case of unbonded length in the mild steel, the strain penetration occurs on both sides of the unbonded region.
- $l_{ub}$  = unbonded length of the mild steel

The total and strain penetration displacement are evaluated as follows.

$$\Delta = \theta \cdot (d - c)$$

d= beam section depth

$$\Delta_{sp} = \frac{2}{3} l_{sp} \epsilon_e + l_{sp} \epsilon_p$$

$l_{sp}$ = length of strain penetration ( $0.15 f_y d_{bl}$ )

$\epsilon_{e,p}$ = elastic and plastic component of the steel deformation (Fig. 3.3)

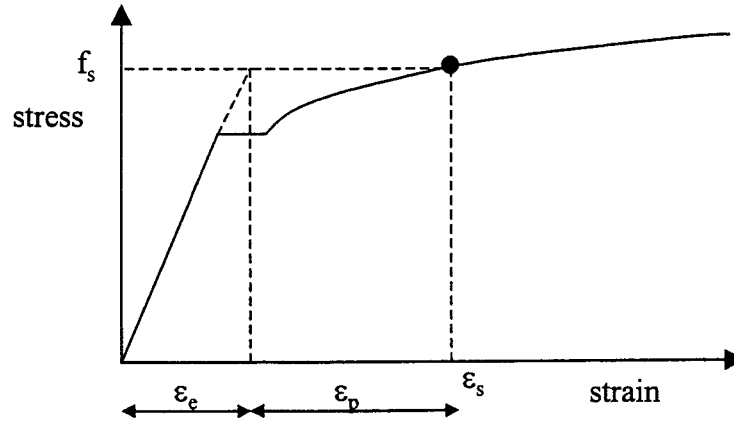


Figure 3.3 – Elastic and plastic steel strain components

substituting:

$$\epsilon_p = \epsilon_s - \epsilon_e$$

$$\epsilon_e = \alpha \cdot \epsilon_y$$

we obtain:

$$\epsilon_s = \frac{[\Delta - (4/3 l_{sp} \alpha \epsilon_y - 2 l_{sp} \alpha \epsilon_y)]}{(l_{ub} + 2 l_{sp})}$$

which can be simplified into:

$$\epsilon_s = \frac{(\Delta + 2/3 l_{sp} \alpha \epsilon_y)}{(l_{ub} + 2 l_{sp})}$$

Having evaluated the strain in the steel, it's necessary to determine the strain in the concrete with an accurate relationship that can no longer rely on classical linear distribution hypothesis.

Assuming a correct complete stress-strain relationship for the concrete, the problem consists in a system of two unknowns, namely the neutral axis depth  $c$  and the concrete strain  $\epsilon_c$ . Two equations should thus be introduced: section equilibrium and a sort of member compatibility.

In this first stage, triangular or rectangular stress-block assumptions can provide an acceptable approximation. No need of calculation of  $\epsilon_c$  would result, and the procedure is reduced to a trial and error iteration on the unique unknown  $c$ .

5. Section equilibrium: new value of neutral axis depth  $c'$

The compression resultant in the concrete is calculated from equilibrium consideration in the section:

$$C - T_s + C'_s = T_{pt}$$

where the post-tension compressive force, acting into the section ( $T_{pt}$ ) as an external force, is given by the sum of the initial post-tensioning and the increment due to the deformation of the beam:

$$T_{pt} = T_{in} + f(\epsilon_{pt})A_{pt},$$

and  $T_s$  and  $C'_s$  are the tension and compression forces in mild steel reinforcement, if present in the section.

The neutral axis depth  $c'$  is then derived from the compression resultant in the concrete  $C$  depending on the hypotheses on the stress-strain behavior of the concrete. A simplified approach can be to assume a linear distribution of the stress in the initial deformation range and a Whitney stress-block hypothesis for certain higher levels.

## 6. Iterative procedure until convergence

At each step (after the first one), the neutral axis depth *guessed*  $c$  is imposed to be equal to the value  $c'$  as estimated at the previous step, until convergence is reached.

Rigorously, the initial hypotheses on the relation between the elastic and plastic components in the PT steel strain  $\varepsilon_{pt}$ , based on the value of the constant  $\alpha$  ( $\varepsilon_e = \alpha \varepsilon_y$ ), should be cross-checked, and the value  $\alpha$  updated with the one calculated after the iteration on  $c$ . Therefore a second iteration should be developed with the new value of  $\alpha$ . Few “double” iterations (on  $c$  and  $\alpha$ ) should be performed to reach convergence on both the parameter  $c$  and  $\alpha$ .

It should anyway be underlined that the influence of the  $\alpha$ -iteration, becomes clearly important at small level of strains (thus at small level of rotation-drift). The larger the rotation, the more the deformation enters the plastic domain and the elastic component becomes negligible, as well as the influence of an incorrect estimation of its real value.

## 7. Evaluation of Moment Capacity and Tensile Force in the tendons

Last step, the moment resistance capacity of the section  $M$ , corresponding to the fixed rotation  $\theta$ , is evaluated with a rotational equilibrium around any convenient point of the section, as the middle height of the section (where the PT tendons are located).

### 3.2. Member Compatibility Condition: the “Monolithic Beam Analogy”

As previously mentioned, when a refined stress-strain relationship is adopted for the concrete behavior, instead of approximate stress block assumptions, we should solve a system of two unknowns (i.e. the neutral axis position  $c$  and the strain in the concrete  $\varepsilon_c$ ).

The proposed procedure to solve the problem of strain compatibility in presence of unbonding concepts introduces the necessary second equation, based on the whole beam member behavior.

The relationship between these local parameters is defined introducing an analogy, in terms of global behavior (displacement), between the precast connection and an equivalent monolithic one.

Assuming conventionally that the point of contraflexure, occurring in the beam due to lateral loads, is localized at mid-length, the end displacement of two different cantilever schemes are compared (Fig. 3.4). In the precast case, the opening of a gap at the beam-column interface will result in a rigid rotation  $\theta_{imp}$ . The contribution to the total beam-edge displacement due to such a rigid rotation can be simply derived:

$$\Delta_{imp} = \theta_{imp} L_{cant}$$

where:

$L_{cant}$  represents the distance from the interface and the point of contraflexure (length of the cantilever scheme).

Adding the contribution due to elastic deformation it will result:

$$\Delta_{tot(preicast)} = \Delta_{imp} + \Delta_{el}$$

In the general case of a monolithic cantilever the total displacement  $\Delta_{tot}$  would be given by the sum of an elastic and a plastic contribution, where the latter is provided by the rigid rotation around the plastic hinge centroid.

$$\Delta_{tot(monolithic)} = \Delta_p + \Delta_{el}$$

Assuming that the two beams are identical in terms of geometry and reinforcement, and imposing the same total displacement, we lead to equate the “plastic” contributions. In the precast case the inelastic deformation is localized at the interface, in the monolithic one is distributed along a plastic hinge (and approximately considered concentrated at its centroid).

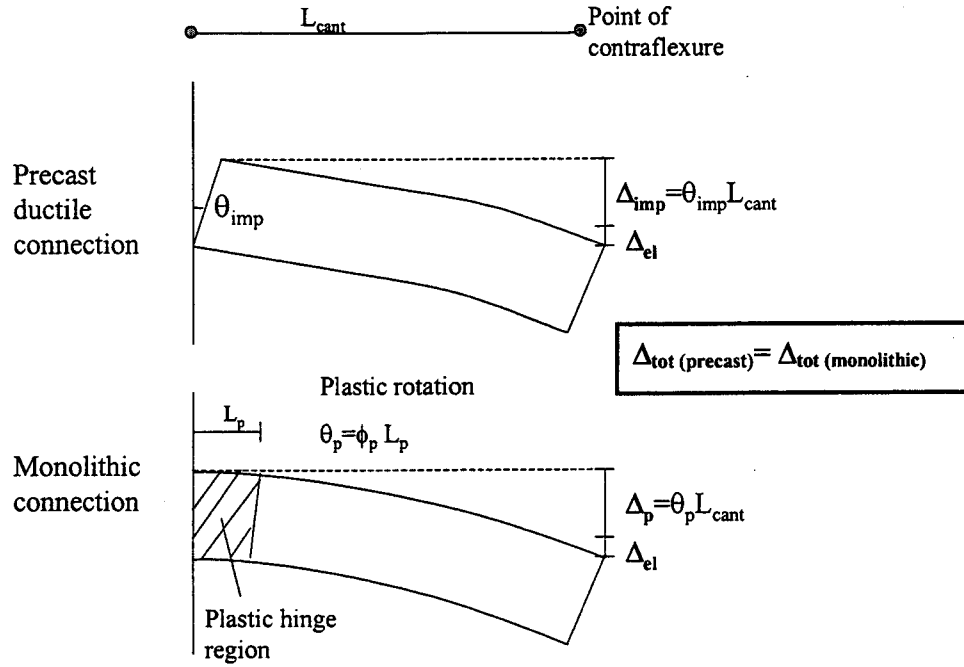


Figure 3.4 – Monolithic beam analogy

Hence:

$$\begin{aligned} \Delta_{tot(precast)} &= \Delta_{tot(monolithic)} \\ \Delta_{imp} + \Delta_{el} &= \Delta_p + \Delta_{el} \\ \Delta_{imp} &= \Delta_p \\ \Rightarrow \quad \theta_{imp} L_{cant} &= \Delta_p \end{aligned} \quad (a)$$

We can thus utilize in the monolithic case the ultimate and yielding curvature ( $\phi_u$  and  $\phi_y$ ) concepts:

$$\Delta_p = \theta_p \left( L_{cant} - \frac{L_p}{2} \right) = (\phi_u - \phi_y) L_p \left( L_{cant} - \frac{L_p}{2} \right) \quad (b)$$

where  $L_p$  is the plastic hinge length.

Combining equation (a) and (b) we obtain:

$$\theta_{imp} L_{cant} = (\phi_u - \phi_y) L_p \left( L_{cant} - \frac{L_p}{2} \right)$$

$$(\phi_u - \phi_y) = \frac{(\theta_{imp} L_{cant})}{\left(L_{cant} - \frac{L_p}{2}\right) L_p}$$

$$\phi_u = \frac{\varepsilon_c}{c} = \frac{(\theta_{imp} L_{cant})}{\left(L_{cant} - \frac{L_p}{2}\right) L_p} + \phi_y$$

$$\Rightarrow \varepsilon_c = \left[ \frac{(\theta_{imp} L_{cant})}{\left(L_{cant} - \frac{L_p}{2}\right) L_p} + \phi_y \right] \cdot c$$

$$\varepsilon_c = f(c)$$

The introduced additional condition on the global member displacement satisfies the member compatibility and results in a simple relationship between concrete strain and neutral axis position. For each guessed value of the neutral axis position, the member compatibility relationship provides a unique value of concrete strain, which should eventually respect section equilibrium considerations. If the local equilibrium is violated a different value of neutral axis depth  $c$  should be guessed, resulting in a trial and error procedure.

The whole procedure can thus be summarized as follows:

1. Impose a rotation  $\theta_{imp}$
2. Guess an initial neutral axis position  $c$
3. Member compatibility : calculate  $\varepsilon_c = f(c)$
4. Evaluate corresponding compressive force  $C = f(\varepsilon_c, c)$
5. Check Section Equilibrium:
  - If it's verified, evaluate moment  $M$  corresponding to the  $\theta_{imp}$
  - If not, guess new neutral axis  $c'$  and start back from point 2.

### 3.3. Alternative Approximate Procedure

In the case of hybrid connections the presence of mild steel suggests the possibility of a closed-form equation to directly evaluate the strain in the concrete from the strain in the mild steel. If the mild steel was completely bonded at the interface, a linear relationship could be adopted, since a section strain compatibility between mild steel and concrete strain would be valid. In fact, although the hypothesis of “plane sections remain plane” likely seems to be violated when considering the whole section depth, we have to consider that the mechanism of opening/closing of the gap at the interface differs significantly from the hypothesis of a continuum element at the base of the classical Bernoulli-Navier assumption. It should therefore be expected in such conditions that the bonded mild steel and the concrete at the extreme fiber of the section would exhibit linearly-related strains.

Under these considerations, the presence of mild steel can provide an auxiliary support, alternative to a “monolithic beam analogy”. It would appear natural to directly modify the formula to determine the ideal strain in the mild steel assuming an ideal case of unbonded length equal to zero:

$$\varepsilon_s = \frac{(\Delta + 2/3 l_{sp} \alpha \varepsilon_y)}{(l_{ub} + 2l_{sp})} \quad (c)$$

Assuming  $l_{ub}=0$   $\Rightarrow \varepsilon_s^* = \frac{(\Delta + 2/3 l_{sp} \alpha \varepsilon_y)}{2l_{sp}}$  (d)

In reality a zero value for  $l_{ub}$  can't be supported by the original formula introduced to determine the strain  $\varepsilon_s$

$$\varepsilon_s = \frac{(\Delta - \Delta_{sp})}{l_{ub}} \quad (e)$$

which after simplifications yields:

$$\varepsilon_s = \frac{(\Delta + 2/3 l_{sp} \alpha \varepsilon_y)}{(l_{ub} + 2l_{sp})}$$

The initial formula can thus be modified to:

$$\varepsilon_s = \frac{\Delta}{(l_{ub} + 2l_{sp})} \quad (f)$$

assuming  $l_{ub}=0 \quad \Rightarrow \quad \varepsilon_s^* = \frac{\Delta}{2l_{sp}}$

Let's note that the (f) differs from the (e) only by the term  $2/3 l_{sp} \alpha \varepsilon_y$  which for medium and high level of rotations is negligible when compared with the main term  $\Delta$ .

The concrete strain is then evaluated assuming a linear distribution of the strain in the section:

$$\varepsilon_c = \frac{\varepsilon_s^*}{(d - c)} \cdot c$$

$$\Rightarrow \quad \varepsilon_c = \frac{\theta_{imp}}{2l_{sp}} \cdot c$$

At the step where the equilibrium conditions on the section are verified, the real strain value  $\varepsilon_s$  is used, while  $\varepsilon_s^*$  is adopted solely for determining the concrete strain (compatibility condition).

Although this approximate procedure is not based on global displacement considerations, as in the case of the previously proposed "monolithic beam analogy", the results of an analytical-experimental comparison are still very satisfactory (as later shown in Figs. 3.10-3.11 ). In fact, the two expressions adopted in the different procedures for the concrete strain  $\varepsilon_c$  are similar:

### Monolithic Beam Analogy

$$\varepsilon_c = \left[ \frac{(\theta_{imp} L_{cant})}{\left( L_{cant} - \frac{L_p}{2} \right) L_p} + \phi_y \right] \cdot c$$

which, assuming  $L_{cant} \approx \left( L_{cant} - \frac{L_p}{2} \right)$ , can be simplify in

$$\varepsilon_c = \left( \frac{\theta_{imp}}{L_p} + \phi_y \right) \cdot c$$

#### Approximate procedure

$$\varepsilon_c = \left( \frac{\theta_{imp}}{2l_{sp}} \right) \cdot c$$

Furthermore for the case herein considered:

- ✓ the plastic hinge length, evaluated as  $0.08 L + l_{sp}$ , is approximately equal to  $2l_{sp}$
- ✓ the yield curvature  $\phi_y$  is, for medium-high level of drift, negligible in comparison to the term  $\theta_{imp}/L_p$

Such considerations can be carefully extended to any general hybrid connection with similar geometric and mechanical characteristic. From the noted similarities we can also derive that the “monolithic beam analogy” method seems to be able to represent the section behavior not only by explicitly assuming global behavior considerations (member strain compatibility) but also by implicitly following rational local considerations.

On the other hand in presence of mild steel (conceptual limit of validity for the approximate procedure) an analogous closed-form equation can be provided with alternative considerations to directly relate the strain in the concrete to the strain in the steel, simply neglecting the contribution due to the elastic deformation of the beam ( $\phi_y$ ). In reality even in this second approach we are still assuming a “monolithic beam analogy” with the condition  $\varepsilon_c = \mathbf{f}(\mathbf{c})$ .

The approximation results from a single simplification of:

$$\varepsilon_c = \phi_u \cdot c = (\phi_p + \phi_y) \cdot c \quad \text{monolithic beam analogy}$$

into

$$\varepsilon_c = \phi_p \cdot c \quad \text{simplified approach}$$

### 3.4. Preliminary Validation of the Procedure

In order to obtain a preliminary validation of the proposed analytical procedure, a comparison with experimental results, deriving from tests conducted at the National Institute of Standard and Technology (NIST) (mentioned in Chapter 2) on hybrid post-tensioned beam-to-column connections subjected to reverse cyclic loading, is performed. A brief summary of testing procedure and specimen details is given in the following paragraph: more detailed information can be found in Cheok et Stone (1994) and in Stanton et al. (1997).

Two different specimens, referred to as M-P-Z4 and O-P-Z4, are herein studied, comparing the moment rotation behavior of the interface sections. Since the test results are reported in terms of global force-tip-displacement of the whole specimen, in order to realize an analytical-experimental comparison, the different additional contributions to the deflection must be taken into account, namely panel-zone shear deformations and elastic element (beam and column) deflections.

Only the contribution due to the panel-zone is herein neglected, while the other ones are easily estimated, remembering that their contributions on the overall behavior are significantly reduced when the rotation is increased (approaching and then entering the inelastic behavior).

Since, as the tests showed, the post-tensioned steel did not yield before the failure occurred (generally due to fracture in the mild steel bars), such specimens should be considered as “over-reinforced” beam connections, with all the problems in the prediction of the behavior previously mentioned.

For any drift value, the proposed procedure is applied, and the moment rotation behavior curve evaluated.

The trilinear idealization, within its limit of applicability, was adopted to find out the decompression and the linear limit state point. While the decompression point can be computed for the hybrid connection similarly to the way suggested for the unbonded tendon connection, the calculation of the point corresponding to linear limit state can't be performed, as in the case of unbonded tendons, because a general underestimation of the rotation and, more consistent, of the moment resistance can be observed.

### **3.5.1. Specimen Description, Details and Test Procedure (NIST Phase IVb)**

Four different hybrid beam column connections (1/3 scale) were tested at NIST in the Phase IVb of the aforementioned experimental campaign on precast concrete ductile connections.

The main objective of this phase was to optimize the combination of mild steel and Post-Tensioned unbonded steel as well as examine the effects of the use of an alternative type of mild steel to improve the energy dissipation capabilities of the whole connection.

The limited number of specimens influenced the possibility of an extensive parametric investigation on the mild/PT steel ratio. Proportion of the mild steel and PT unbonded steel resulted in ratios between the mild steel moment contribution and the total moment resistance of 35% and 47%, corresponding to two and three #3 bars respectively located at the top and at the bottom of the beams and three 13 mm PT Grade 270 ( $f_{pu}=1862$  MPa) strands.

Similar moment contribution ratios were chosen for the remaining specimens, only substituting the Grade 60 mild steel with 304 stainless steel bars (same yielding resistance  $f_y=414$  MPa).

The higher total strain deformation capacity of the stainless steel (50%, as compared to 20% for the Grade 60 bars), was expected to postpone the failure of the specimen, due to fracture of mild steel as recorded in the previous Phase IVa, improving the energy dissipation potential at high drift levels. In order to limit the deformation in the PT steel and guarantee an elastic clamping force at higher drift levels, the PT steel was placed at the centroid of the section and partially unbonded (through the joint and for a distance on either side of column).

Figure 3.5 shows the ideal unbonded length of the test subassembly, as conceived from the prototype. The decision of measuring the load in the PT steel through a load cell localized at the end of the specimen, imposed an asymmetric distribution of the unbonded length (Fig. 3.6). The mild

steel was also debonded 25 mm on either side of the beam-column interface to postpone the fracture of the bars. The tendons were post-tensioned in order to guarantee, after the losses, an average stress of  $0.44 f_{pu}$ . Constant axial load of approximately  $0.4 f'_c A_g$  was applied to the column. Concentrated loads (20 kN) simulating gravity loads on the beam were applied to each beam at approximately 89 mm from the column face and maintained constant throughout the tests.

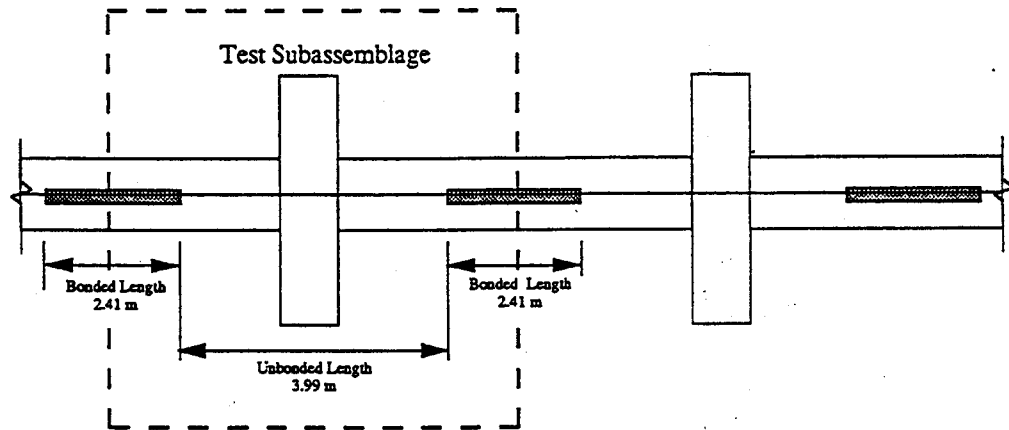


Figure 3.5 – Beam-column connection in the prototype building (from Cheok and Stone, 1994)

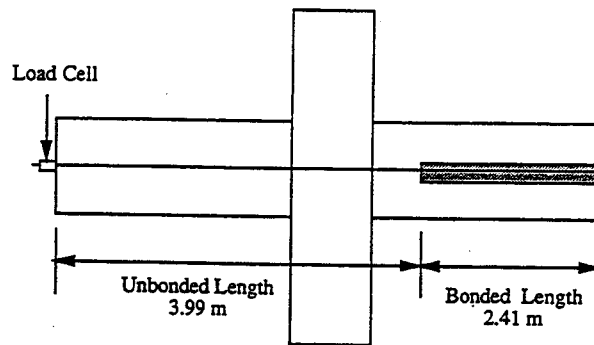


Figure 3.6 – Bonding of PT steel in Model Connections (from Cheok and Stone, 1994)

A scheme of the test set up, with dimension of the test specimens, reinforcement details and material properties are illustrated in the following Figures 3.7-3.8 and in Table 3.1.

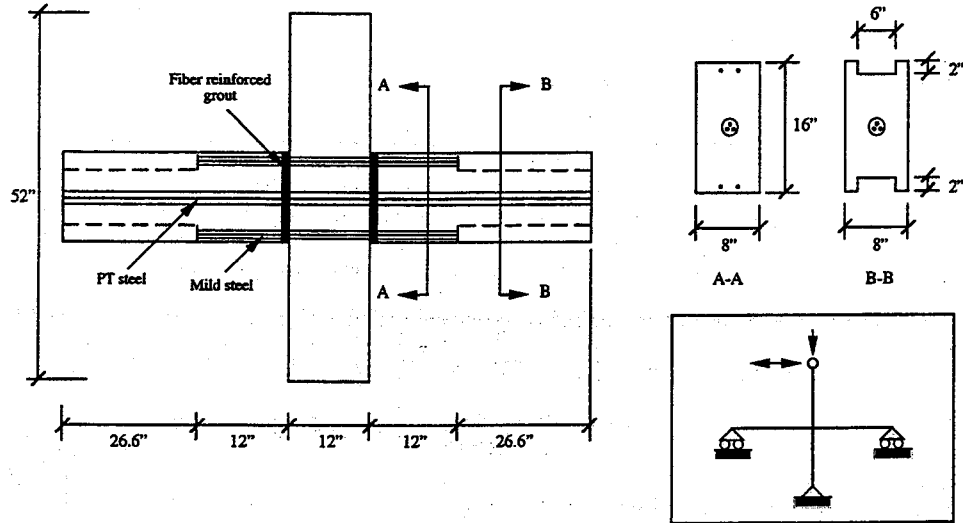


Figure 3.7 – Test set-up  
(from Cheek and Stone, 1994)

Table 3.1 - Reinforcement details of test specimens (Stanton et al., 1997)

Specimen	Bars	$f_{y,nom}$ (ksi)	$f_{y,exp}$ (ksi)	$f_{u,exp}$ (ksi)	Strand	$f_{p,e}$ (ksi)
M-P-Z4	2#3 Grade 60	60	61	98	3 - 1/2 in.	120
N-P-Z4	2 SS 304*	60	75	100	3 - 1/2 in.	120
O-P-Z4	2#3 Grade 60	60	61	98	3 - 1/2 in.	120
P-P-Z4	2 SS 304*	60	62	101	3 - 1/2 in.	120

Note: 1 in. = 2.54 mm; 1 ksi = 6.895 MPa

\*Stainless steel 304

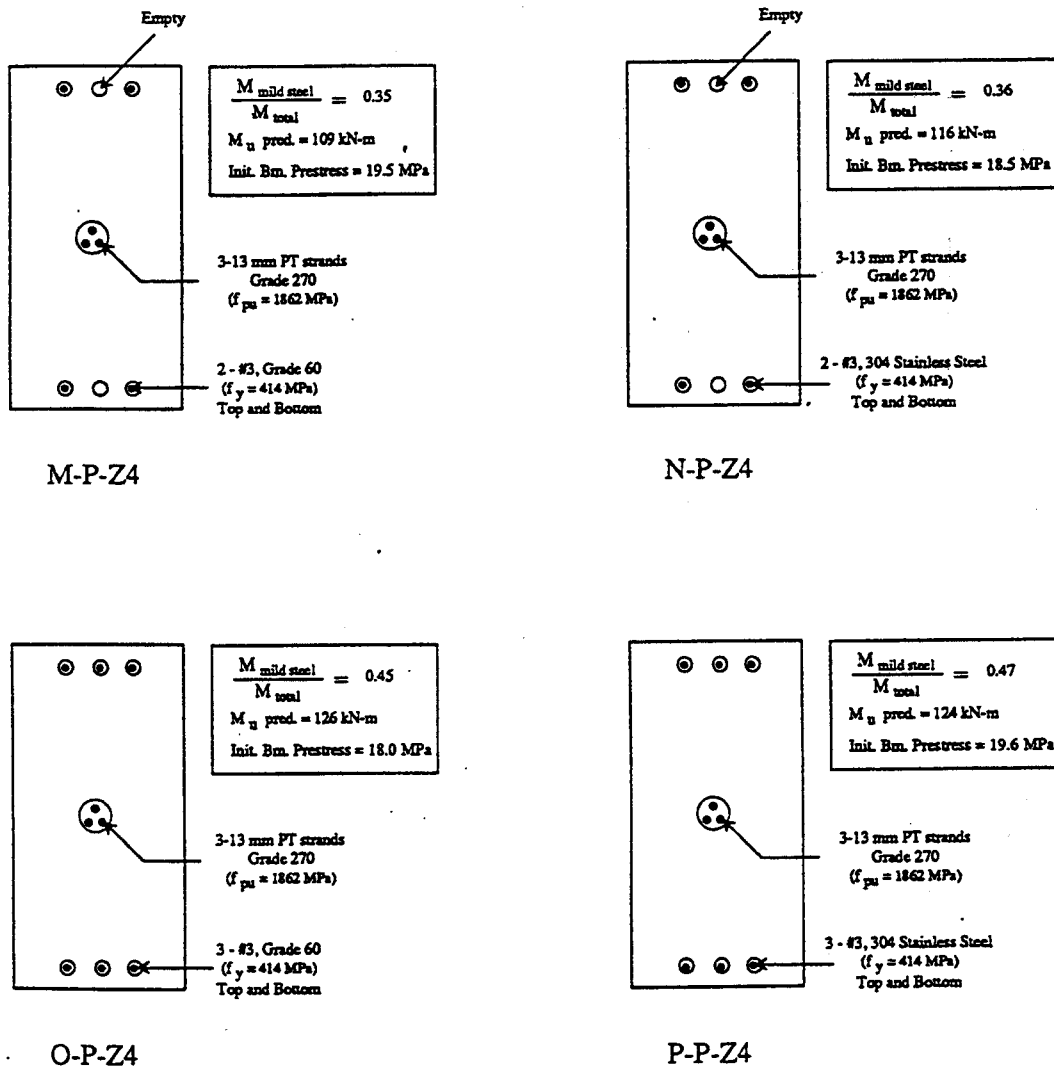


Figure 3.8 – Beam section reinforcement  
(from Cheek and Stone, 1994)

The displacement history shown in Figure 3.9, based on a story drift as recommended for use in the PRESSS Program was applied at the top of the column. At each level of drift three cycles were performed, followed by a cycle at 30% of the previous cycle peak displacement.

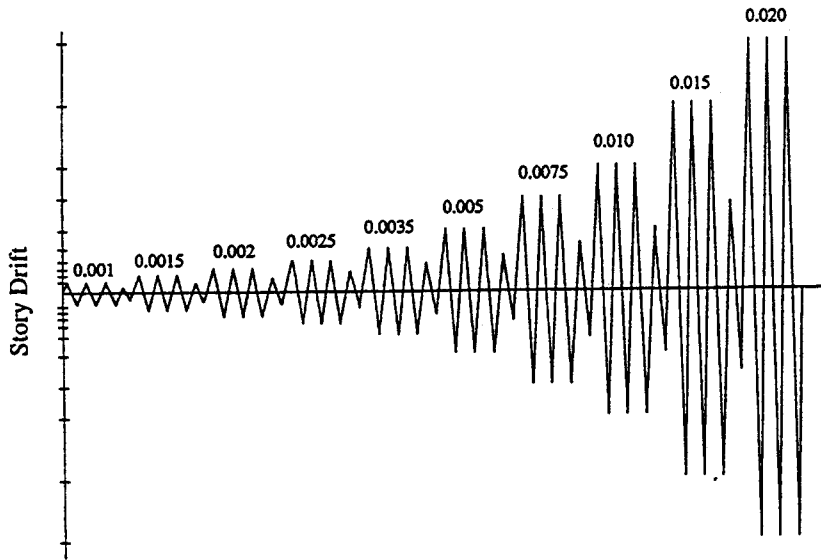


Figure 3.9 – Imposed Displacement History for NIST Phase IVb specimens  
(from Cheok and Stone, 1994)

### 3.5.2. Steel Behavior Modeling

The steel behavior characteristics are directly taken from the uniaxial tensile tests on the coupon of steel bars as adopted in the specimens (Cheok and Stone, 1994). The stress-strain relationship is obtained from the constitutive equations suggested by Dodd and Restrepo-Posada (1995):

$$f_s = E_s \varepsilon_s \text{ for } \varepsilon_s \leq \varepsilon_y$$

$$f_s = f_{su} + (f_y - f_u) \left( \frac{\varepsilon_{su} - \varepsilon_s}{\varepsilon_{su} - \varepsilon_{sh}} \right)^p \text{ for } \varepsilon_y < \varepsilon_s \leq \varepsilon_y$$

$$p = \frac{\log \left( \frac{f_{su} - f_x}{f_{su} - f_y} \right)}{\log \left( \frac{\varepsilon_{su} - \varepsilon_x}{\varepsilon_{su} - \varepsilon_{sh}} \right)}$$

where  $(\varepsilon_s, f_s)$  represents a generic stress-strain situation,  $(\varepsilon_y, f_y)$  corresponds to the yielding point,  $(\varepsilon_{sh}, f_y)$  defines the onset of the hardening,  $(\varepsilon_{su}, f_{su})$  defines the ultimate strength, and  $(\varepsilon_x, f_x)$  is a data point on the hardening behavior.

### 3.5.3. Concrete Behavior Modeling

The compression stress-strain relationship for concrete is defined according to the Mander model (Mander et al. 1988), which takes into account the confinement effects:

$$f_c = \frac{f'_{cc} x^r}{r-1+x^r}$$
$$f'_{cc} = f'_c \left( 2.254 \sqrt{1 + \frac{7.94 f'_l}{f'_c}} - \frac{2 f'_l}{f'_c} - 1.254 \right)$$
$$x = \frac{\varepsilon_c}{\varepsilon_{cc}}$$
$$\varepsilon_{cc} = 0.002 \left[ 1 + 5 \left( \frac{f'_{cc}}{f'_c} - 1 \right) \right]$$
$$r = \frac{E_c}{E_c - E_{sec}}$$
$$E_{sec} = \frac{f'_{cc}}{\varepsilon_{cc}}$$

where  $f'_{cc}$  and  $\varepsilon_{cc}$  are the concrete stress and strain at peak stress and  $f'_l$  is the effective lateral confining stress (in the case where  $f'_l = 0$ , the equation simplifies to the expression for unconfined concrete).

### 3.5.4. Experimental-Analytical Comparison

The Figures 3.10-3.11 report the experimental-analytical comparison in terms of moment-rotation behavior for the M-P-Z4 and O-P-Z4 specimens. The predicted monotonic curves, developed with the proposed procedure, represent an extremely satisfactory envelope of the cyclic experimental behavior, for both tests.

The slight difference in the initial elastic behavior of the O-P-Z4 specimen should be attributed to the approximations adopted in the calculation of the member deflection elastic contributions.

Furthermore, the presence of mild steel (unbonded for a small length at the beam-column interface) in addition to the unbonded tendons can justify the use of the alternative approximate procedure to directly define the concrete strain from the steel strain value (Par. 3.4), without

explicitly using any “monolithic beam analogy”. As previously mentioned, similar results are expected, since analogous formulas to evaluate the value of concrete strain are adopted in the two cases.

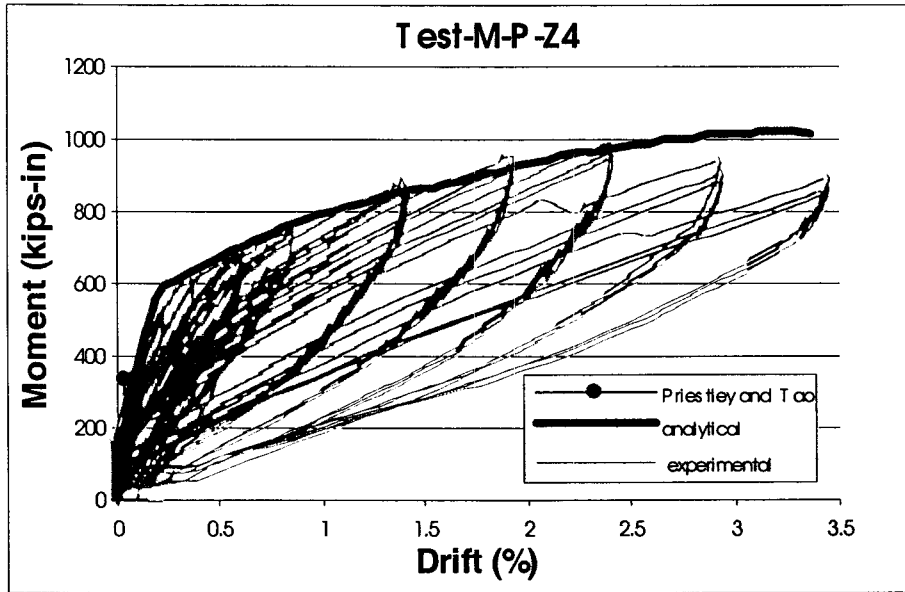


Figure 3.10 – Validation of the analytical procedure: NIST hybrid specimen M-P-Z4

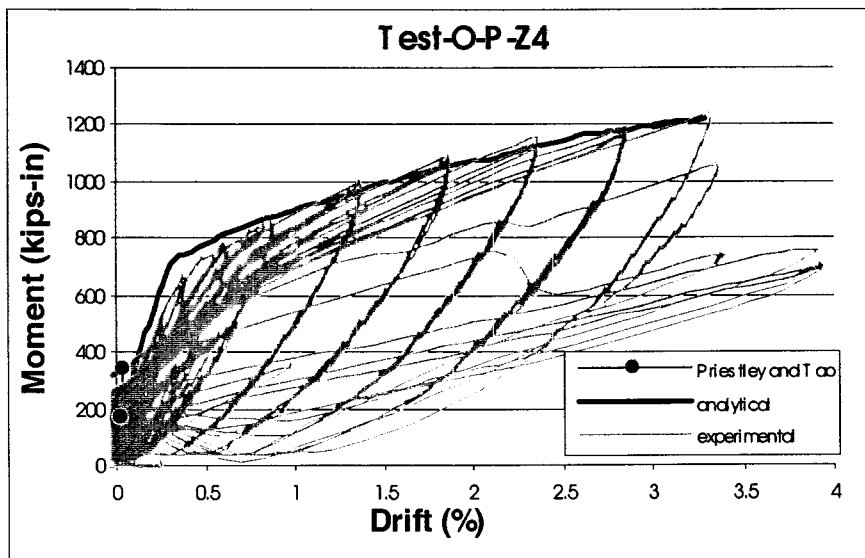


Figure 3.11 – Validation of the analytical procedure: NIST hybrid specimen O-P-Z4

When comparing the monotonic behavior of the connection M-P-Z4 computed using the two proposal procedures, it can be seen that the results are identical (Fig. 3.12).

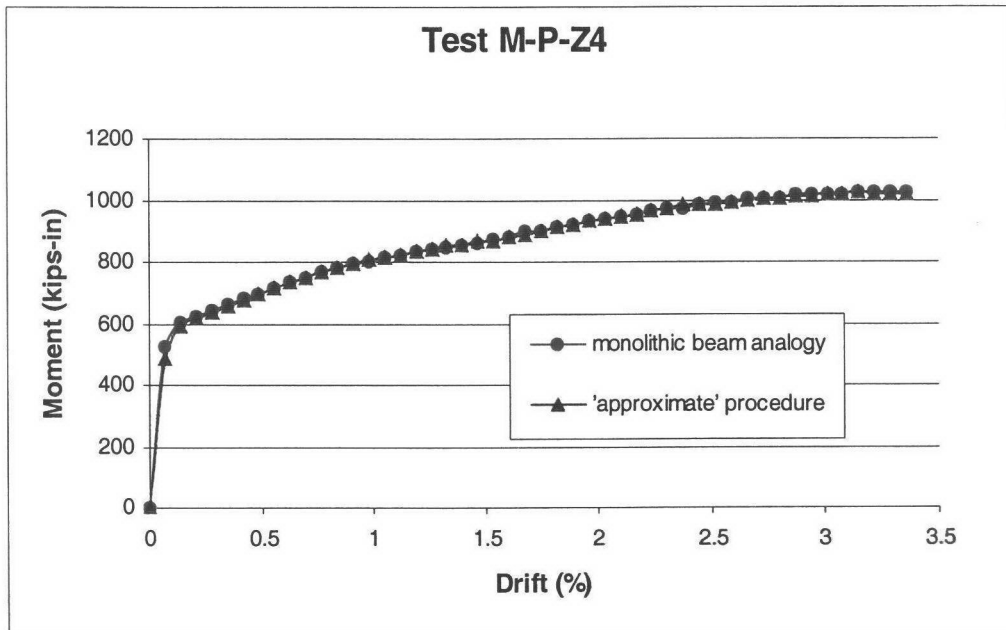


Figure 3.12 – “Monolithic beam analogy” and approximate procedures: cross-comparison

The comparison with the experimental results is shown in Figure 3.13: in this case the contribution of the member elastic deformation to the total displacement are not are taken into account, resulting in a obvious artificial overestimation of the initial stiffness.

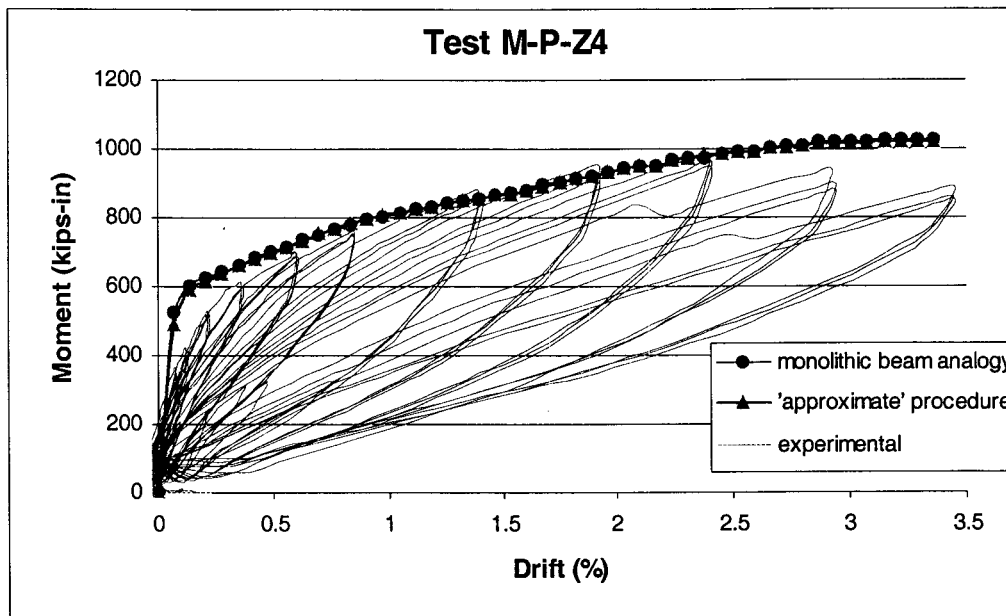


Figure 3.13 – “Monolithic beam analogy” and approximate procedures: comparison with test results.

### 3.6. Conclusions

Based on simple assumptions on the global member behavior, a rigorous section analysis procedure, as defined and commonly adopted for the analysis and design of ordinary (cast-in-place) reinforced concrete structures, has been introduced. Looking at the “member compatibility” condition as nothing more than an external constraint condition, the whole procedure can be simply implemented as in the case of a traditional moment-curvature section analysis for RC concrete.

The peculiarity of the mechanism governing the behavior of a precast connection at the interface reduces the trial and error iterations to satisfy equilibrium, when compared with a traditional reinforced concrete section. In fact, the initial estimation of the neutral axis position can be, in most of the cases, easily realized, as discussed in the following chapter.

The procedure above proposed has then been satisfactory validated with test results on hybrid-connection beam-column subassemblies. As anticipated in the first paragraph, the generality of the method allows to adapt it to numerous particular cases in which the concept of “unbonding” is utilized.

Subsequently, the four different connections used in the PRESSS (Phase III) five-story precast concrete building have been studied and modeled according to this procedure in order to realize a reliable analytical model to predict the simulated seismic response of the building in the frame direction.

In the following Chapters 4 and 5 an overview of the test program, including design concepts, structural features, test procedures as well as main assumptions for the analytical modeling of the two frame systems is presented. In conclusion, a preliminary experimental-analytical comparison of the overall response of the building is given.

## CHAPTER 4

### ANALYTICAL MODELING OF FRAME SYSTEMS:

#### 4.1. The PRESSS Test-Building

At the conclusion of the PRESSS (PRecast Seismic Structural Systems) coordinated research program a large scale five-story precast concrete building, composed of a super-assemblage of different solutions investigated in the previous phases, was tested at the University of California, San Diego –UCSD (Priestley et al. 1999).

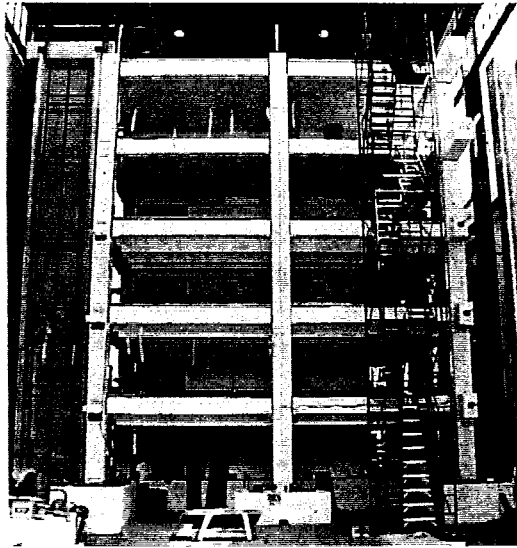


Figure 4.1 – The Test Building: elevation view

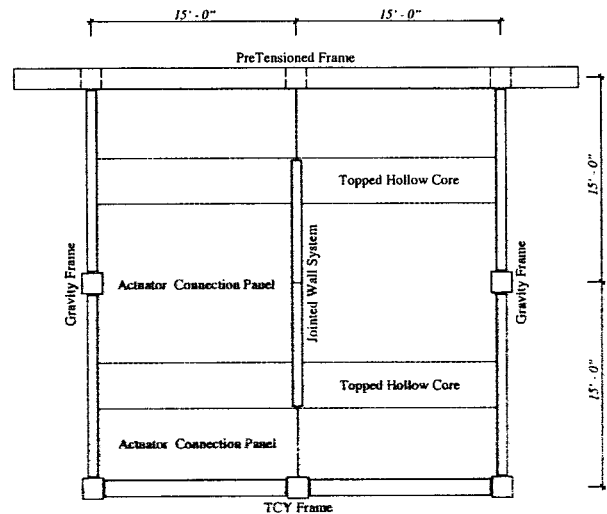


Figure 4.2 – Plan view

The prototype building is a five-story precast office building, 100 x 200 ft (30.5 x 61m) in plans, with 12 ft 6 in. (3.81 m) story height and 25 ft (7.62 m) bay length, with seismic resisting frames in the longitudinal direction and shear wall in the transverse one. The dimensions of the test building (Figs. 4.1-4.2), which represent a 60% scale of the prototype, were decided according to the size of the Charles Lee Powell Structural Laboratory at UCSD, and thus limited to 30 x 30 ft (9.14 x 9.14 m) in plan and two-bay by two-bays (15 ft-4.57m long) configuration.

The seismic resistance of the test building is provided by two seismic resisting frames (Figs. 4.3-4.4), which include four different beam-column connections, in one direction and a shear wall system in the other.

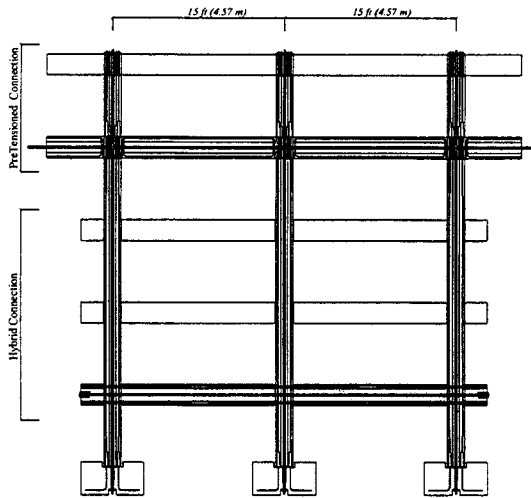


Figure 4.3 – Prestressed Frame – elevation

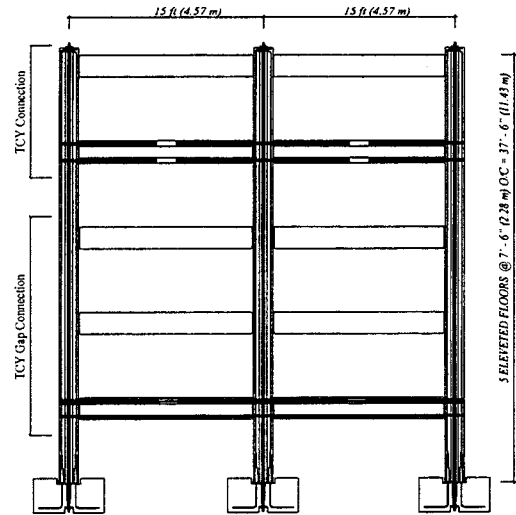


Figure 4.4– TCY Frame - elevation

The wall consists of unbonded post-tensioned panels connected with special u-shape shear energy dissipation devices: the panels are designed to rock on the foundations, while the dissipators, located in vertical joints, are activated by the relative displacements of two adjacent panels (Figs 4.5-4.6).

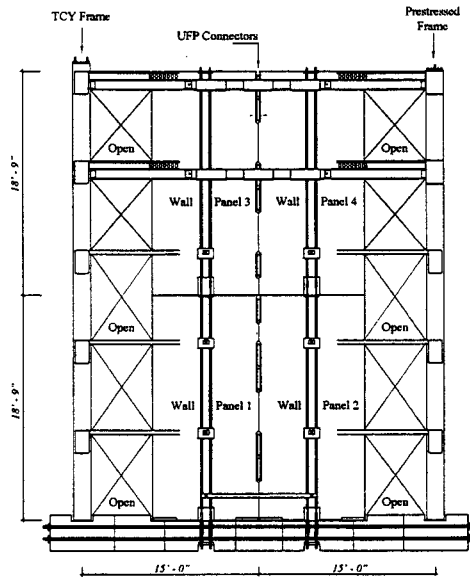


Figure 4.5 – Wall System- elevation

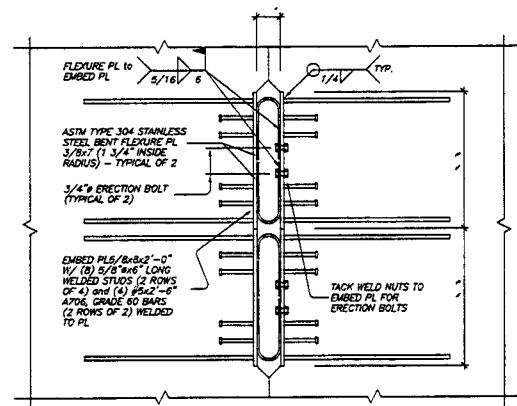


Figure 4.6 – Dissipating device

Two different floor systems were included in the building: pretopped double tees for the first three floors and hollow-core panels with in-situ topping at the upper floors.

The work presented herein focuses only on the frame direction. In a companion report the analytical modeling of the wall direction is discussed (Conley et al. 1999). Design details of both the wall system and frame connections can be found in (Stanton et al. 2000).

#### 4.2. The Frame Systems

The co-existence of different types of connections in the same frame system on different floors of the same building, is unusual in common design practice and complicates analytical-experimental comparison of the performance of each connection.

In order to provide designers with a synoptic view of the seismic behavior of several alternatives, for the development of a flexible and versatile design procedure of precast concrete buildings in seismic zones, four different types of “dry” ductile connection systems were adopted in the two frames of the PRESS III test building:

- Hybrid
- Pretensioned
- TCY
- TCY-Gap

A preliminary difference is found in the construction methodology: while the pretensioned connection uses multibay beams and single-story columns, appropriate for floor by floor construction, all the other connections consist of multistory columns and single-bay beams, more appropriate “up and out” construction.

Each frame is characterized by the presence of two different kinds of connections, distributed along the elevation according to the scheme shown in Table 4.1.

Table 4.1 – Distribution of the different type of connections in the test-building

Floor	PRESTRESSED FRAME	NON PRESTRESSED (TCY) FRAME
1,2,3	Hybrid	TCY Gap
4,5	Pretensioned	TCY

## Pretensioned connection

Unbonded tendons, partially bonded only with respect to the column joint, are located in a multi-bay continuous pretensioned beam (Fig. 4.7). The longitudinal reinforcement of the single-story column segment passed through sleeves located in the joint. A hysteretic behavior, essentially non-linear elastic, with self-centering property, characterizes this connection. On the other hand, very limited energy dissipation capability can be provided.

## TCY connection

Only mild steel is present in this connection (Fig. 4.7), which is expected to behave similarly to a monolithic case, according to the “emulation of cast in place concrete”.

Yielding in tension and compression guarantees good energy dissipation, but low self-centering capability. A short unbonded length is used in the sleeves in the proximity of the interface, to avoid high level of strain (damage) in the steel.

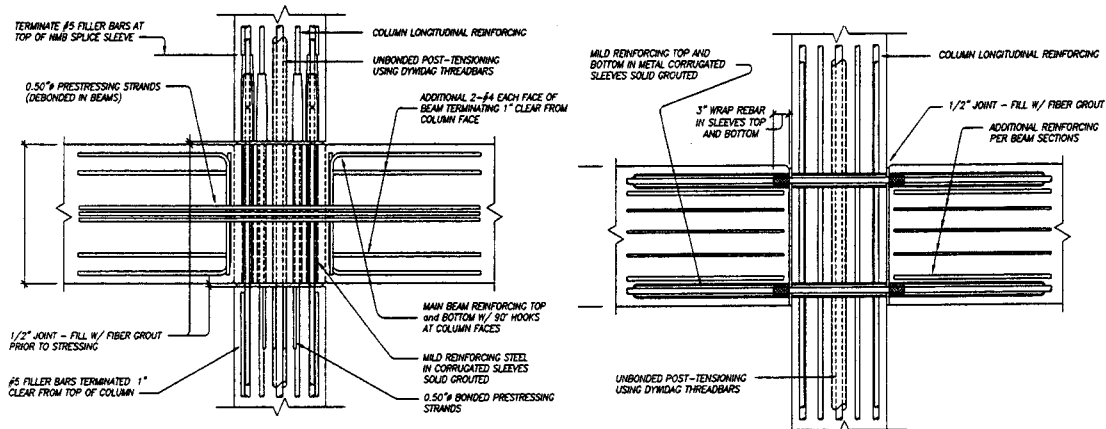


Figure 4.7 - Prestressed and TCY connections (Sritharan et al. 2000)

## Hybrid Connection

Conceptually developed as a compromise between the Non Linear Elastic (NLE) and the TCY (Tension Compression Yielding) systems, this connection is characterized by the simultaneous presence of unbonded tendons and mild steel (Fig. 4.8). An elastic clamping force, with self-centering properties, is provided by the tendons located in ungrouted PVC sleeves, designed to remain in the elastic range. Energy dissipation is provided by the mild steel, unbonded for a short length only in proximity to the beam-column interface.

## TCY-Gap Connection

Based on the TCY system concepts, this connection is substantially different from all others presented herein. A net gap (Fig. 4.8) at the beam-column interface is used to reduce the level of damage in the precast elements due to the elongation of the beam during seismic action and the bumping, with crushing of the concrete, of the beam against the column. Post-tensioned tendons provide compressive action through a fiber grout pad in the bottom side, guaranteeing shear resistance by means of Coulomb friction and acting as a pivot point for the section rotation (no clamping force is thus provided). Top mild steel (partially bonded at the interface) provides flexural strength and energy dissipation.

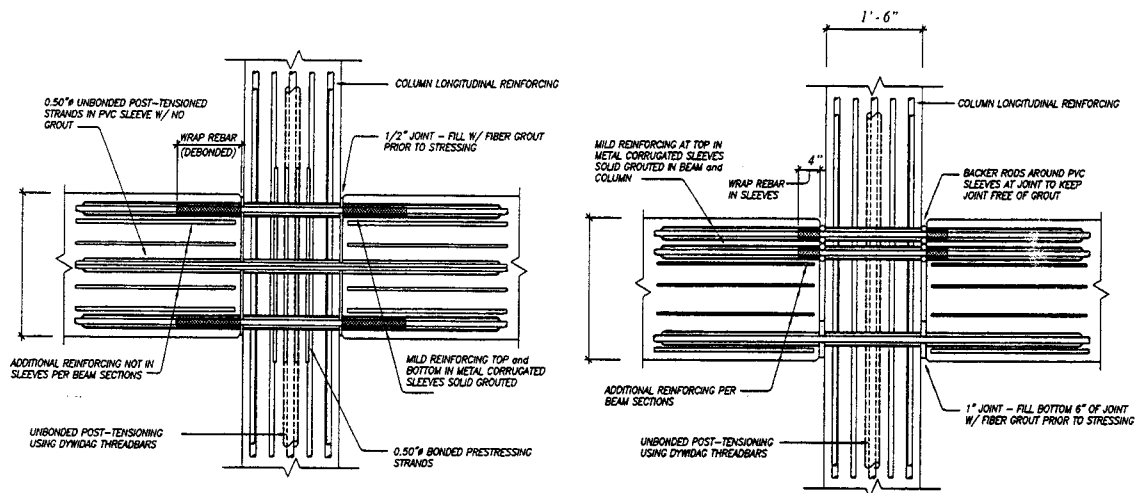


Figure 4.8 – Hybrid and TCY-Gap connections (Sritharan et al. 2000)

### 4.3. Design Philosophy

Limitations and drawbacks of the commonly accepted Force-Based Design approach have been demonstrated (Priestley, 1998) and seem to be emphasized in the case of precast concrete structures with ductile connections which rely on the unique properties of a precast system.

The approach places particular importance on elastic stiffness of the structure and its elements, whose evaluation is often delicate and critical. Erroneous assumptions derive from considering the initial stiffness as a section property, independent of the strength, while the yielding curvature seems to be a more representative section property. In a precast system, additional complications are introduced due to the different (when compared to equivalent monolithic systems), conceptual role of the initial stiffness, which is related to a precompressed stage, and of the post-elastic behavior.

On the other hand the hysteretic characteristics of ductile precast connections do not follow the elasto-plastic scheme commonly adopted in the evaluation of the reduction factor R (or behavior factor q) for ordinary reinforced concrete frames. Due to the lack of detailed experimental evidences, code provisions commonly suggest reduction factors analogous to, when not smaller than, those prescribed for equivalent cast-in-place reinforced concrete systems.

The real structural efficiency of these precast connections is thus overlooked, resulting in excessively conservative design.

Therefore the prototype building was designed according to a direct displacement based design approach (DBD) (Priestley, 1998) to sustain a maximum drift of 2% under a design level earthquake compatible with the UBC +1997 Zone 4 and intermediate soil type  $S_e$  (UBC, 1997). The drift limit of 2% was chosen to correspond to typical code limits to control non-structural damage, and on the basis of satisfactory performance of beam column sub-assemblages tested in Phase II of the PRESSS program which were required to exhibit stable response at deformations 50% above the design drift limit (i.e. 3% drift).

Since displacement spectra are not provided by the UBC provisions, the spectra suggested in the Appendix G of the SEAOC Bluebook (PBSE-SEAOC, 1998) were adopted.

As a result of applying a displacement based design procedure, instead of a traditional force-based design approach, less conservative design base shears were obtained (Nakaki et al., 1999), which would result in significant cost savings.

#### **4.3.1. DBD Procedure**

Starting from a design drift of 2% and having assumed an equivalent viscous damping of  $\xi=20\%$  the displacement based design procedure illustrated in Figure 4.9 was adopted.

Table 4.2 shows design values in terms of target displacement at the effective height, defined according to the "substitute structure method" (Shibata and Sozen, 1976), and base shear.

Building base shear as well as frame base shear are also shown

Table 4.2 – Design parameters according to the DBD procedure

	PROTOTYPE	TEST BUILDING
Design drift $\theta_d$	0.02	0.02
Target Displ. $\Delta_d$	0.264 m ( 10.39 in.)	0.158 m (6.23 in.)
<b>Building Base Shear</b>	<b>6598 kN (1484.5 kips)</b>	<b>1187 kN (267.2 kips)</b>
<b>Frame Base Shear</b>	<b>3299 kN ( 742.2 kips )</b>	<b>593.8 kN (133.5 kips )</b>

A design evaluation of the frame model was performed independent of the official design of the PRESSS Program (conducted at the University of Washington (Seattle)) in order to compare ideal design internal forces (demand) and actual strength predicted with the analytical non-linear model at the design drift level (capacity). The results presented below are those from the independent UCSD design evaluation.

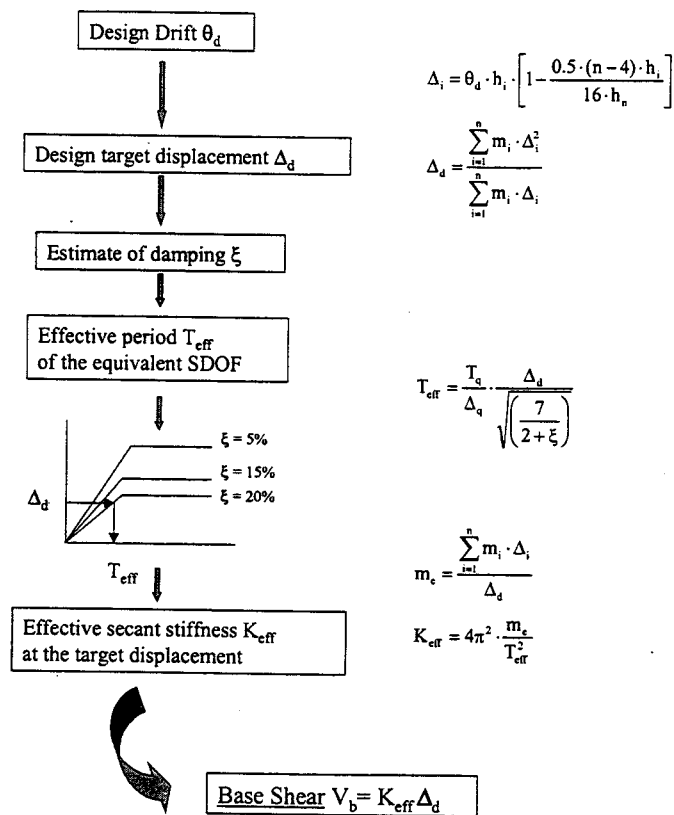


Figure 4.9 – DBD procedure adopted

The base shear calculated according to the DBD procedure is distributed along the elevation (Tab. 4.3) in proportion to the vertical mass and displacement profiles:

$$F_i = V_b \cdot \frac{m_i \cdot \Delta_i}{\sum_{i=1}^n m_i \cdot \Delta_i}$$

Table 4.3 - Lateral force distribution from DBD design

	DBD lateral force distribution			
	Prototype		Test Building	
	(kips)	(kN)	(kips)	(kN)
Floor 5	249.6	1110.0	44.9	199.8
Floor 4	199.6	887.8	35.9	159.8
Floor 3	149.0	662.8	26.8	119.3
Floor 2	97.8	434.8	17.6	78.3
Floor 1	45.8	203.8	8.2	36.7
	Frame Base Shear $V_b$			
	<b>742.2</b>	<b>3299.0</b>	<b>133.5</b>	<b>593.8</b>

The verification of the internal forces under the designed lateral loads, was conducted through an elastic static analysis with lateral loads assuming the actual dimensions (as designed) of the beam and column elements (Fig. 4.10).

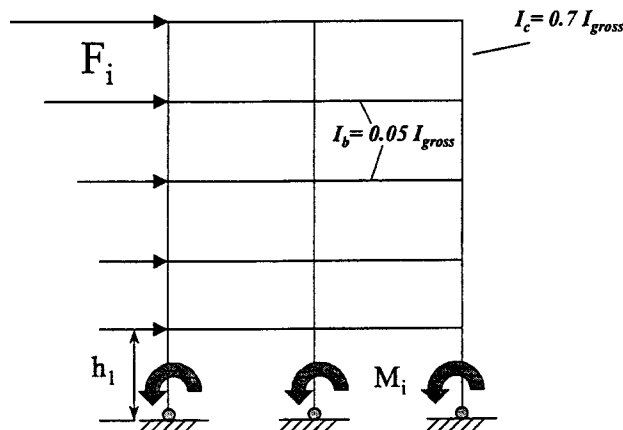


Figure 4.10 – Model for the static elastic analysis

Effective stiffness representative of conditions at maximum displacement response were adopted (Priestley, 1998), according to the substitute structure approach (Shibata and Sozen, 1976). The column stiffness  $I_c$  was assumed to be 70% of the uncracked value  $I_{gross}$ , while in the case of the beams the effective stiffness took into account the significant softening of the behavior of the connections after yielding. The beam stiffness  $I_b$  was thus taken as 5% of  $I_{gross}$ .

It has been shown (Loeding et al., 1998) that member forces are not particularly sensitive to the level of stiffness assumed, and this was confirmed in the analyses realized herein.

In order to model the plastic hinges formation at the design level state, hinges are placed at the base level of the elastic model with initial imposed moment  $M_{bi}$ , representing the flexural capacity of the base-column section. Assuming a point of contraflexure at 60% of the first floor height, the moment at the base can be found from lateral equilibrium of the frame as:

$$\sum_{i=1}^n M_{bi} = V_b \cdot (0.6h_1)$$

where  $V_b$  is the resultant of the imposed lateral forces (base shear).

A realistic distribution of the moments within the column base-sections, can be obtained calculating the moment capacity of each column based on the axial load levels resulting from the first static analysis with equal applied base moments (Tab. 4.4).

The static analysis at the next step provides reliable values of the design internal forces (Tab.4.5). Comparison between elastic design forces and analytical estimates of the actual capacity at the design drift level are shown later.

Table 4.4– Imposed column base moments

<b>COLUMNS</b>	<b>External-1</b>		<b>Internal</b>		<b>External-2</b>	
<b>Base Moment</b>	(kip-in)	(kNm)	(kip-in)	(kNm)	(kip-in)	(kNm)
<b>STEP 1</b>	2101.9	237.5	2101.9	237.5	2101.9	237.5
<b>STEP 2</b>	1538.1	173.8	2193.0	247.8	2754.1	311.2

Table 4.5 – Internal design forces: beam and column moments

	<b>Beam moments</b>							
	<b>External columns faces</b>				<b>Internal column faces</b>			
	<b>M+</b>		<b>M-</b>		<b>M+</b>		<b>M-</b>	
	(kip-in)	(kNm)	(kip-in)	(kNm)	(kip-in)	(kNm)	(kip-in)	(kNm)
<b>Floor 5</b>	1098.2	124.1	1090.3	123.2	1061.1	119.9	1069.0	120.8
<b>Floor 4</b>	1386.4	156.7	1380.8	156.0	1371.1	154.9	1375.8	155.5
<b>Floor 3</b>	1724.6	194.9	1722.2	194.6	1702.7	192.4	1705.1	192.7
<b>Floor 2</b>	1976.3	223.3	1971.5	222.8	1952.9	220.7	1956.0	221.0
<b>Floor 1</b>	2033.9	229.8	2051.9	231.9	2018.2	228.1	2010.0	227.1

	<b>Column moments</b>					
	<b>External1</b>		<b>Internal</b>		<b>External</b>	
	(kip-in)	(kNm)	(kip-in)	(kNm)	(kip-in)	(kNm)
<b>5top</b>	1130.1	127.7	2029.3	229.3	1122.8	126.9
<b>Floor 5</b>	-614.2	-69.4	-44.2	-5.0	-616.2	-69.6
<b>4top</b>	1819.7	205.6	2314.7	261.6	1820.0	205.7
<b>Floor 4</b>	-397.3	-44.9	260.6	29.5	-404.9	-45.7
<b>3top</b>	1744.8	197.2	2500.6	282.6	1745.6	197.2
<b>Floor 3</b>	139.4	15.8	904.9	102.3	175.6	19.8
<b>2top</b>	1337.7	151.2	2166.5	244.8	1327.7	150.0
<b>Floor 2</b>	959.0	108.4	1855.0	209.6	743.6	84.0
<b>1top</b>	548.5	62.0	1330.3	150.3	603.4	68.2
<b>Floor 1</b>	1538.1	173.8	2193.0	247.8	2761.2	312.0

#### 4.4. Modeling of the Monotonic Behavior

For each connection a complete monotonic moment-rotation behavior was derived according to the analytical procedure (based on the “monolithic beam analogy”) presented in the previous chapter.

In the case of Hybrid, TCY and Pretensioned connections the main general procedure can be adopted with simple modifications to take into account the peculiarities of each system (i.e. presence or absence of unbonded tendons, unbonded length in the mild steel).

On the other hand, the singularity of the TCY-Gap connections suggested to investigate its behavior by an independent analytical procedure.

Experimental tests on beam-column subassemblies with Gap-type connections were performed at the University of Texas at Austin (Saqa, 1995) and at University of Minnesota (Palmieri, 1996).

In the first case the specimen UT-GAP (Fig 4.11-4.12) incorporated tapered threaded couplers in the column to mate with mild reinforcement in the cast-in -place topping of the beam. High strength vertical rods anchored in a corbel provided the bottom horizontal connection and resistance to beam-end uplift.

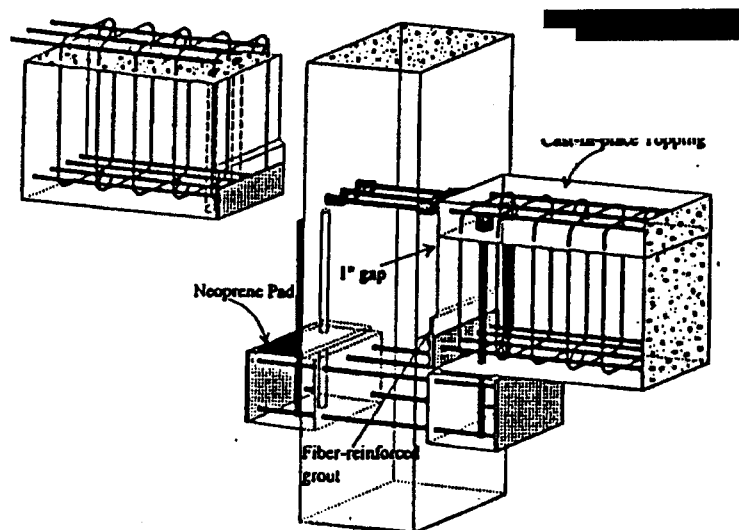


Figure 4.11 – UT-Gap specimen (from Palmieri et al., 1994)

Fiber reinforced grout was placed in the bottom of the gap at the beam column interface to transfer the compression force. When compared to the test-building TCY-Gap connection, significant differences in design details are incorporated in this specimen.

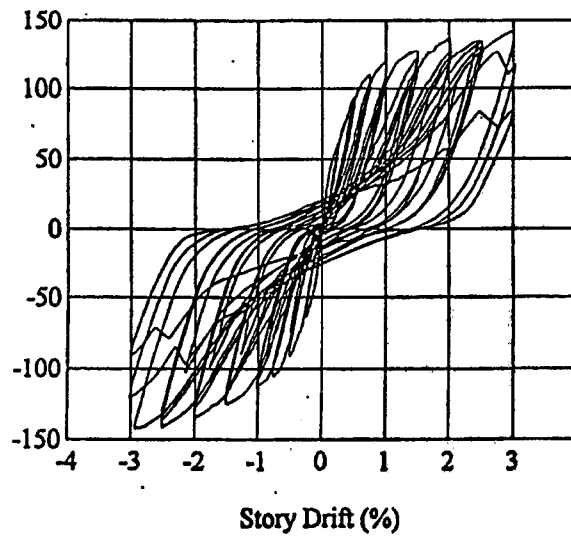


Figure 4.12 – UT-Gap hysteretic behavior (from Palmieri et al., 1994)

On the other hand, the specimen UMn-GAP tested at the University of Minnesota provides adequate analogies to the PRESSSS building connection typology. The only difference is the presence in the UMn-Gap specimen of spiral transverse reinforcement in the post-tensioned region (Fig. 4.13) to increase, through adequate confinement, the concrete strength and deformability.

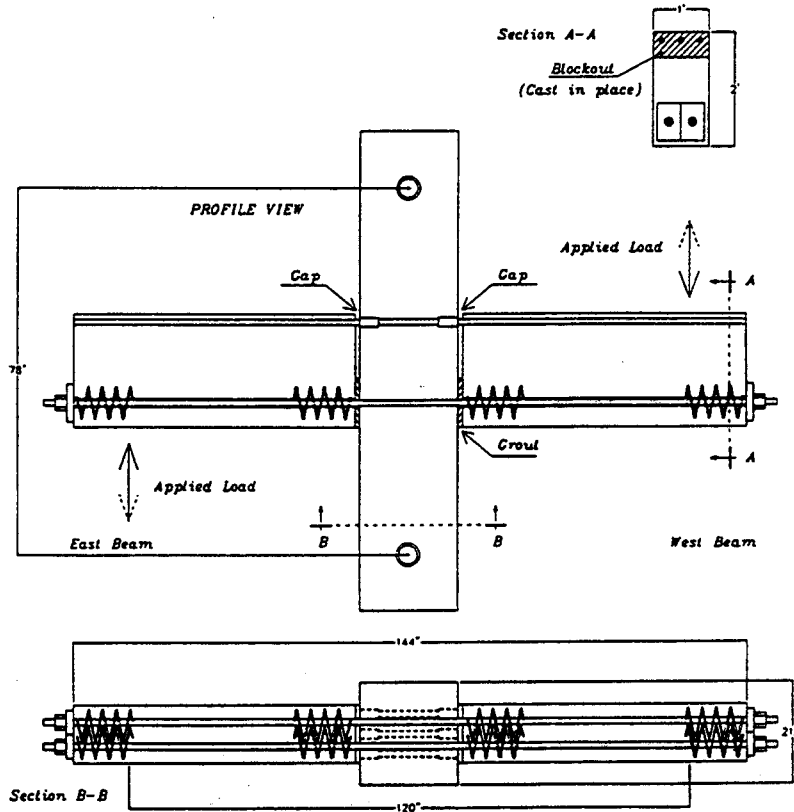


Figure 4.13 – UMn-Gap specimen: dimensions and connection details (from Palmieri, 1996)

#### 4.4.1. The TCY-Gap Connection Physical Model

When the gap opens the top mild steel bars are subjected to a tensile force ( $T_s$ ). The compression force in the concrete grout pad must therefore equilibrate both the tension  $T_s$  and the “external” compression force due to the post-tensioned unbonded tendons:

$$C = T_s + T_{pt}$$

The neutral axis position is limited by the size of the grout pad and the maximum value of the compression zone corresponds to the depth of the grout itself.

A simple approach, generally adopted at the design level, was to assume the unbonded tendons as pivot point of the section rotation. This implies fixing the neutral axis (n.a.) at the level of the tendons, which can not be correct for both the opening and closing phases.

Theoretical moment-rotation curves of the single beam-column interface derived for the test conducted at the University of Minnesota showed stiffer and stronger behavior when the gap opens than when the gap closes (Fig. 4.14), which would not be noticeable in the global lateral force- top displacement behavior.

Due to the test-setup, positive loading means opening on the gap on the west side and closing of the gap on the east side.

Such an asymmetry in the section behavior can be attributed to the neutral axis position. When the gap opens it is reasonable to assume a pivot point at the centroid of the tendons: an iterative trial and error procedure, similar to the one proposed, with an initial guess of the neutral axis depth and a cross-check of the equilibrium of the section, would show a fluctuation around that position. When the gap closes, the rotation occurs around the top region of the grout, so that the n.a. depth can be assumed to be at the grout-end level. This can justify the difference in stiffness: in the opening case (n.a. at level of the tendons), we would have, for the same rotation, a higher width  $\Delta$  which implies higher strains in the top steel  $\epsilon_s$  and thus a stiffer behavior.

On the other hand the compression force in the concrete during this same phase (absent or negligible when the gap closes) would contribute to the moment capacity of the section, resulting in an increase of the strength for the same assumed rotation.

Such considerations were included in the physical model of the TCY-Gap, resulting in satisfactory analytical results when compared to the experimental tests (Fig. 4.15).

The basic general iterative procedure, as described in the previous chapter, can, in this case, be simplified, assuming a fixed neutral axis depth and iterating over the concrete strains to verify the equilibrium. The first point of the moment-rotation behavior is again evaluated as the decompression point.

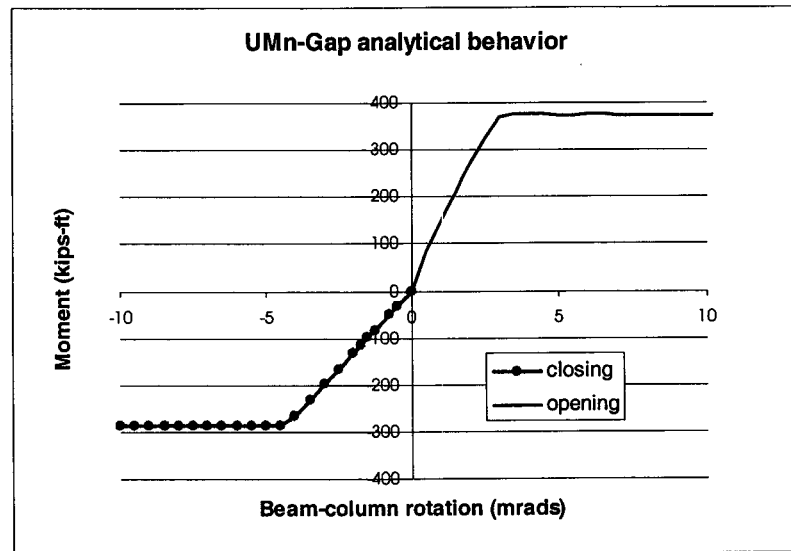


Figure 4.14 – UMn-Gap specimen: analytical moment-rotation behavior (from Palmieri, 1996)

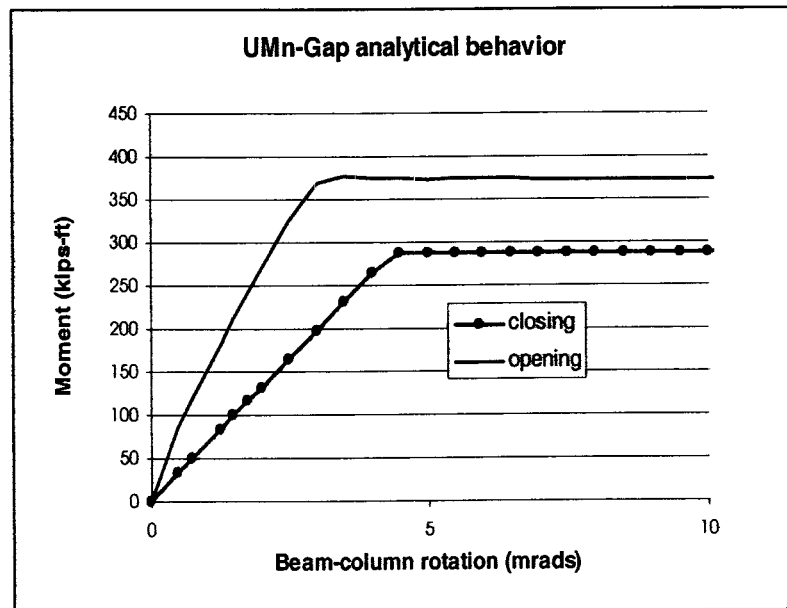


Figure 4.15 – UMn-Gap specimen: analytical moment-rotation behavior (from Palmieri, 1996)

#### 4.4.2. The Frame Finite Element Model

The finite element code RUAUMOKO (Carr, 1998) was utilized to create a plane model of the two frames. The columns are modeled with a beam-column element, with lumped plastic properties at the ends, taking also into account the effects of the variation of the axial loads on the moment

capacity. Moment curvature relationships are calculated for the column sections with monolithic behavior and the parameters introduced to define the end-sections hysteretic behavior.

Since in precast ductile connections a moment-rotation curve is more fundamental than a moment-curvature curve (an ideal infinite value of curvature should be assumed at the section interface), rotational inelastic springs were adopted to model the connections between precast elements. The rotational springs were assigned the bi-linear or tri-linear moment-rotation characteristics computed using the proposed procedure, under complete monotonic push.

In fact, all the inelastic demand is concentrated in the connection, while the beam elements are supposed to suffer low damage. For the beam members either an elastic behavior with a cracked stiffness value or a more detailed bilinear elastic scheme with initially uncracked and then cracked stiffness can be used. Since the panel-zone shear behavior was not modeled, a certain flexural deformability was introduced, as a sort of compensation, modeling that region with elastic beam elements (cracked properties), instead of rigid offsets, as commonly used.

#### **4.4.3. Pushover Analysis**

Pushover analyses were performed on the two frames, in order to obtain preliminary information on the seismic performance of the building in the frame direction. Slowly increased lateral loads, distributed along the elevation according to the first mode shape of the frame, were applied at the floor levels, as concentrated forces on the external column nodes.

In RUAUMOKO the pushover analysis is performed as a dynamic analysis with a slow ramp loading function which multiplies an imposed initial lateral load pattern. The slope of the ramp (rate of increasing load) should be small enough in order to guarantee that inertia forces are negligible.

The analyses showed significantly different behaviors for the two frames, with the non-prestressed-frame (TCY) initially softer but generally stronger than the prestressed-frame. In Figure 4.16 base shear-top drift displacement curves are illustrated: the base shear values corresponding to the design drift level are pointed by arrows (in parentheses the values in kips), indicating a substantial overstrength of the non-prestressed frame, as designed.

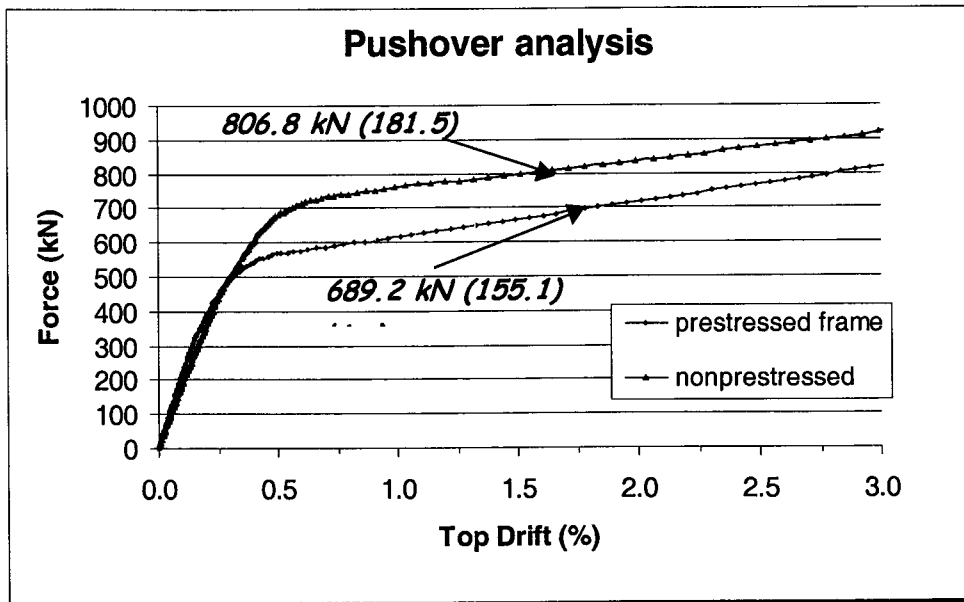


Figure 4.16 – Pushover analysis

The deformed shapes, as shown in Figure 4.17 are quite different from the distribution assumed in the DBD approach, due to an over-strength of the connections of the 4<sup>th</sup> and 5<sup>th</sup> floors (Prestressed and, particularly, TCY).

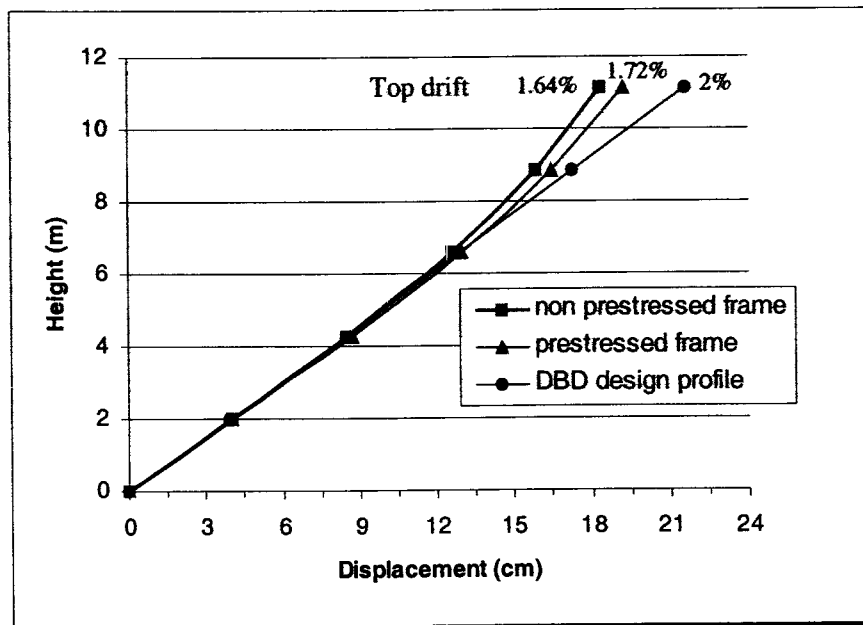


Figure 4.17 –Design and analytical displacement pattern (2% base drift)

The maximum desired interstory drift of 2% will occur at the first floor while a smaller drift is computed when considering the top drift (displacement of the top floor divided by the total

height of the building), as clearly shown in Figure 4.18. This fact should be taken into account when comparing base shear values at the design drift level.

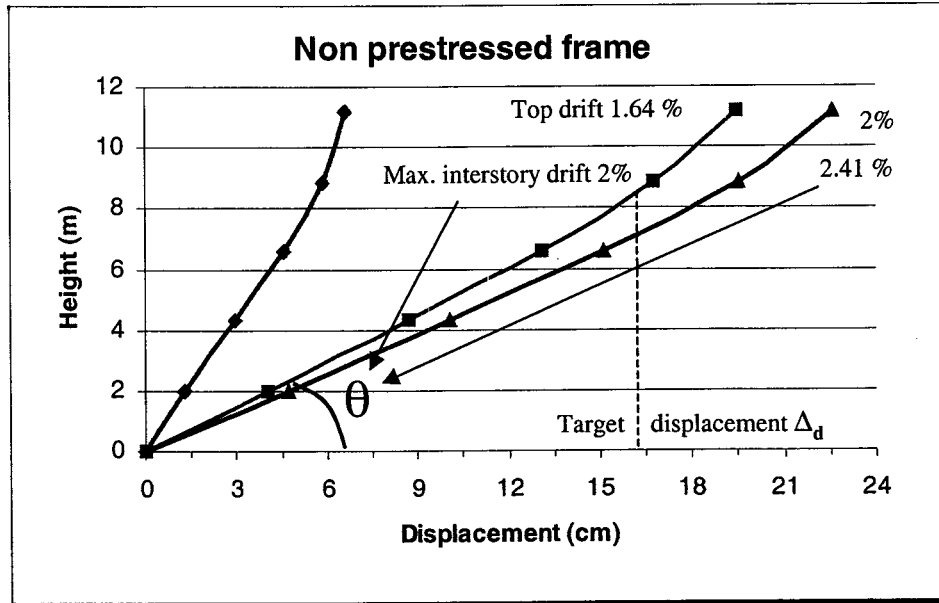


Figure 4.18 – Difference between Top floor and First floor drifts

Single connections and overall frame overstrength factors have been evaluating, comparing the maximum beam moments and total base shear (Tab. 4.6-4.7 respectively). A simple average value of the connection overstrengths seem to reproduce the whole frame situation satisfactory. In the TCY-Gap connection both the opening and closing behavior are considered to obtain bound values.

Table 4.6 – Design vs. actual estimated capacities: prestressed frame

		Beam moments					
		Elastic analysis		Pushover analysis			
Prestressed frame		DBD procedure		2% max drift		Overstrength	
Floor	Connection	(kips-in)	(kNm)	(kips-in)	(kNm)	RATIO C/D	Average
5	Prestressed	1098.3	124.1	1191.2	134.6	1.08	1.18
4	Prestressed	1386.4	156.7	1573.5	177.8	1.13	
3	Hybrid	1724.6	194.9	2093.0	236.5	1.21	
2	Hybrid	1976.4	223.3	2178.9	246.2	1.10	
1	Hybrid	2033.9	229.8	2727.6	308.2	1.34	
BASE SHEAR		(kips)	(kN)	(kips)	(kN)	RATIO	
		133.6	593.8	155.1	689.2	1.16	

Table 4.7 – Design vs. actual estimated capacities: non-prestressed (TCY) frame

		Beam moments					
		Elastic analysis		Pushover analysis			
Non Prestressed frame		DBD procedure		2% max drift		Overstrength	
Floor	Connection	(kips-in)	(kNm)	(kips-in)	(kNm)	RATIO C/D	Average
5	TCY	1098.29	124.10	1224.84	138.40	1.12	1.40
4	TCY	1386.44	156.66	1872.66	211.60	1.35	
3	TCY-Gap	1724.60	194.87	2877.13 (2024.8)	325.1 (228.8)	1.67 (1.17)	
2	TCY-Gap	1976.38	223.32	3331.14 (2470.9)	376.4 (279.2)	1.69 (1.25)	
1	TCY-Gap	2033.91	229.82	3756.82 (2861.2)	424.5 (323.3)	1.84 (1.4)	
BASE SHEAR		(kips)	(kN)	(kips)	(kN)	RATIO	
		133.61	593.80	181.53	806.80	1.36	

An average overstrength of 16% in the prestressed frame and 36% in the non-prestressed frame appear from the analyses. While the first result can be accepted and justified as an intrinsic effect of the design (due to the use of safety factors), the second can lead to complications during the testing phase with:

- 1) torsional effects in a force control test (inverted triangular load)
- 2) asymmetric distribution of the actuator floor forces between the two sides of the building in the frame direction in a displacement control test (pseudodynamic)

Furthermore, difficulties in the validations of the DBD procedure are expected when comparing the experimental base shear and the deformed shape at design drift level with the design assumptions.

#### 4.5. Modeling of the Cyclic behavior

Once the procedure to model the monotonic behavior of unbonded-type connections was completed, the cyclic behavior could be obtained from the same physical model by implementing a procedure of unloading from a defined level of displacement (or rotation). Cyclic constitutive laws of steel and concrete must be included in the procedure.

Otherwise simple assumptions can be made to determine the full hysteretic rule of the section from the already known monotonic curve. The idea is to refer to the basic concepts characterizing the different connections (NLE or TCY) and model each component separately in order to easily manage any possible combination (Hybrid).

According to this approach the contribution of the mild steel, which provides good energy dissipation capability, and of the unbonded tendons, which guarantee self-centering properties, should be separately computed and represented with different hysteretic rules. The modeling of the hybrid connection can be obtained by an adequate combination of a non-linear elastic and TCY-type hysteretic rule, resulting in an approach perfectly consistent with the nature of this connections.

### **Prestressed Connection**

The presence of tendons, unbonded along the bay length and bonded only in the joint region, imposes an ideal nonlinear elastic behavior. Such a behavior is thus modeled in the hysteretic rule of the corresponding rotational spring, maintaining the properties of the previously defined monotonic envelope curves.

### **TCY connection**

Since the behavior is expected to be similar to an equivalent monolithic connection, it seems natural to adopt a hysteretic rule typical of ordinary reinforced concrete sections.

The modified Takeda rule (Takeda et al., 1970) was thus used. The unloading stiffness is determined as  $K = K_o \cdot (1/\mu^\alpha)$ , where  $K_o$  is the initial stiffness,  $\mu$  is the ductility level and  $\alpha$  was taken as 0.5. Another parameter  $\beta$  defines the characteristics of the curve in the reloading phase. The experimental test results suggest to set  $\beta=0.2$ .

Actually, a TCY connection is expected to have slightly different energy dissipation when compared with a monolithic connection. In particular the unloading stiffness of the model should be reduced. An overestimation of the damping properties should thus be expected from the model, as confirmed by the experimental pseudo-dynamic test results. Additional comments about this topic are given later in this contribution.

## TCY-Gap Connection

Similarly, a modified Takeda rule was adopted, even if the behavior is more complicated than a TCY connection. Although the unbonded tendons are not providing the same level of self-centering capability than a prestressed connection, it's reasonable to assume that when the gap is closing their contribution can no longer be negligible. It would signify a further underestimation of the energy-dissipation capability of the model. This effect is added to that caused by the use of the Takeda model, as previously discussed.

## Hybrid Connection

The behavior of the hybrid connection can be analyzed adequately combining the different contributions: mild steel, concrete and unbonded tendons.

It would seem reasonable to model such a connection respecting its own nature, using rotational springs in parallel (subjected to the same interface rotation) which represent the contribution of each component (Fig. 4.19).

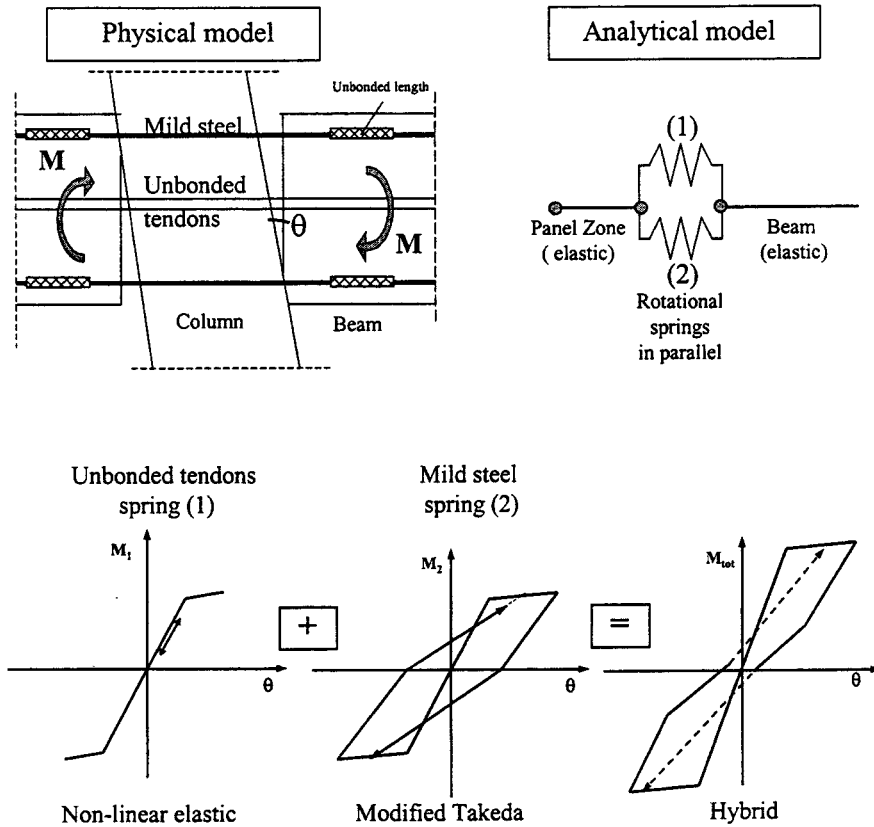


Figure 4.19 – Analytical model of hybrid connection

Starting from the moment-rotation curve as calculated with the procedure previously discussed, the moment capacity contribution of mild steel, tendons and concrete can be evaluated with a rotation equilibrium around any section point.

If concrete and mild steel are combined together, we can assign to the resultant monotonic envelope a Takeda hysteretic rule model, typical of reinforced concrete. A nonlinear elastic behavior envelope, resulting from the contribution of the unbonded tendons, should then be applied to the moment-rotation.

#### 4.5.1. Quasi-static Cyclic Analysis

The modeling of the cyclic behavior, by means of rotational spring with adequate hysteretic rules, was included in the general finite element model of the two frames and preliminary predictions of the overall response under a quasi-static cyclic load were performed.

The Base Shear-Top drift displacement behaviors, illustrated in Figures 4.20-4.21, confirm the expected differences in the response of the prestressed and non-prestressed frames, regarding the two often mentioned parameters: self-centering and energy dissipation capabilities. The prestressed frame shows significant level of self-centering, after the load is removed, which should result in a significant reduction of the residual displacements under seismic loads.

Equivalent viscous damping values, related to the secant stiffness to the design drift level of 2% were calculated from the conventional formula:

$$\xi = \frac{E_c}{4\pi \cdot E_e}$$

where  $E_c$  is the dissipated energy in the complete cycle, and  $E_e$  the elastic energy at peak displacement.

The equivalent viscous damping coefficients were evaluated as  $\xi_p=14.5\%$  and  $\xi_{np}=20.3\%$  for the prestressed and non-prestressed frame respectively. An average value for the whole building in the frame direction would thus be in general agreement with (even if slightly smaller than) the value assumed in the DBD procedure ( $\xi=20\%$  for the whole building in the frame direction). The reduced damping should result in increased displacements, which would tend to compensate for the influence of extra strength (discussed previously) which would have the opposite effect.

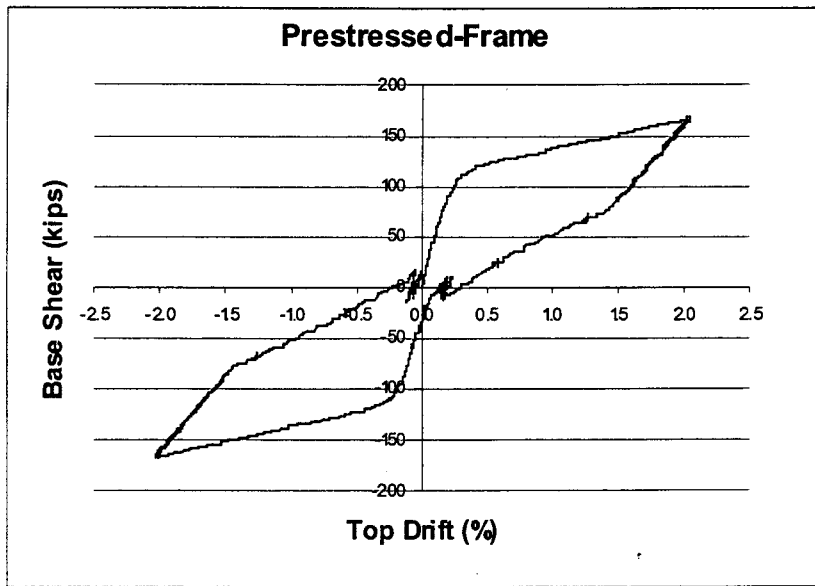


Figure 4.20 – Analytical hysteretic behavior –Prestressed frame

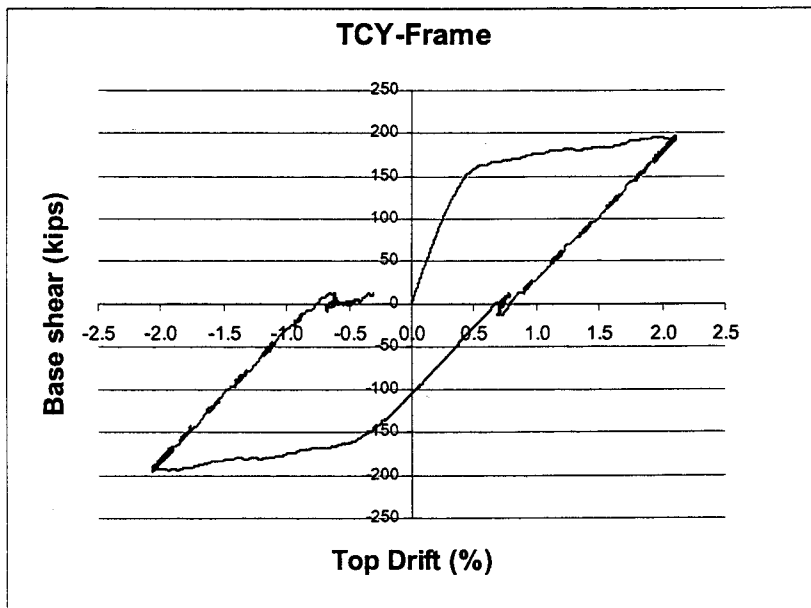


Figure 4.21– Analytical hysteretic behavior –Non-Prestressed (TCY) frame

## CHAPTER 5

### EXPERIMENTAL RESULTS AND PRELIMINARY ANALYTICAL-EXPERIMENTAL COMPARISON

#### 5.1. Test Plan

The simulated seismic test of the PRESSS five-story precast concrete building was conducted independently in the two orthogonal directions: The wall system was first tested followed by the frame system. Different schemes, namely pseudo-dynamic, inverse triangular load and flexibility tests, were carried out integrating and supporting the whole test-procedure.

Most of the test was carried out with a pseudo-dynamic procedure using a control algorithm developed at UCSD as part of a 5-story masonry building test (Igarashi et al., 1994), and modified to apply to the PRESSS building [Sritharan et al 2000].

##### 5.1.1. Pseudo-dynamic Procedure

The pseudo-dynamic procedure is a method which combines numerical computation, on-line control of the actuators and experimental measurements to simulate the response of a structure under dynamic external loads.

The conceptual scheme of this procedure is shown in Figure 5.1.

The equations of motion of the M.D.O.F. system subjected to a dynamic force vector  $f(t)$  are calculated based on the initial conditions for the mass, stiffness, and damping matrices.

Due to scaling effects, the mass matrix of the test-building is not the actual one, but the "conceptual" one, scaled from the prototype's mass. The initial stiffness matrix is calculated through a flexibility test, while the damping matrix is modeled analytically. The resultant displacement vector is thus applied to the structure and the actuator restoring forces  $r(t)$  (based on a generally non-linear behavior) are measured and fed-back into the equation of motion for the evaluation of the target displacement vector at the next step.

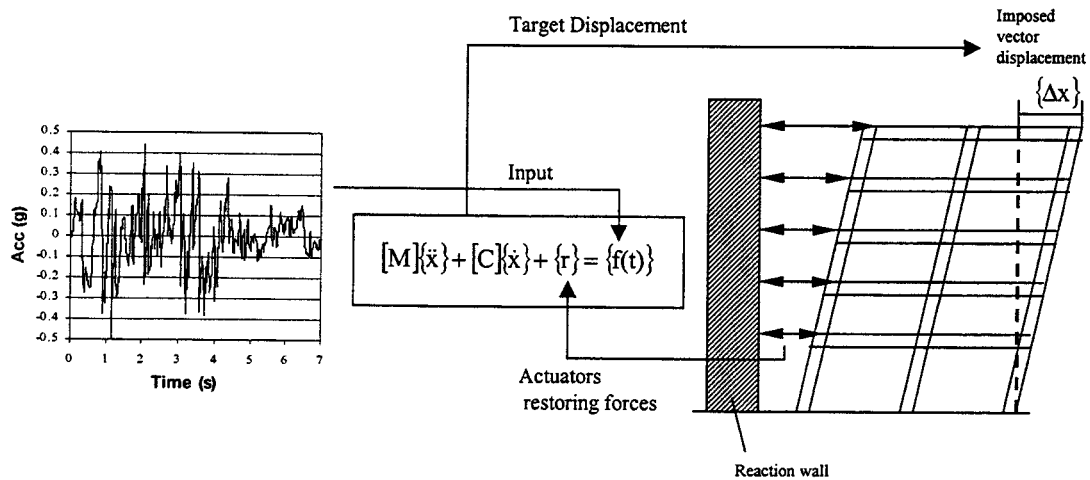


Figure 5.1 – Conceptual scheme of the pseudo-dynamic procedure

### 5.1.2. Input Ground Motions

In order to investigate the performance of the test-building under different increasing levels of seismic ground shaking, several input motions were selected corresponding to progressively increasing return periods.

Recorded past earthquakes were modified to be compatible with the four levels of performance based spectra (from EQ-I to EQ-IV) as recommended by PBSE Ad-Hoc SEAOC Committee (1998), corresponding to frequent, occasional, rare and maximum credible earthquakes (Fig.5.2)

EQ-III represents the design level spectrum, while EQ-IV is obtained by multiplying the acceleration spectrum ordinates of EQ-III by 1.5.

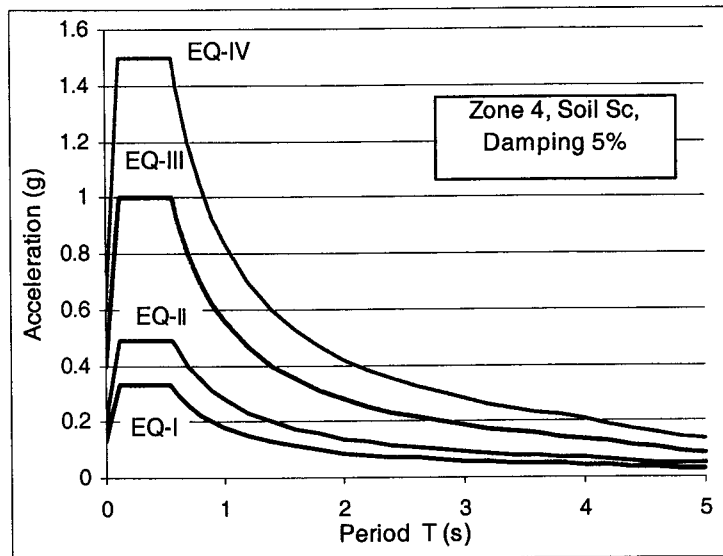


Figure 5.2 – Acceleration design spectra (SEAOC 1998)

The accelerograms were chosen over synthetic spectrum compatible records, generated with the program SHAPE (Earth Mechanics 1998). Unrealistic high frequency content, typical of synthetic records, could have lead to significant negative effects during the pseudo-dynamic test. Artificial increases of the actuator forces, oscillating at high frequency, would have been expected, causing complications regarding both control aspects (risks of instability and lack of convergence) and structural behavior (due to the maximum design level of floor shear forces).

Since such effects become significantly important at medium levels of drift, the accelerogram corresponding to EQ-III level was modified with a low-pass filter. Compatibility with the medium-high period range of the acceleration and displacement spectra were thus respected (Fig.5.3) , consistent with the adopted DBD approach, based on secant stiffness (medium to high periods) concepts.

In order to speed up the test, short segments were extracted from the real recorded accelerogram and then modified, according to the following criteria:

- The cycle with the peak ground acceleration must be contained in the segment
- The starting time of each segment is defined such that the first occurring acceleration peak exceeds 0.05 for EQ-I level input motion and 0.1g for EQ-II to EQ-IV

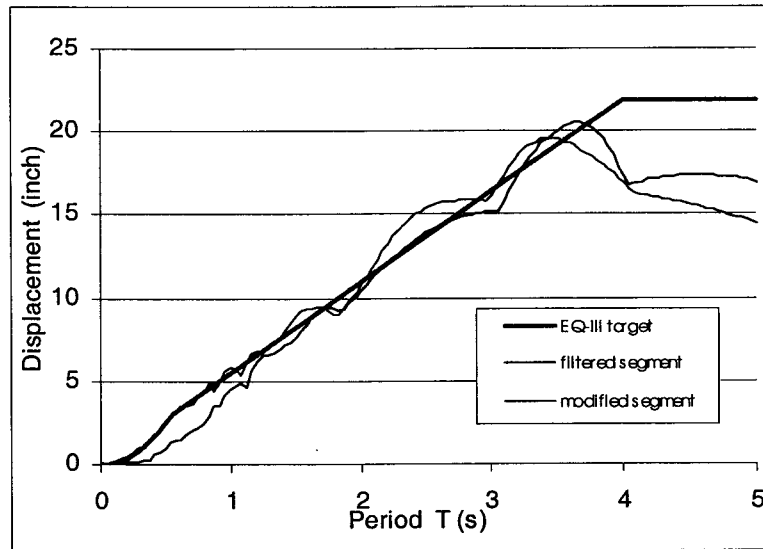


Figure 5.3 – Design and response displacement spectra

### 5.1.3. Flexibility Test and Inverse Triangular Test

At each level of the pseudo-dynamic test, the stiffness matrix was updated through the flexibility tests in order to:

- 1) improve the convergence of the pseudo-dynamic test based on implicit integration schemes
- 2) compare experimental stiffness values, at different displacement level, with the effective stiffness  $K_{eff}$  of the equivalent single degree of freedom adopted in the DBD procedure
- 3) monitoring structural damage levels using stiffness as a damage indicator

In the flexibility test, lateral forces were sequentially applied at each floor level and the corresponding vectors of lateral displacement were measured. Lateral force levels were chosen to be as large as possible while still ensuring elastic structural response of the frame connections.

Furthermore, at the conclusion of each pseudo-dynamic test, the building was subjected to a quasi-static cyclic test with inverse triangular lateral loads, which imposed a deformed shape close to the first mode of vibration, the top floor displacement being equal to the maximum

reached in the previous test. Two complete cycles with maximum positive and negative top floor displacements were performed.

Since in the design phase, either in a force-based or displacement-based approach, the internal forces are evaluated assuming an inverse triangular distribution of the lateral acceleration, useful information can be provided when comparing test-results and design assumptions.

The equivalent viscous damping, critical parameter in the design phase, can be evaluated at different levels of drift.

## **5.2. Experimental Results**

### **5.2.1. Damage Level Observations**

The two frames were subjected to a series of pseudodynamic tests (0.25 EQ-I, 0.5 EQ-I, EQ-I, EQ-II, EQ-III), with inverse triangular load tests, applied after each earthquake level. Both frames displayed a really satisfactory performance and a limited level of damage in general.

Particularly efficient was the prestressed frame, with the Hybrid and Pretensioned connections, while the TCY-Gap connection suffered, starting from the EQ-III design level (corresponding to an average experimental drift of 2.2 %), some shear slipping at the beam-column interface with increasing levels of damage, crushing and spalling of the concrete.

Preliminary interpretation of this unexpected phenomenon would indicate the occurrence of inter-related factors: an over-strength of the compression mild steel longitudinal bars reduced the net compression across the grout joint. Thus the grout pad slipped and was progressively damaged, reducing the resisting area with a consequent increase of the stress state in the critical region which caused crushing and spalling of the cover concrete.

In retrospect, increased safety against slipping could have been provided by:

- increasing the PT bar compression force
- increasing the friction coefficient

On the other hand an increase in the amount of fibers in the grout would have caused the grout pad to behave plastically, avoiding a brittle failure.

Such interventions represent viable solutions which can be simply realized at the design stage.

A photo report of the building response at different level of excitation is presented in Appendix A.

In the early stages of loading the response of the building was characterized by low level of damage (Figs. A.1 – A.4 refer to EQ-II level). In the Hybrid and TCY-Gap connections, which represent alternative solutions to the “emulation” of cast in place concrete, the inelastic demand was concentrated, as expected, at the beam-column interface through opening and closing of a unique crack. The level of cracking and damage in the precast elements, outside the critical region, and in the panel zone was minimal, in contrast to what would have been expected in an equivalent monolithic solution. Only the TCY connection, on the other hand, displayed flexural cracking patterns distributed along the beam, similar to a cast-in-place reinforced concrete solution.

Nonetheless, the damage at EQ-III design level was extremely limited as shown in Figures A.5-A.9. No significant problems appeared in the prestressed connection: a neat flexural crack developed at the beam-column interface, acting as a fuse, according to a correct capacity design, for the panel node region.

The experimental behavior of the connections confirms the analytical assumptions regarding the concentration of the inelastic demand at the interface region through a neat opening of the gap ( $\theta_{imp}$ ) with consequent low levels of damage in the precast element. The use of elastic members connected at the interface by concentrated rotational springs appears, therefore, as a correct way to model precast frame systems.

It should be reported that, during testing at EQ-III level, some inward rotation of the hybrid beams around their longitudinal axes was observed. The mechanism of this torsional rotation is illustrated in Figure 5.4. The heavy double-tee floor members were hung off the side of the beams at the lower three floors, causing a torsional moment of significant magnitude. Under inelastic action, the torsion in the hybrid beams was primarily resisted by the compression

zone at the beam-column interface, with a small contribution from dowel action of the mild steel damping bars crossing the interface.

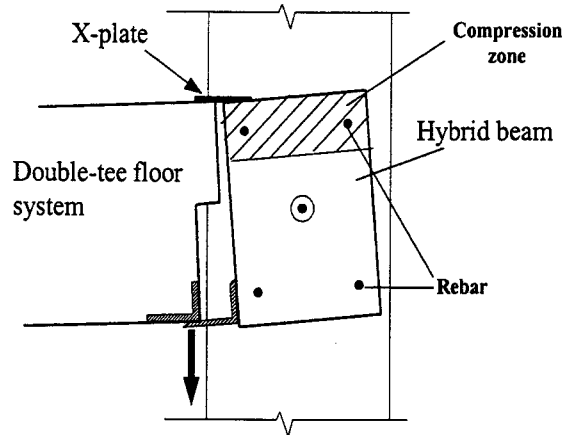


Figure 5.4 – Torsional rotation of hybrid beams

The torsional resistance of these actions was insufficient to prevent the rotation at the three floors of the prestressed frame. The very high floor forces levels also exacerbated the problem, providing additional vertical forces to the floors, which in one direction of response more than doubled the reactions of the double tees on the prestressed beams, and hence increasing the torsion by a similar amount.

Following testing at EQ-III input, the steel base of the floor beams was welded to the brackets on the side of the prestressed beams, effectively locking in the rotation at the existing level, and prohibiting further rotation (Fig. A.14). It is clear that support of these heavy double-tee floor members should be provided as close to the beam centerline as possible to reduce the torsional effect, which would be important whether the frame was precast or cast-in-place.

At the end of the pseudo-dynamic test at the EQ-III level, with a top (roof-level) displacement of 10 in. (254 mm) and average drift of 2.1%, the significant differences in damage levels and, consequently, in the stiffness of the two frames made it difficult to continue with the pseudo-dynamic tests. It was therefore decided to continue with quasi-static cyclic tests (IT4-IT5) at inverse triangular load.

The 3% drift level, corresponding to a top displacement of 12.2 in. (310 mm) was passed without significant additional damages. The structure was further brought to a maximum drift close to 4.5%, corresponding to a top displacement of 17.9 in (454 mm), before failure in the mild steel reinforcement occurred in some connections. On the second cycle to the peak displacement of 17.9 in (454 mm) the control system developed a severe instability, which forced the suspension of the test. At this stage even the hybrid connection experienced some spalling of the cover concrete. In spite of failure of longitudinal reinforcement, reduction in the whole frame strength (base shear) was not observed.

The condition of the various connections after cycling to more than twice the design level are shown in Figures. A.10 – A.13. The hybrid connections performed extremely well at this stage, with only minor damage in the form of cover spalling, and some crushing and incipient break-down of the fiber grout pads between the beams and the columns. No significant increase in width of the joint shear cracks above that sustained at the design level was observed. It is probable that the results from the joint strain gauges will show that substantial reduction in joint reinforcement will be possible with this detail. These results will be published separately in Sritharan et al 2000(2).

In the upper floors of the prestressed frame, the performance of the pretensioned connections was also excellent with damage limited to superficial cover spalling at, or adjacent to the beam-column interface.

In the non prestressed (TCY) frame, sliding at the interface had continued in the TCY-Gap connections during testing levels above the design level. As a consequence of the high tension strains from the seismic response coupled with the dowel bending caused by the interface sliding, a few of the mild steel reinforcing bars crossing the interface fractured in the latter stages of testing. As discussed, the occurrence of the sliding phenomenon with continuous damaging of the grout pad at the interface could have been avoided with simple intervention in the design phase. It should also be observed that early crushing of the cover concrete may be inevitable with this design detail because of the high compressive force across the grout pad when the top bars are in tension. Strengthening the beam ends or some other detail to inhibit crushing may be advisable in future designs. However, the damage level in these connections

at the end of testing appear to be still less than would be expected from a conventional reinforced concrete beam-to-column joint at this level of drift.

Damage to the TCY connections in the upper levels of the non prestressed frame was not significantly different from that at the design level. A small amount of interface sliding continued to occur at these higher levels of response, but crack patterns and spalling did not noticeably change. Some loss of bond between the top level reinforcing bar in the grout ducts was noted at the exterior connections, with the headed reinforcing bar, which were exposed at the ends of the connection being pushed out by up to 1 in. (25 mm). There was no apparent significant strength reduction associated with this action.

The performance of the beam-column joint connections has been so far described. However, as anticipated, the whole building showed an excellent performance, thus including the other structural details or elements:

- seismic columns: only minimal damage was observed at the critical column base section (connection to the foundation), with very minor spalling being observed at some, but not all of the seismic columns (Fig. A.16).
- gravity columns: the consistent details of the whole structures allowed the gravity frame to be subjected to the same maximum displacement reached by the seismic frames, with minimal level of damage given by early stage level of flexural cracking along the element (Fig.A.18). The details adopted at the column base appeared to be extremely adequate to the scope.
- welded X-plates: these connectors between the double-tee floor members and the frame beams also performed well, although exhibiting significant inelastic action and permanent distortion, as illustrated in (Fig. A.16).
- the connection details between the cast-in-place hollow-core topping and the frames, formed by drag bars from the topping connecting into pockets in the top of the frame beams showed only minor cracking, despite the high levels of floor forces.
- the out of plane flexural resistance of the wall was negligible. Due to its flexibility, the level of damage was extremely limited, with only minor flexural cracking in the region close to the foundation (Fig. A.19). Force-Displacement Characteristics

### 5.2.2. Force-Displacement Characteristics

Further information can be derived from preliminary experimental results in terms of force and displacements characteristics reported in Figures 5.5 - 5.21. Base-moment/top-displacement hysteresis responses at different level of seismic excitation, under pseudo-dynamic tests (Fig. 5.13 - 5.16) or inverse triangular quasi-static cyclic tests (Fig.5.17 - 5.19), emphasize the peculiarities of the whole system and of the two individual frames. The differences in terms of energy dissipation and self-centering capabilities are evident, although the dissipation of both the frames was lower than what assumed in the design phase (equivalent viscous damping). Considerations on this topic will be given in the following paragraph when comparing the analytical and experimental results.

The peak displacement profiles up the frame (see Fig. 20(a)) at different levels of excitation confirm the predominance of the first mode of vibration. The evident pronounced curvature (reduction of drift) at the upper stories seems to indicate the predicted excessive overstrength at the upper levels (Par. 4.4.3). Time histories of displacement response, story shear forces and floor forces, at different level of the building are shown in Figures 5.5-5.12. Significant higher mode response, which was becoming particularly evident at increasing level of excitation, leading to unacceptably high floor forces, resulted in a necessity to filter the original design level (EQ-III) accelerogram to reduce the severity of third to fifth mode effect.

Analyses of the structure confirmed that this filtering would not influence the peak displacements or base shear forces, which were primarily influenced by the first (inelastic) and second modes of response.

A considerable amount of higher mode response, however, is still evident from the time-histories of the story shear and floor forces, particularly in the early stages of excitation, being less apparent during the peak response and in the displacement time-history.

This difference in sensitivity to higher modes between the displacement and force response is to be expected, since only the first mode is significantly modified by ductility. Higher modes remain essentially elastic and their contribution in the displacement response is limited by

their large stiffness, while their contribution in the floor force response increases with ductility level.

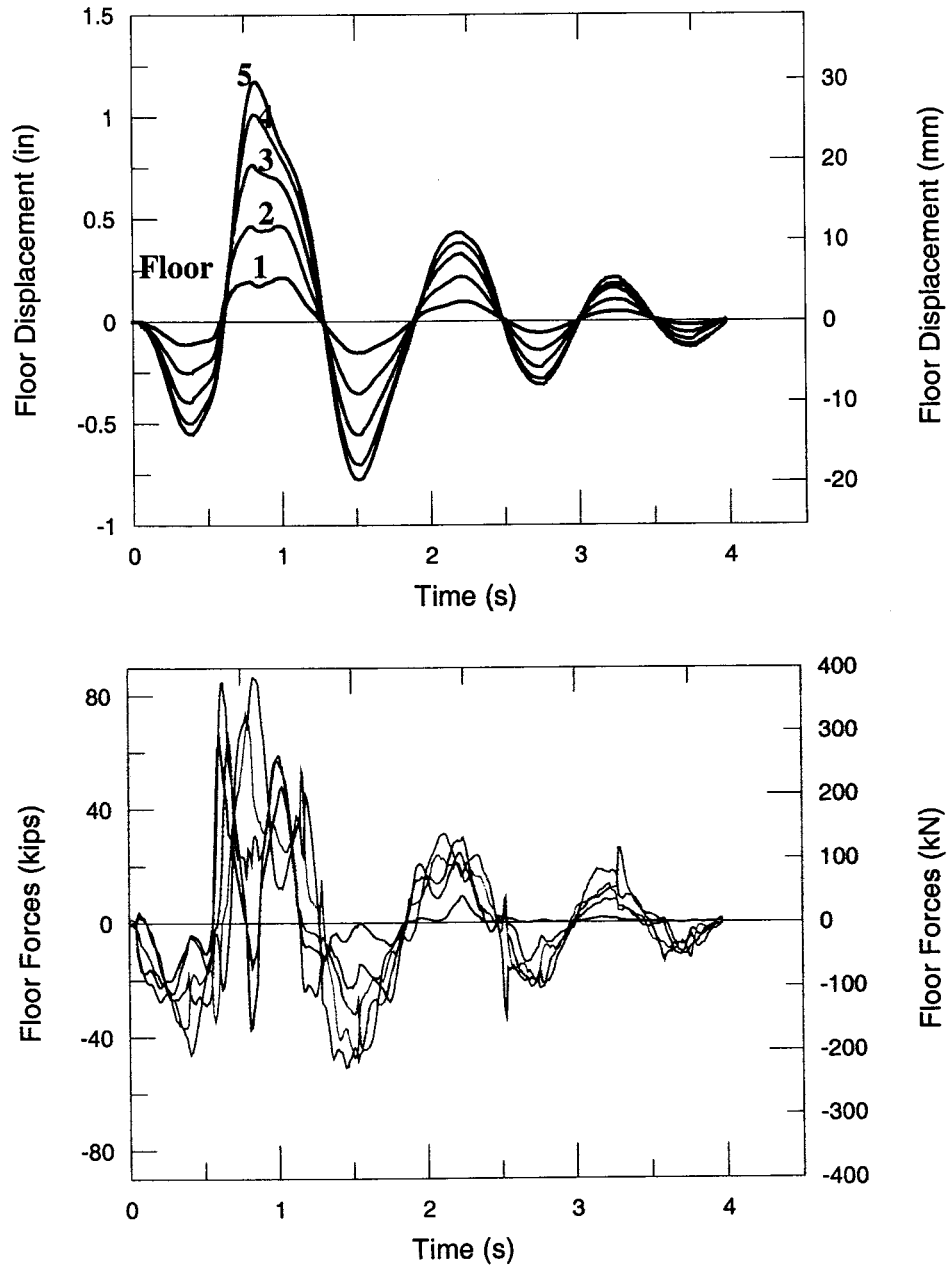


Figure 5.5 – Experimental results (0.5 EQ-1):  
Floor displacement and Story shear Time-histories

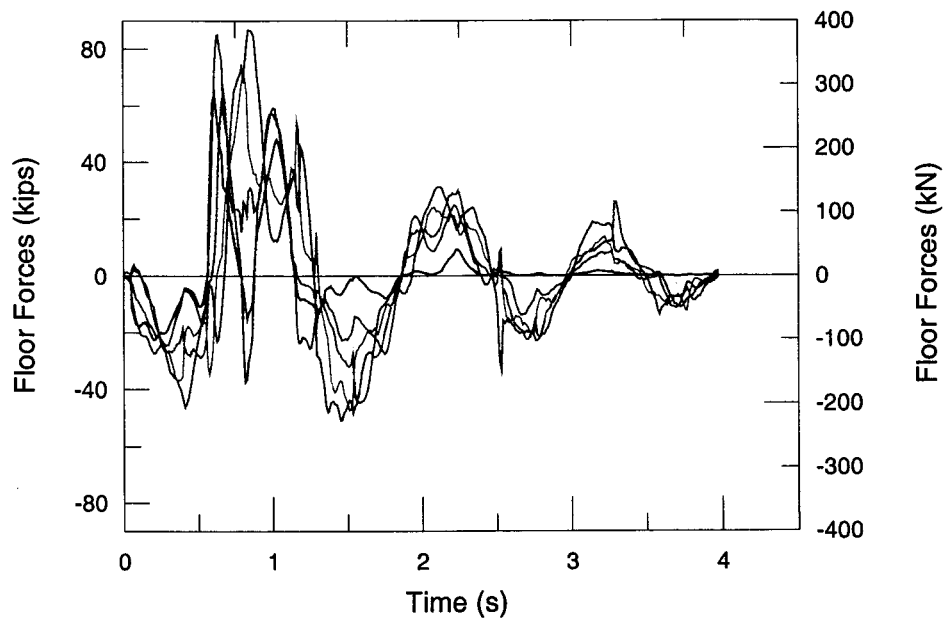


Figure 5.6 – Experimental results (0.5 EQ-I):  
Floor forces Time-history

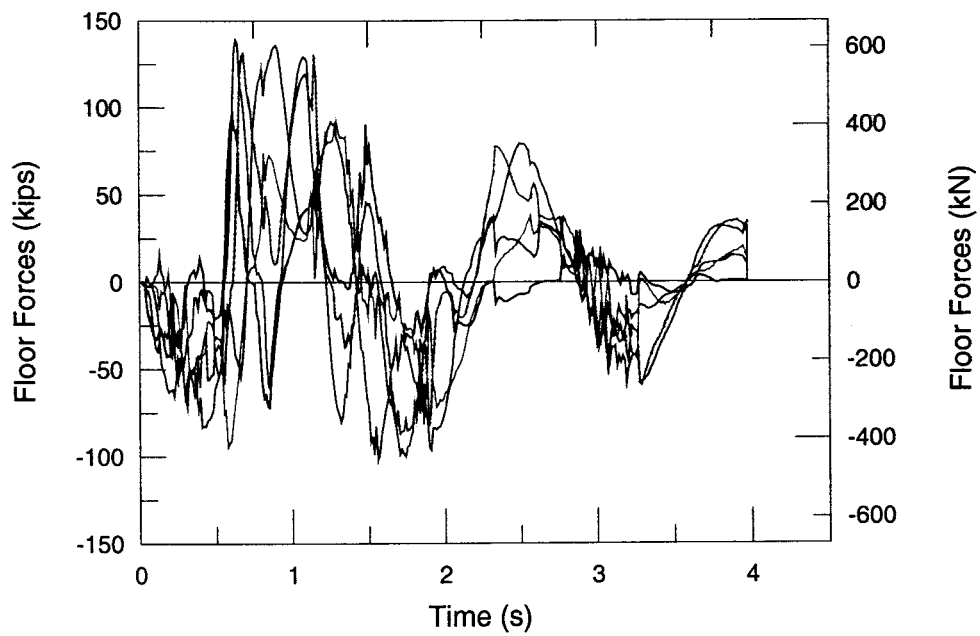


Figure 5.7 – Experimental results (EQ-I):  
Floor Forces Time-history

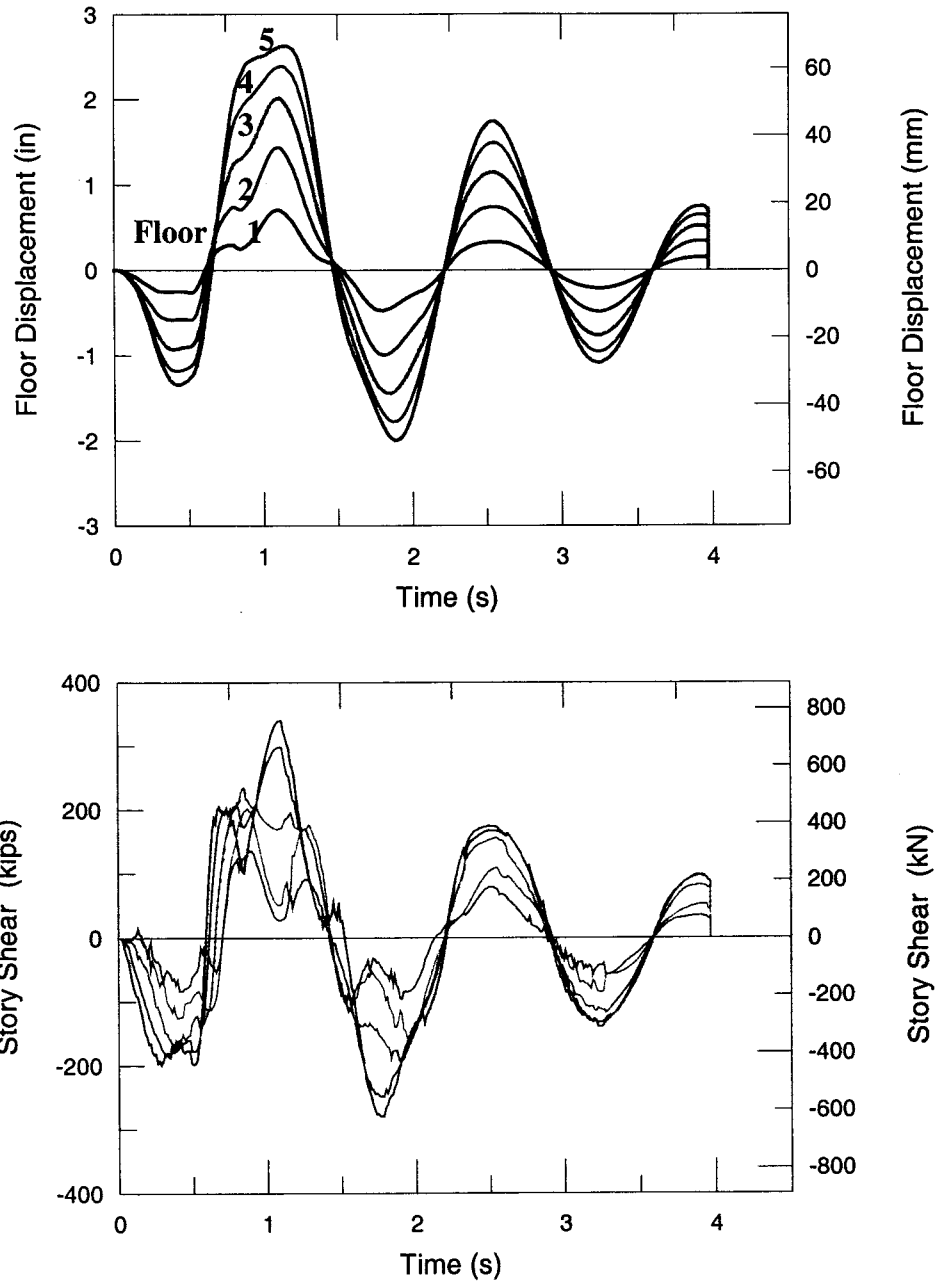


Figure 5.8 – Experimental results (1.0 x EQI):  
Floor displacement and Story shear Time-histories

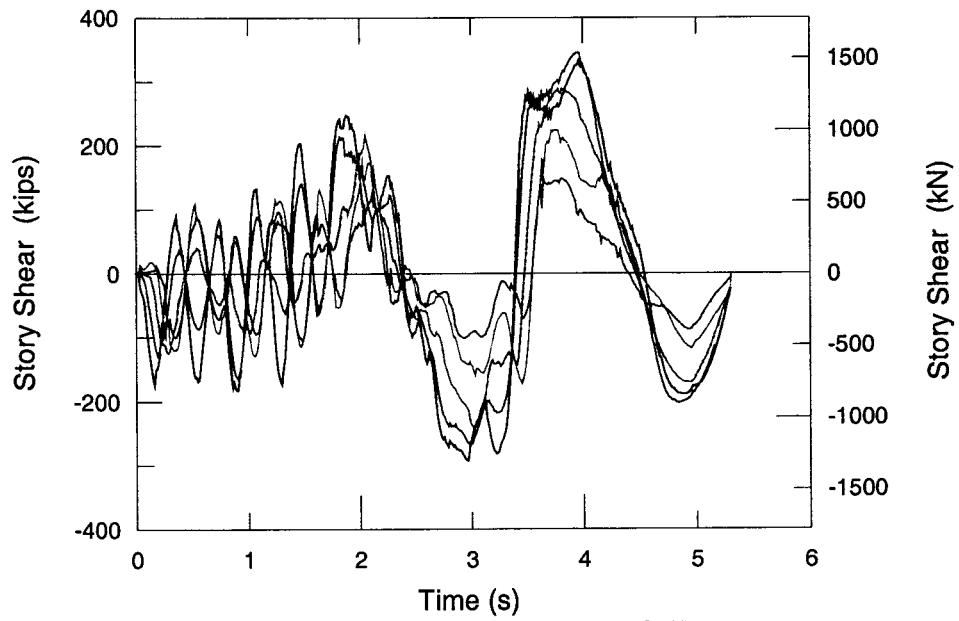
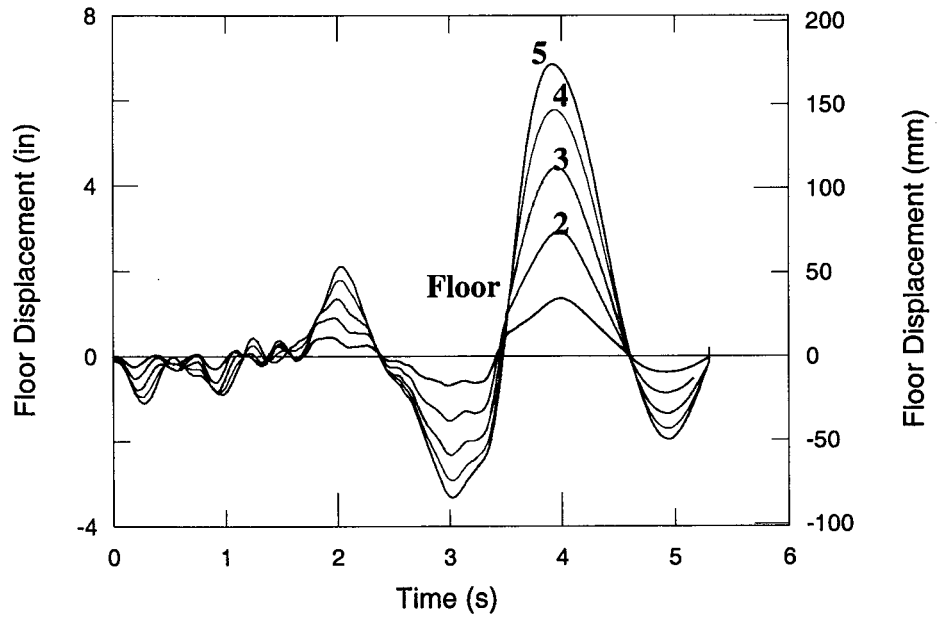


Figure 5.9 – Experimental results (EQ-II):  
Floor displacement and Story shear Time-histories

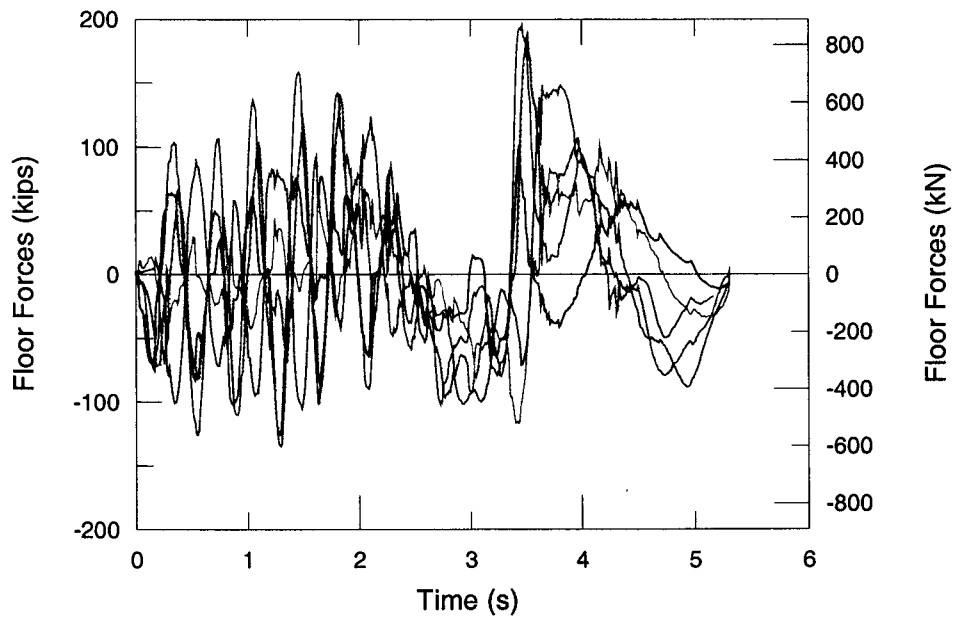


Figure 5.10 – Experimental results (EQ-II):  
Floor forces Time-history

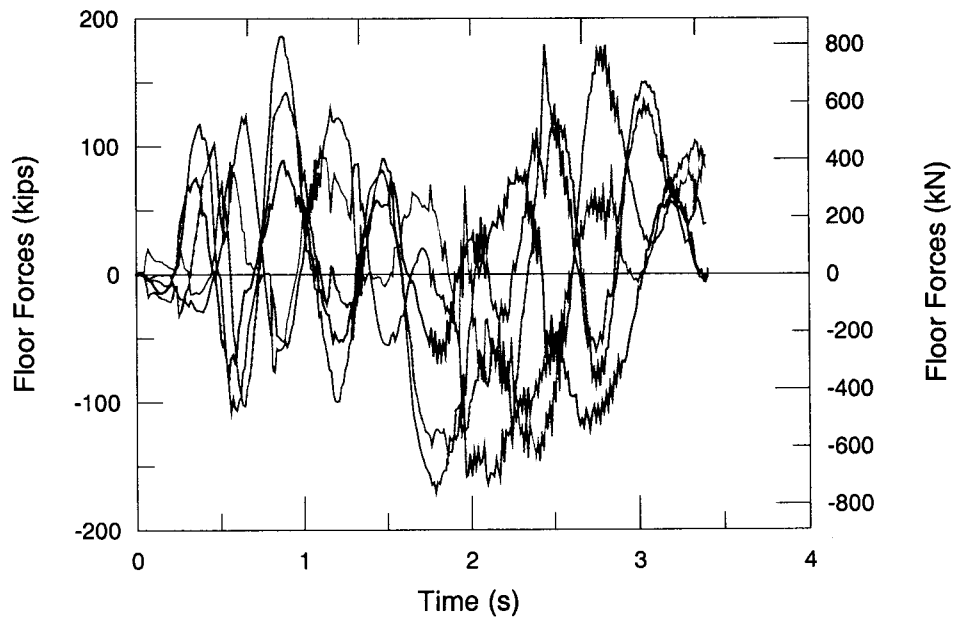


Figure 5.11 – Experimental results (EQ-III):  
Floor forces Time-history

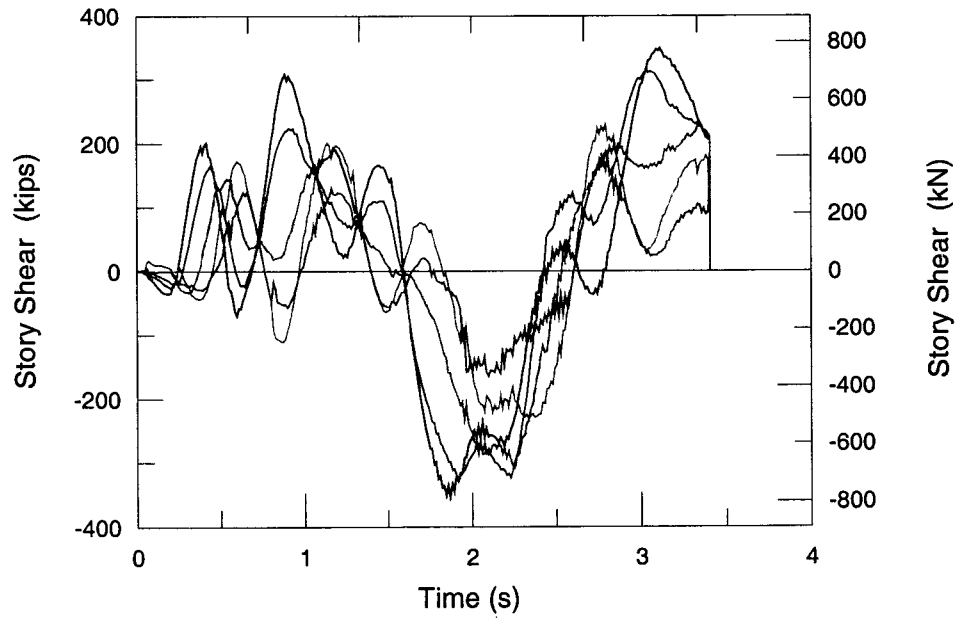
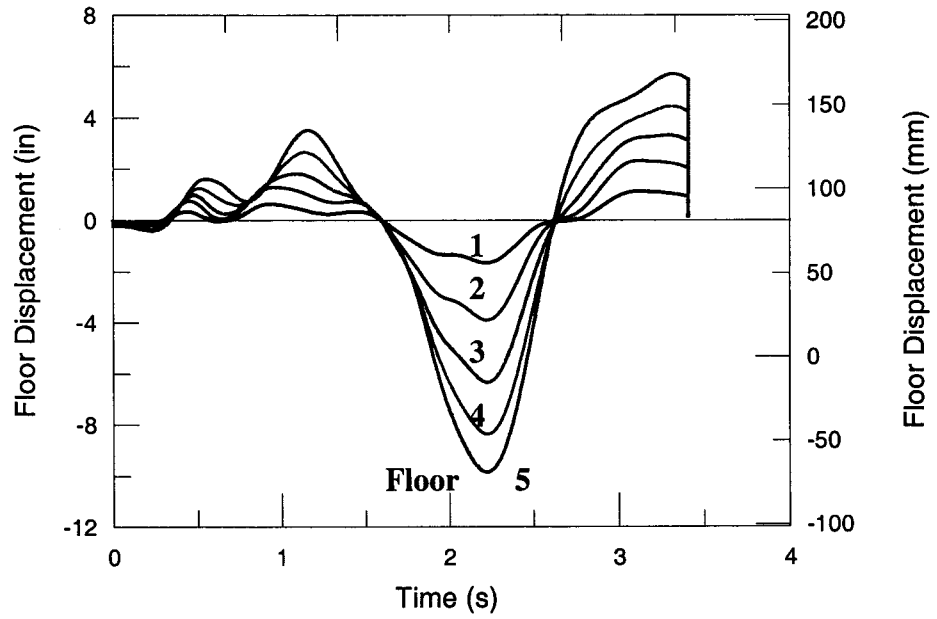


Figure 5.12 – Experimental results (EQ-III):  
Floor displacement and Story shear Time-histories

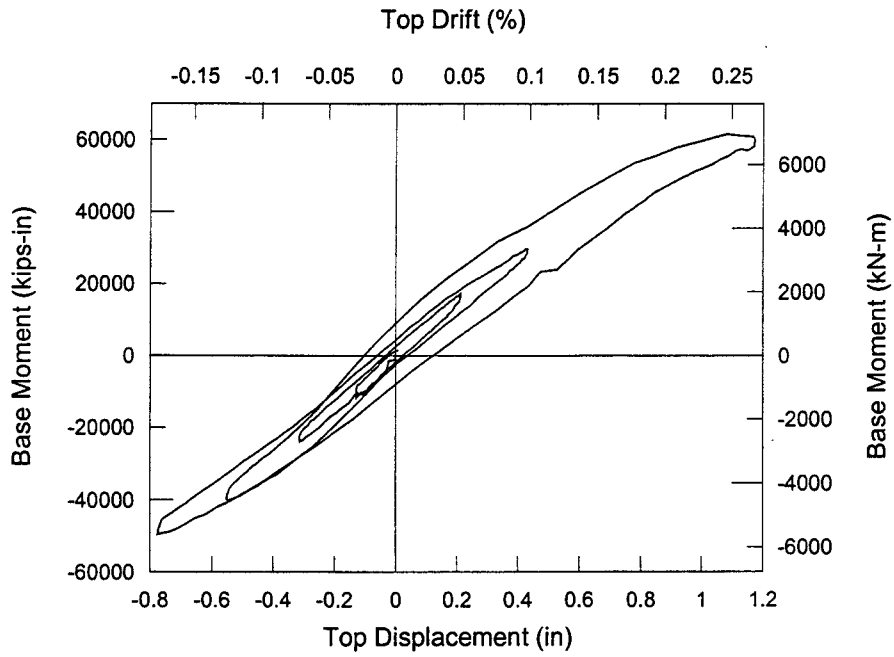


Figure 5.13 – Experimental results (0.5 EQ-I):  
Base Moment- roof displacement hysteresis

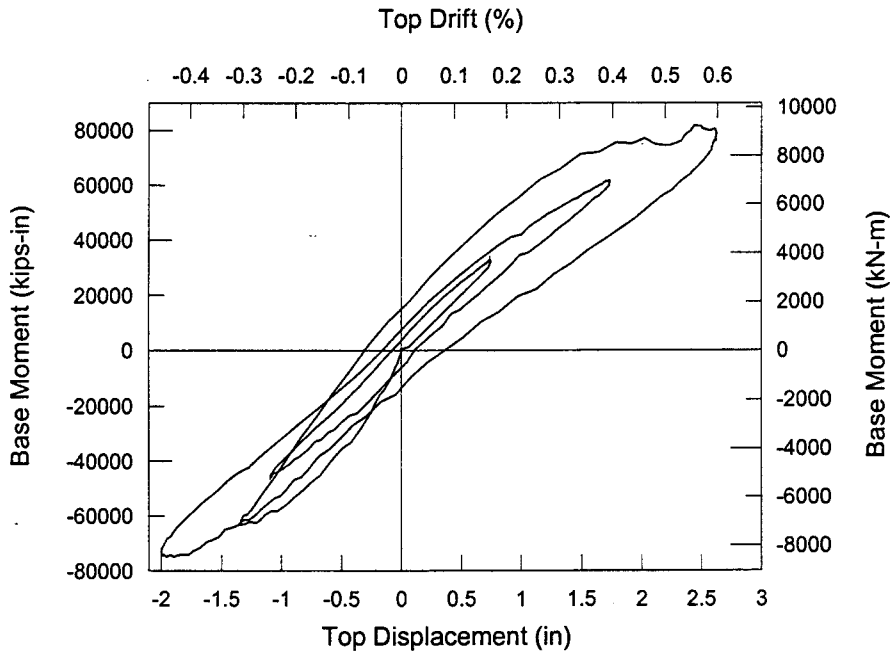


Figure 5.14 – Experimental results (EQ-I)  
Base Moment- roof displacement hysteresis

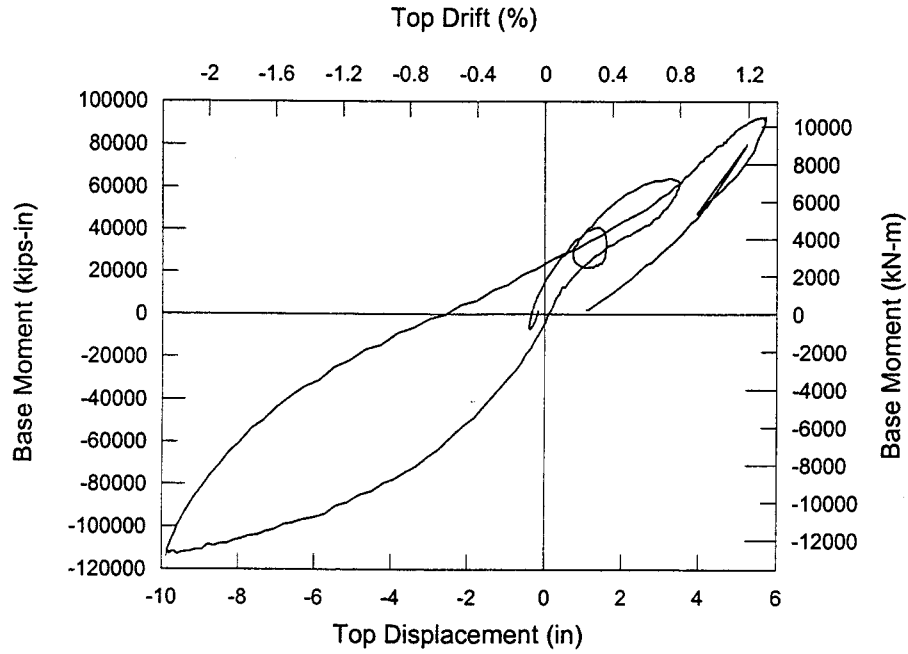


Figure 5.15 – Experimental results (EQ-II)  
Base Moment- roof displacement hysteresis

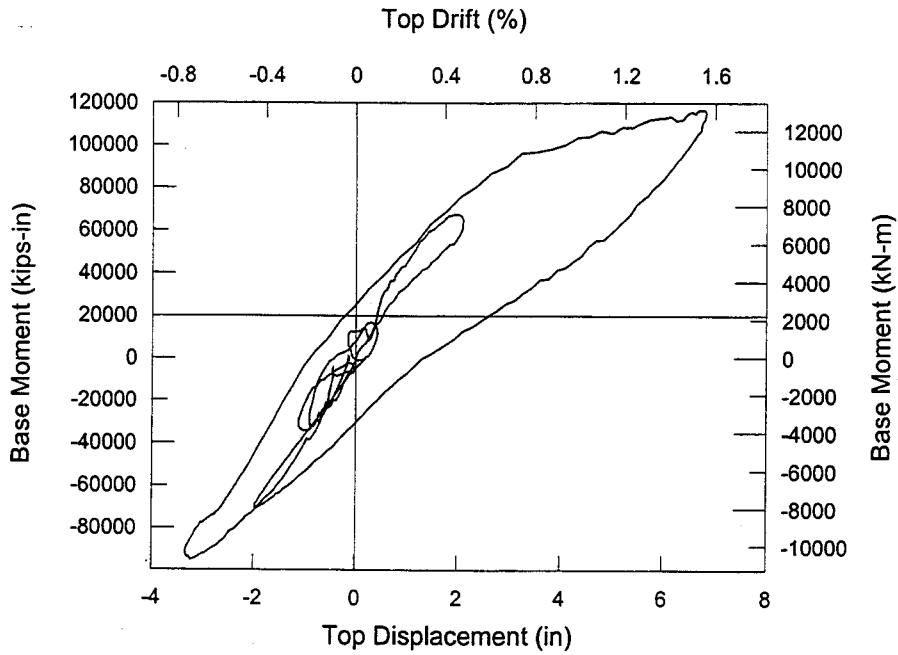


Figure 5.16 – Experimental results (EQ-III)  
Base Moment- roof displacement hysteresis

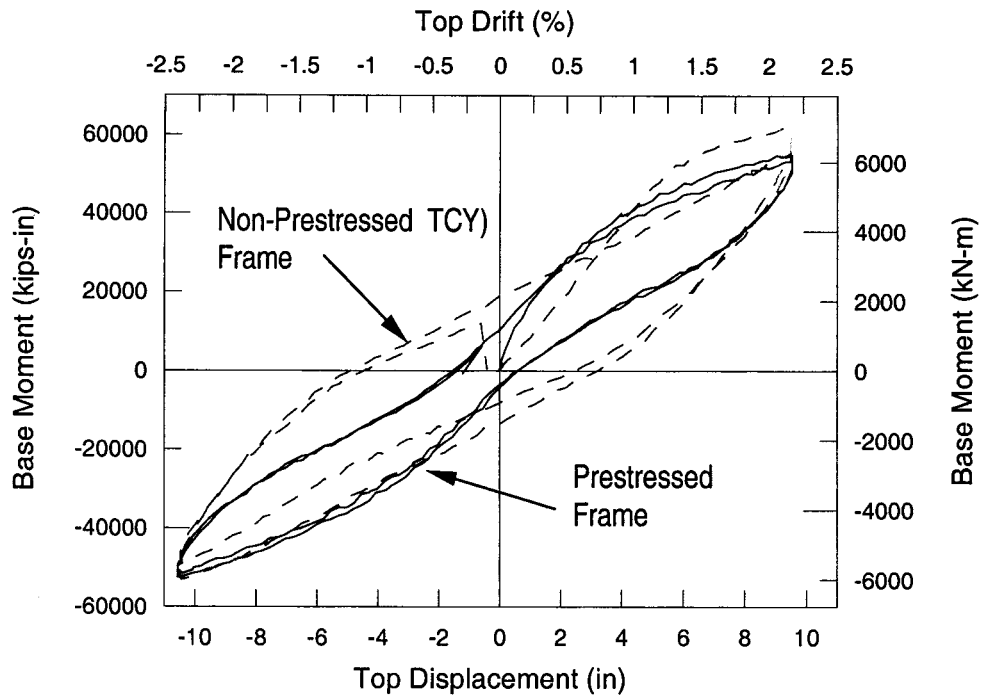
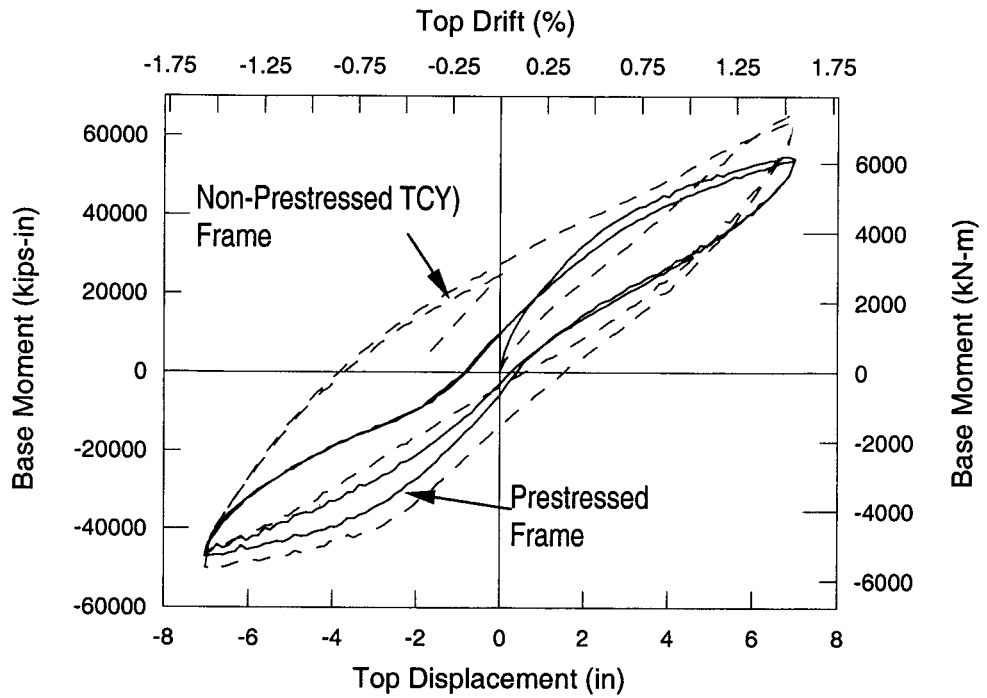


Figure 5.17 – Experimental results (IT2 and IT3)  
Base Moment- roof displacement hysteresis

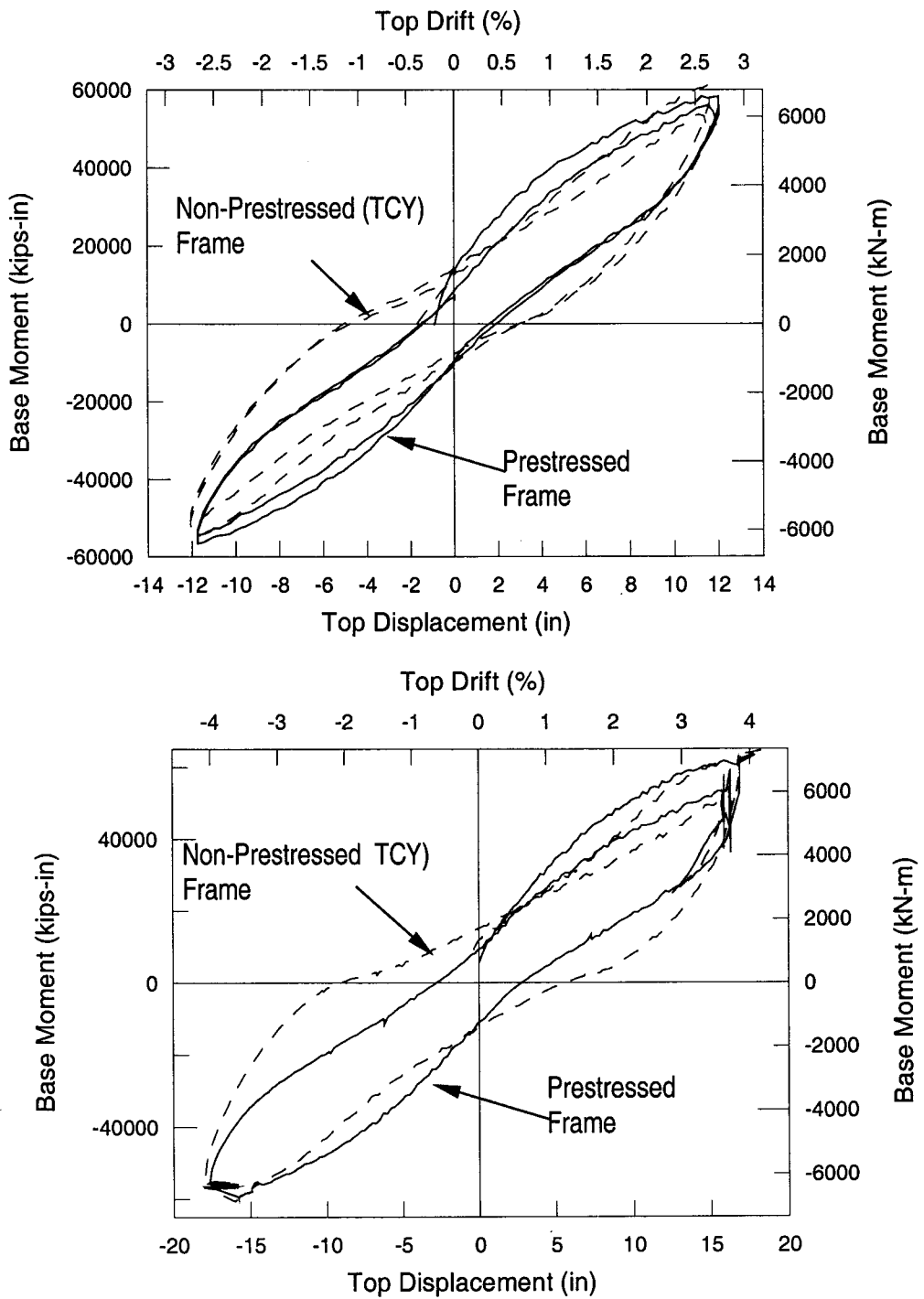


Figure 5.18 – Experimental results (IT4 and IT5)  
 Base Moment- roof displacement hysteresis

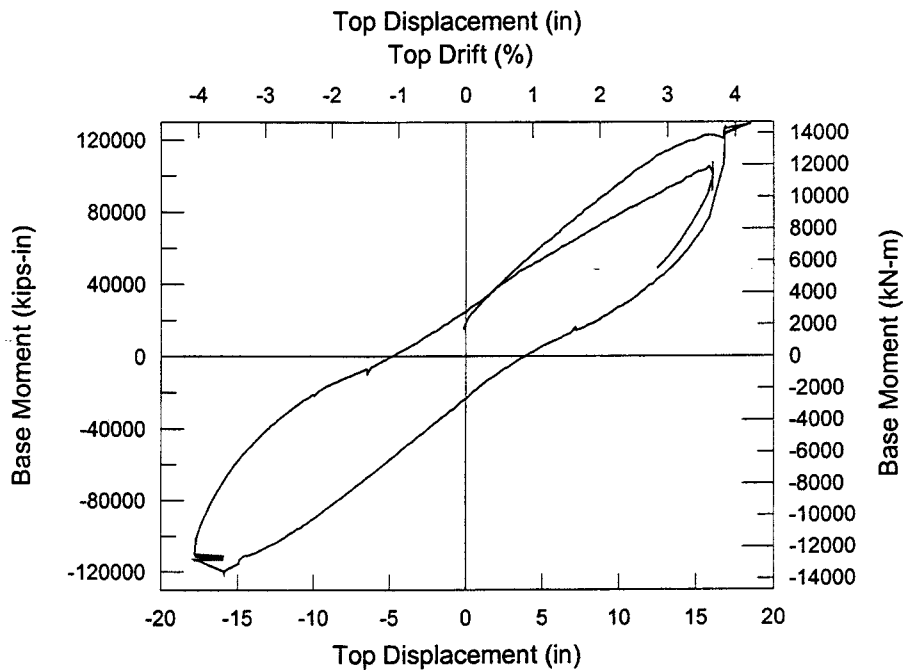
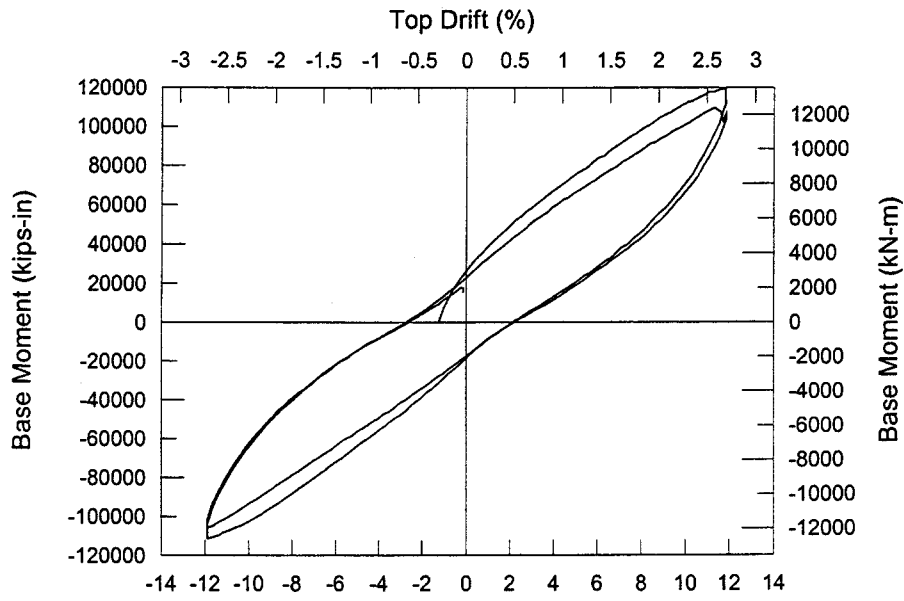


Figure 5.19 – Experimental results (IT4 and IT5)  
Base Moment- roof displacement hysteresis

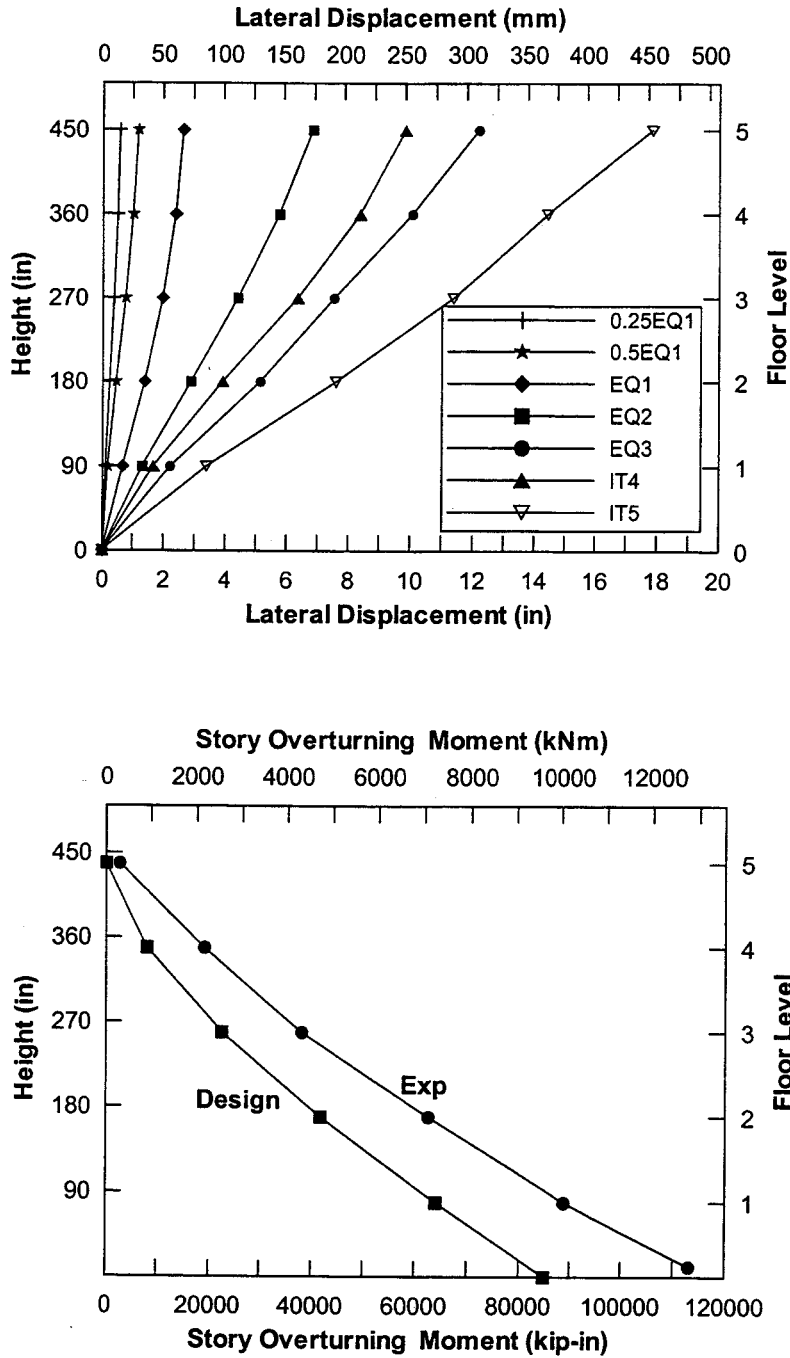


Figure 5.20 – Experimental results

- a) Peak Displacement profiles at different level of excitation
- b) Design vs. experimental story overturning moment envelope

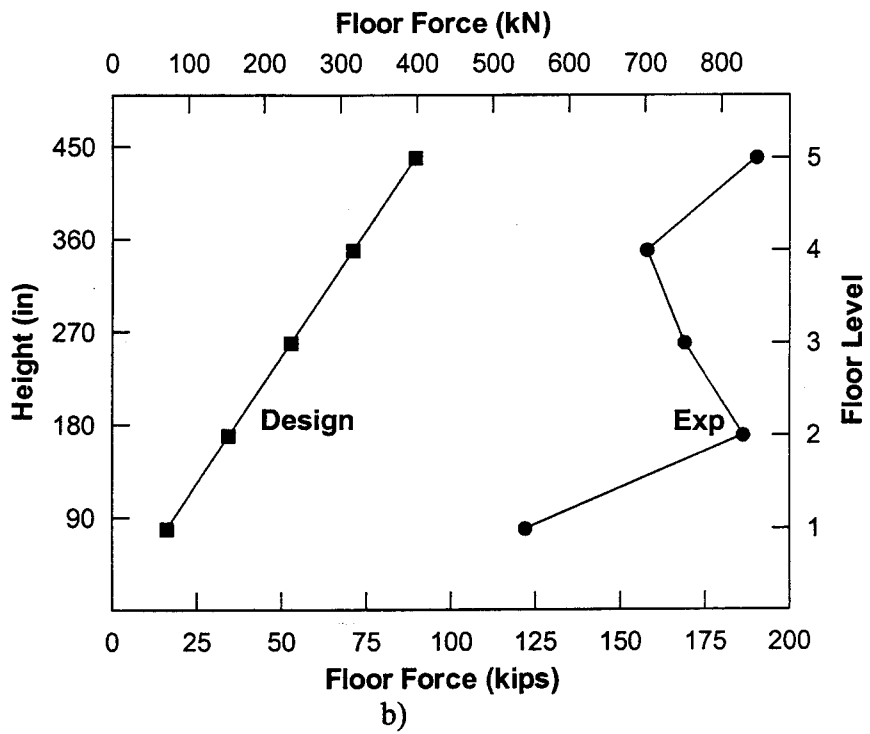
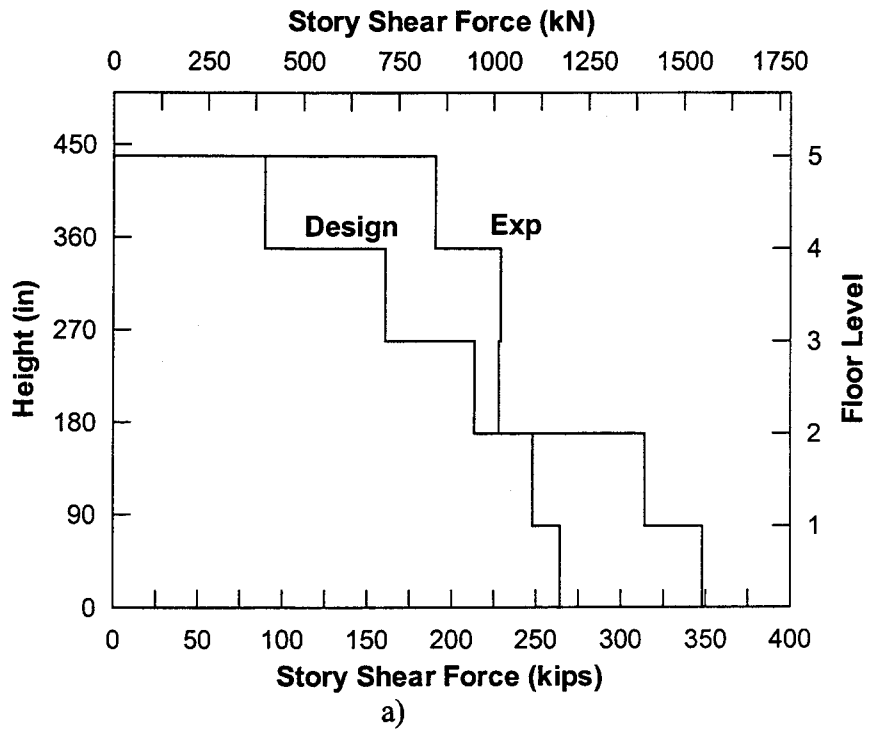


Figure 5.21 – Experimental results  
Design vs. Experimental Envelops a) Story shear forces b) Floor forces

Figures 5.20-5.21 compare the envelopes of experimental overturning moment, story shear forces and story force levels with the design envelopes.

While the expected general overstrength at different floors seems to be confirmed, the effects of higher mode of vibrations on the floor forces levels up to the height of the frames is significant. Floor forces greatly exceeding the design values at all heights of the building do not show any tendency to reduce in the lower levels, as would be expected from a predominantly first mode of response. While not significantly influencing the moment demand at the base, these high floor forces represent the magnitude of the diaphragm forces that must be distributed from floors to lateral forces-resisting elements and should be therefore be carefully addressed in the design phase.

### **5.3. Experimental-Analytical Comparison**

In order to predict the whole building response in the frame direction, the two finite element models of the Prestressed and TCY frames were analyzed in parallel, with the displacements constrained at each floor.

An initial comparison between the predicted and experimental response is provided by the base-moment/roof-displacement envelopes of Fig. 5.22. In this figure, the results from the analytical pushover analysis are compared with the full set of experimental results, including pseudo dynamic tests and inverted triangle tests.

The agreement is satisfactory in the small to moderate displacement range. However, a discrepancy is seen at large lateral displacements, with the analytical model predicting higher lateral strength than the experimental values. The reasons for this discrepancy are primarily the strength degradation of the non-prestressed frame (particularly the TCY-gap connections) at large drifts, and also due to not incorporating softening behavior of the beam-column connections, resulting from concrete crushing and cover spalling in the analytical model.

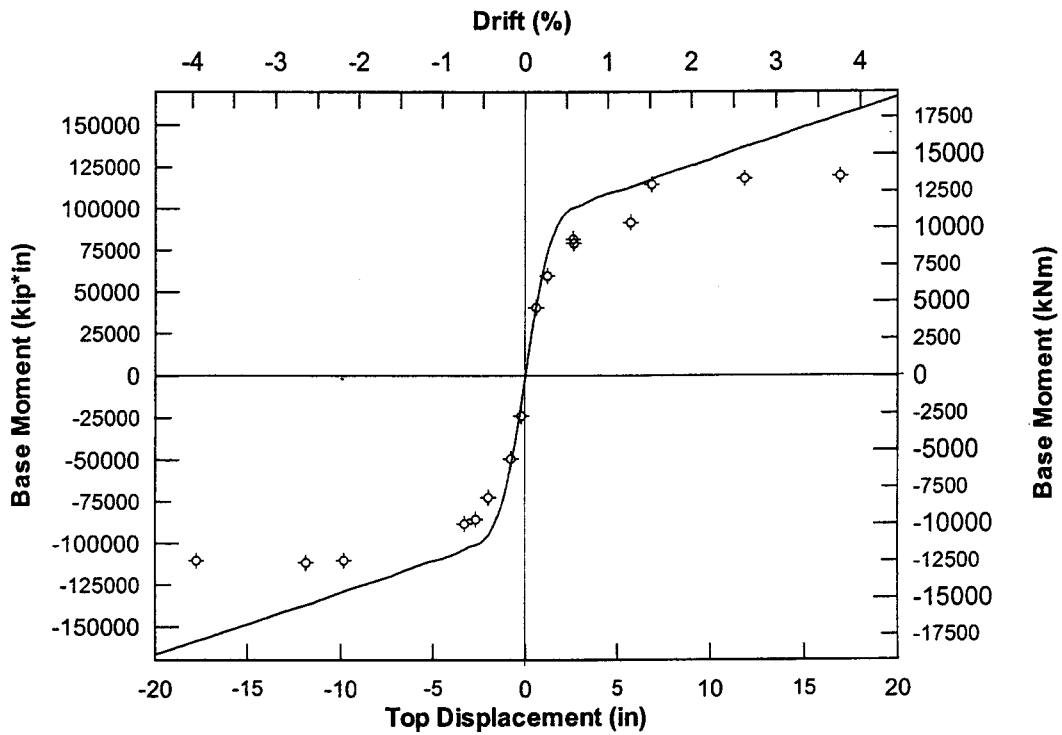


Figure 5.22 – Experimental-analytical comparison  
Moment-roof displacement envelope response

The increasing level of damage during the test was simulated imposing the same sequence of different hazard-level accelerograms, separated by padded windows to allow free oscillations, as illustrated in Figure 5.23.

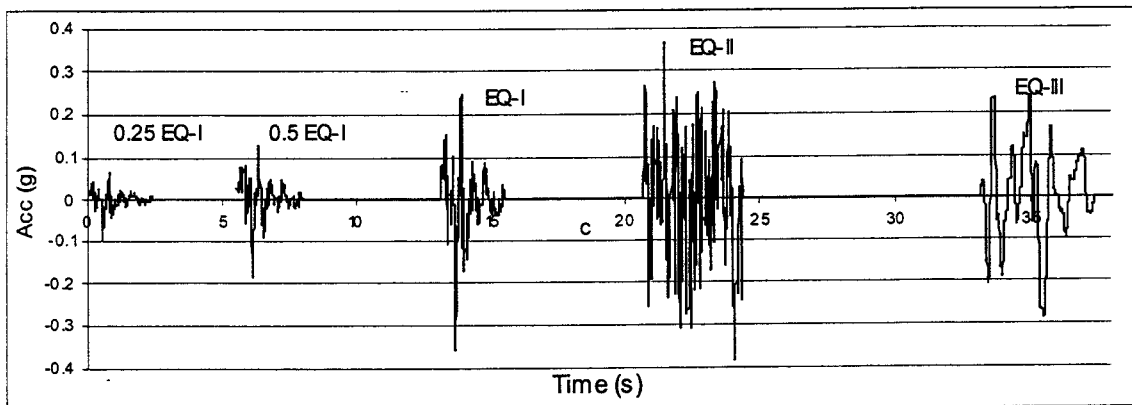


Figure 5.23 – Sequence of input accelerograms

An experimental-analytical comparison of the floor time-history is presented in Figures 5.24-5.25 in terms of floor displacement time-histories at EQ-II and EQ-III levels.

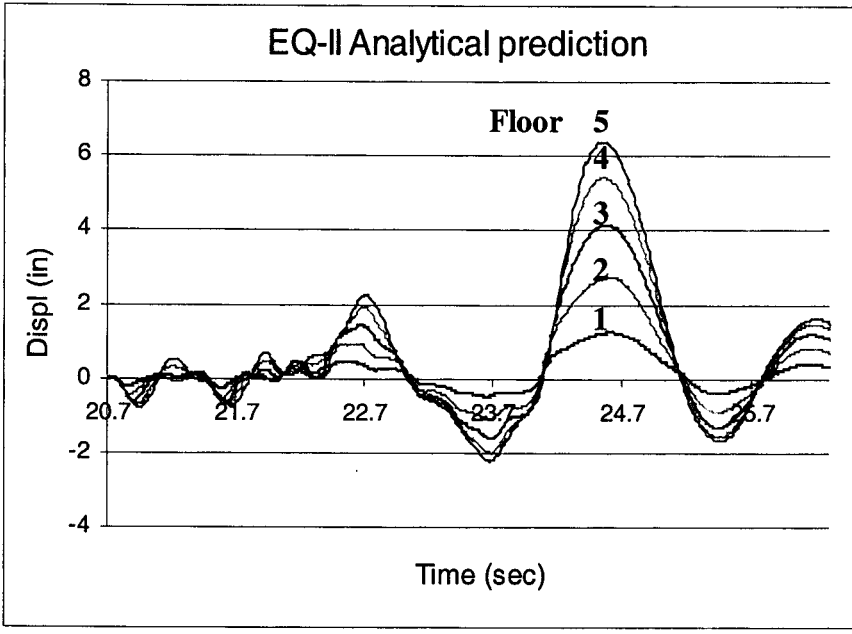
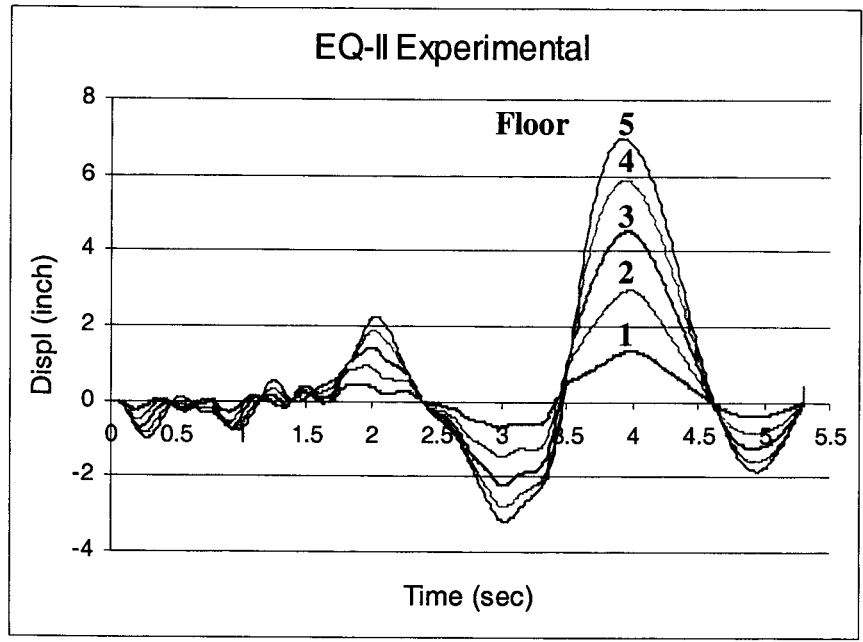


Figure 5.24 – Experimental-analytical comparison at EQ-II level Floors displacement time-history

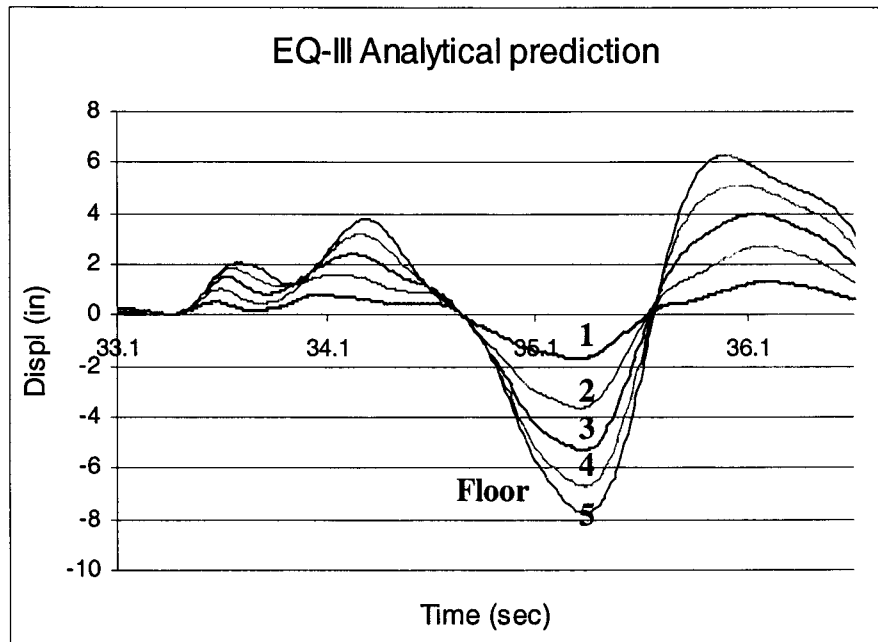
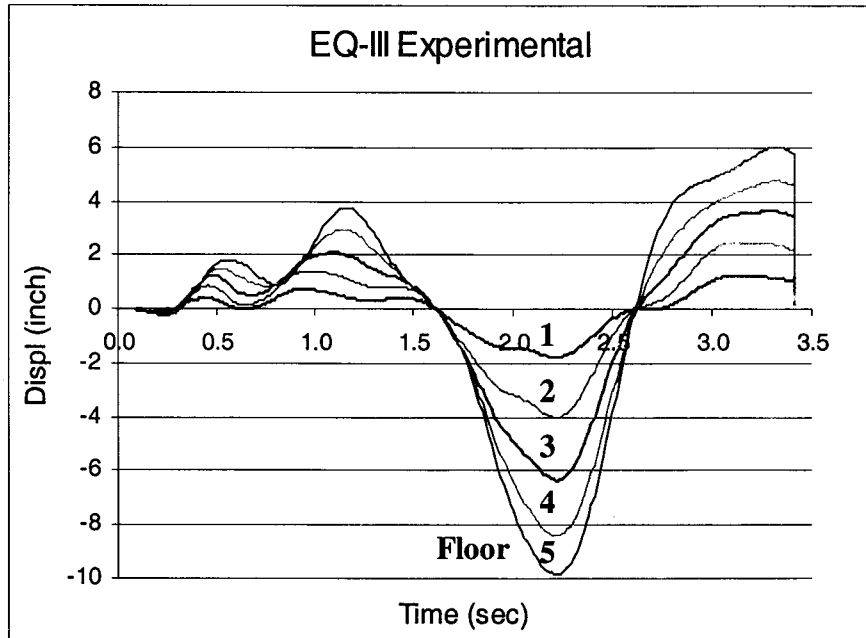


Figure 5.25 – Experimental-analytical comparison at EQ-III level  
Floors displacement time-history

The prediction is extremely satisfactory when taking into account the actual complexity of the test-building. The oscillation of each floor is generally well captured, showing a predominance of the first mode of vibration, as expected.

However, a general underestimation of the displacement peaks in the predictions must be underlined, possibly indicating the presence of excessive damping in the analytical model.

This overestimation of damping in the model was expected, as previously discussed. The analogy with ordinary reinforced concrete behavior, assumed (totally or partially) for all the connections except for the Pretensioned one, was realized using a modified Takeda model which seems to provide an overestimation of the energy dissipation capability of the section for the following reasons:

The unloading stiffness is determined by  $K = K_o \cdot (1/\mu^\alpha)$  where the usual upper-bound value of 0.5 for the coefficient  $\alpha$  can be too restrictive in such precast ductile connections.

Furthermore, the dependence of the unloading stiffness on the initial stiffness of the undamaged structure represents an additional source of excessive damping in the analyses.

The predicted hysteretic curves for the whole frame system have been shown in Chapter 4 and the equivalent viscous damping values evaluated ( $\xi_{pt\_pred}=14.5\%$  and  $\xi_{tcy\_pred}=20.3\%$  for the Prestressed and TCY frame respectively).

Since such predictions were based on ideal undamaged structures, the initial stiffness and, consequently, part of the unloading stiffness (contribution from the Takeda-type connections) were overestimated, when compared to the test structure, which was subjected to different damaging cycles before being tested at the EQ-III design level. An overestimation of the actual energy dissipation results as an obvious consequence, as experimentally observed.

The quasi-static cycles performed after each pseudo-dynamic test, with the top displacement being the maximum displacement reached in the previous test, confirmed the difference in the equivalent viscous damping values.

Figure 5.26 shows the experimental cycles performed at level EQ-III (top displacement 12.2 inch- 310 mm -) in terms of base shear vs. top floor displacement.

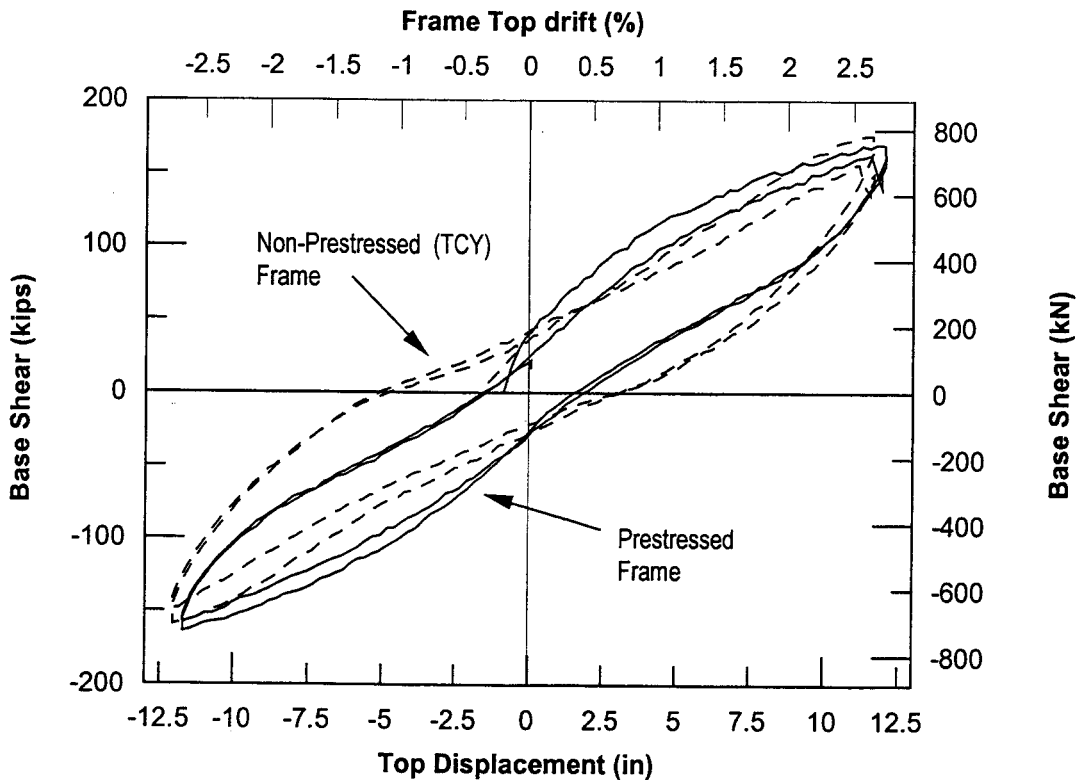


Figure 5.26 – Quasi-static response to inverse triangular loading (EQ-III level)

Equivalent viscous damping values are estimated in  $\xi_{pt\_exp}=11\%$  and  $\xi_{tcy\_exp}=15.6\%$  for the PT and TCY frame respectively, with an average  $\xi_{aver\_exp}=13.2\%$  for the whole structure, resulting in a value significantly lower than the design value ( $\xi=20\%$ ) assumed in the DBD procedure and also in the analytical model.

Once again it should be underlined that such a discrepancy is strongly related to the different initial conditions between the analytical model (undamaged) and the real test-structure:

(damaged). It is reasonable to assume that a comparison of hysteretic cycles within undamaged structures would significantly reduce the discrepancies between analytical and experimental results.

Figures 5.27-5.35 show experimental-analytical comparisons in terms of base shear and base moment time-histories. Again the agreement is satisfactory: the aforementioned effects of the higher modes response (particularly the second mode), which affects the base shear more than the base moment, are well predicted.

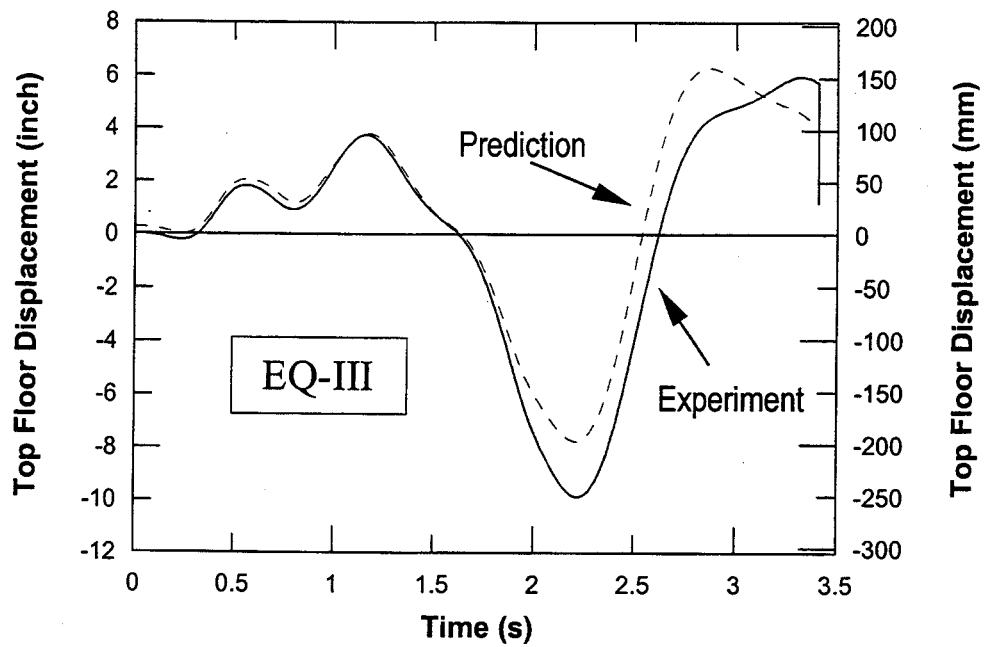
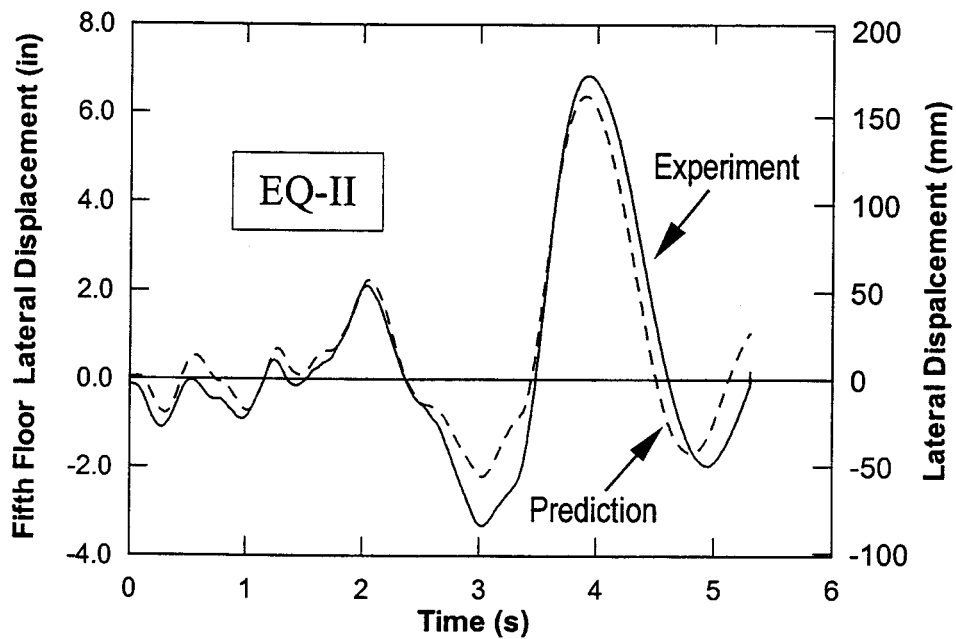


Figure 5.27 – Experimental-analytical comparison  
Roof-level displacement at EQ-II and EQ-III level

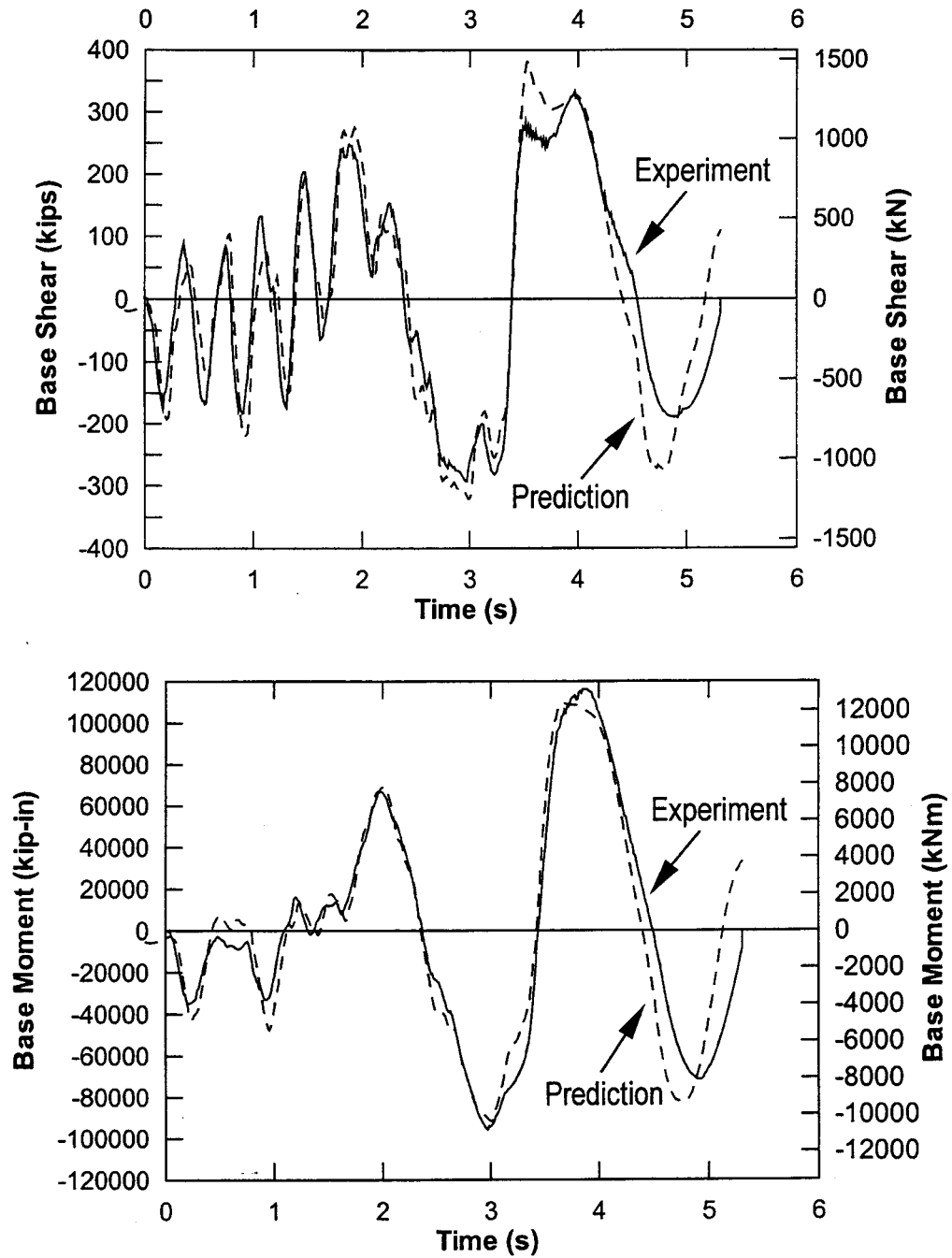


Figure 5.28 – Experimental-analytical comparison  
Base Shear and Base Moment at EQ-II level

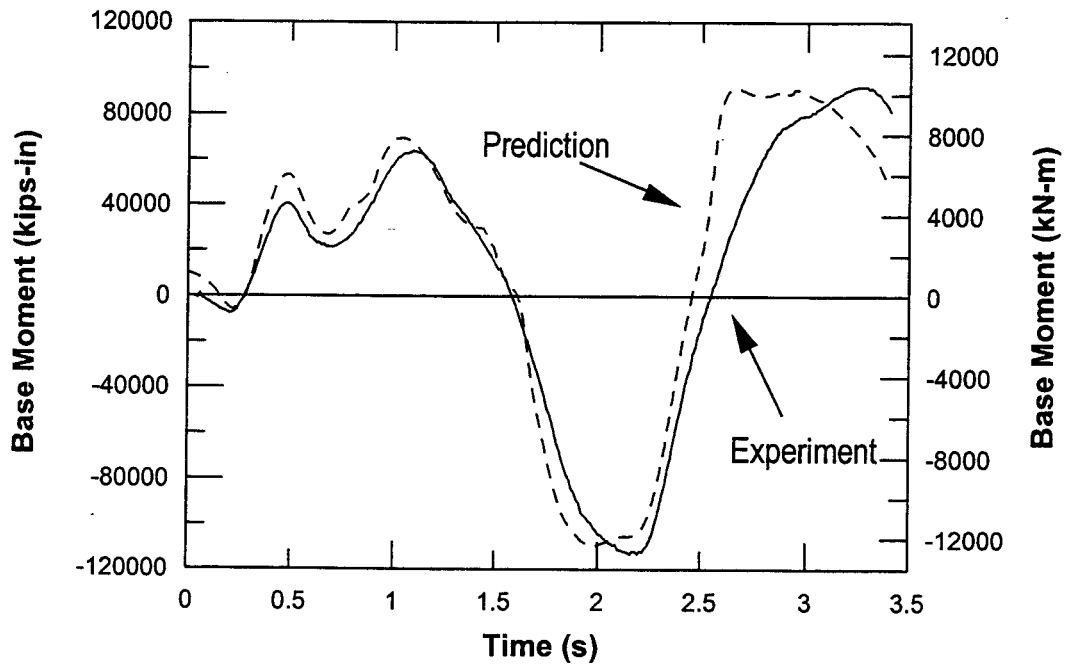
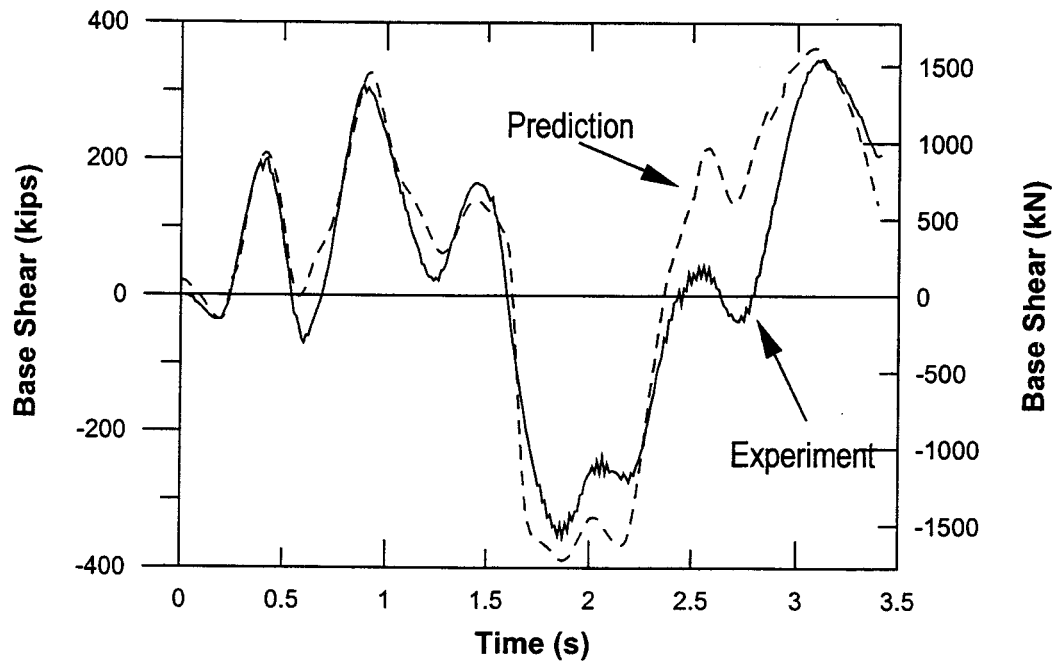


Figure 5.29 – Experimental-analytical comparison  
Base Shear and Base Moment at EQ-III level

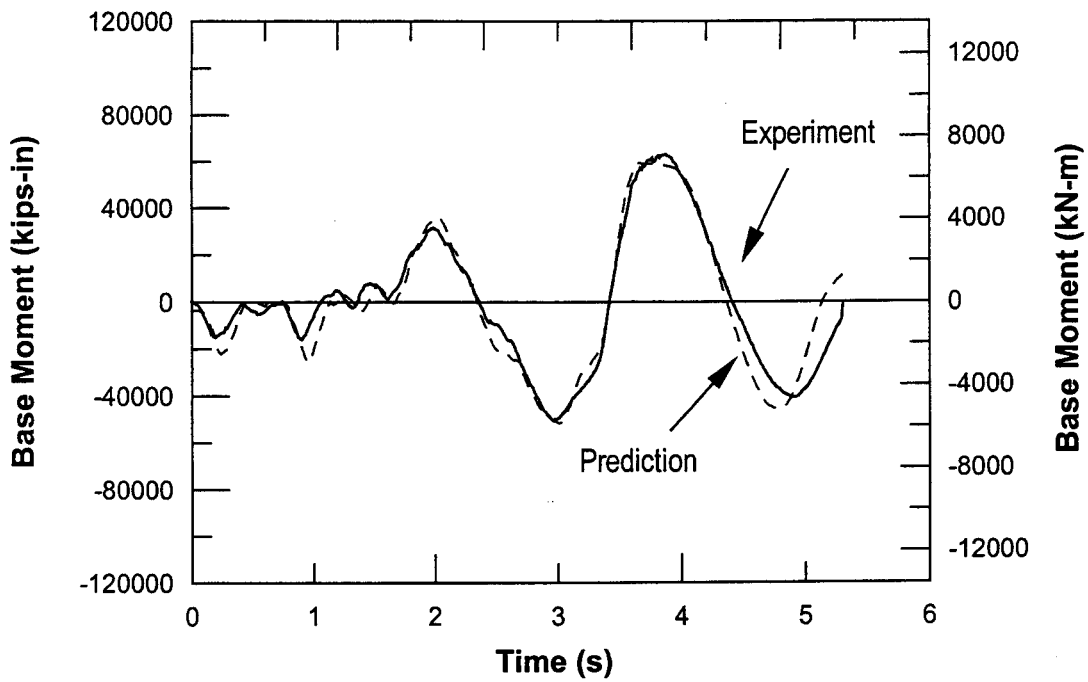
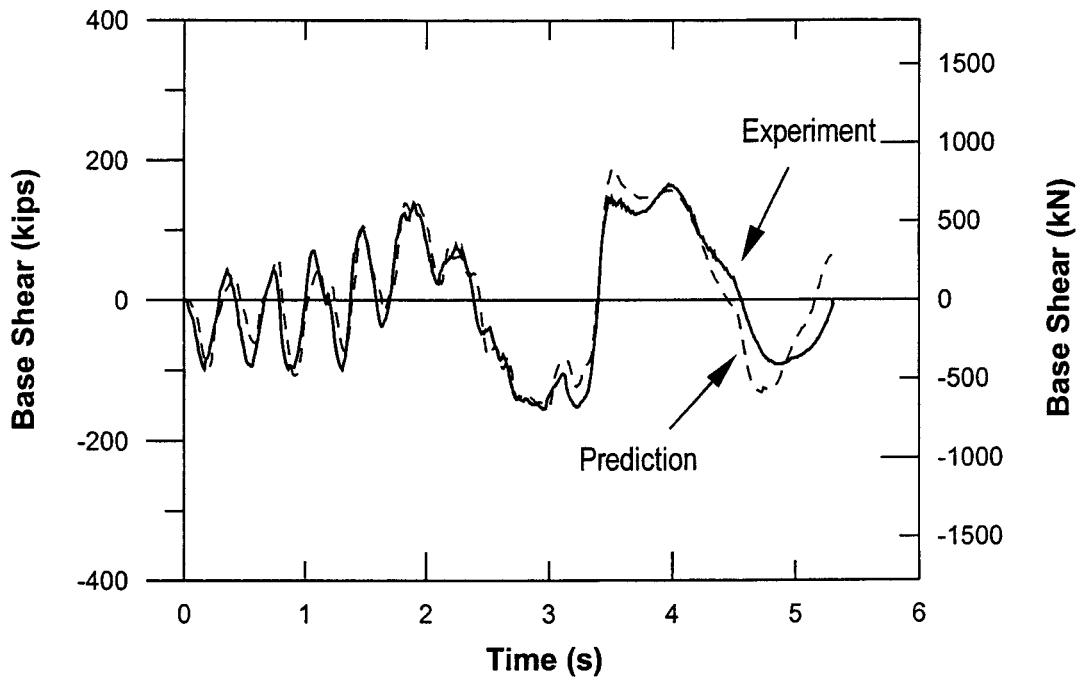


Figure 5.30 – Experimental-analytical comparison  
PT frame response at EQ-II level

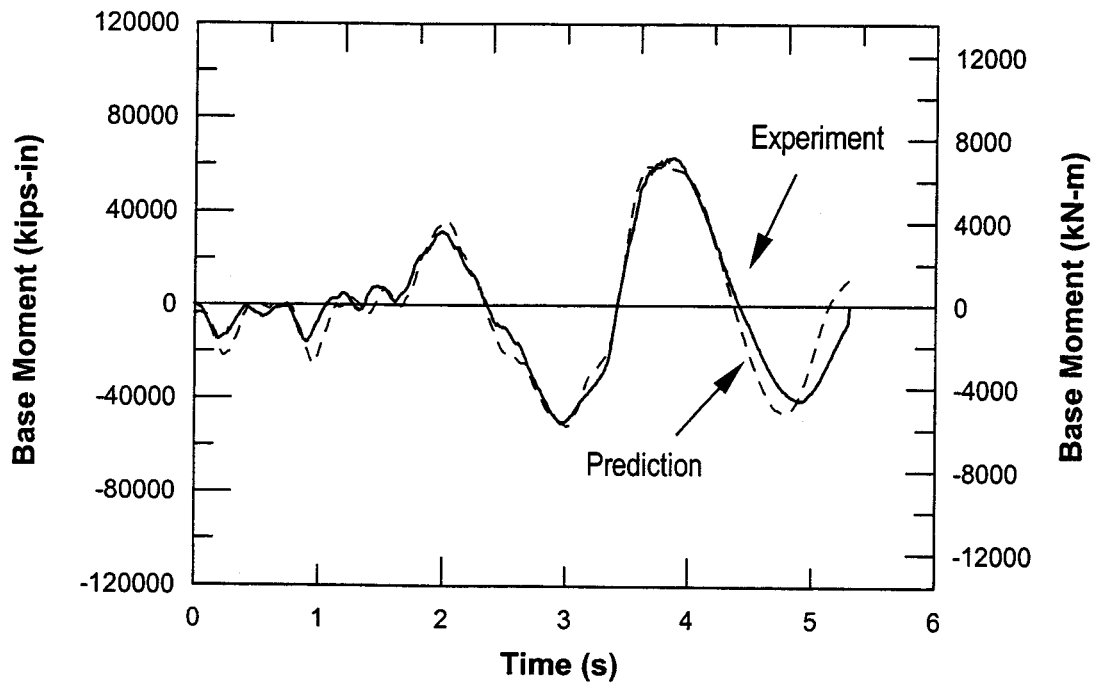
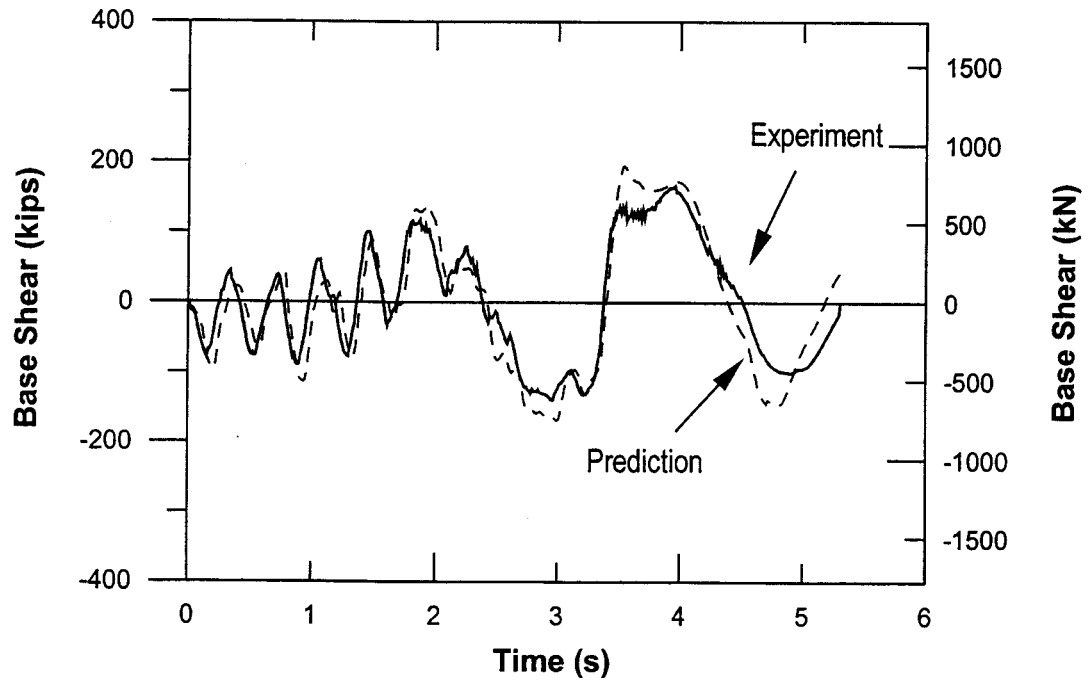


Figure 5.31 – Experimental-analytical comparison  
TCY frame response at EQ-II level

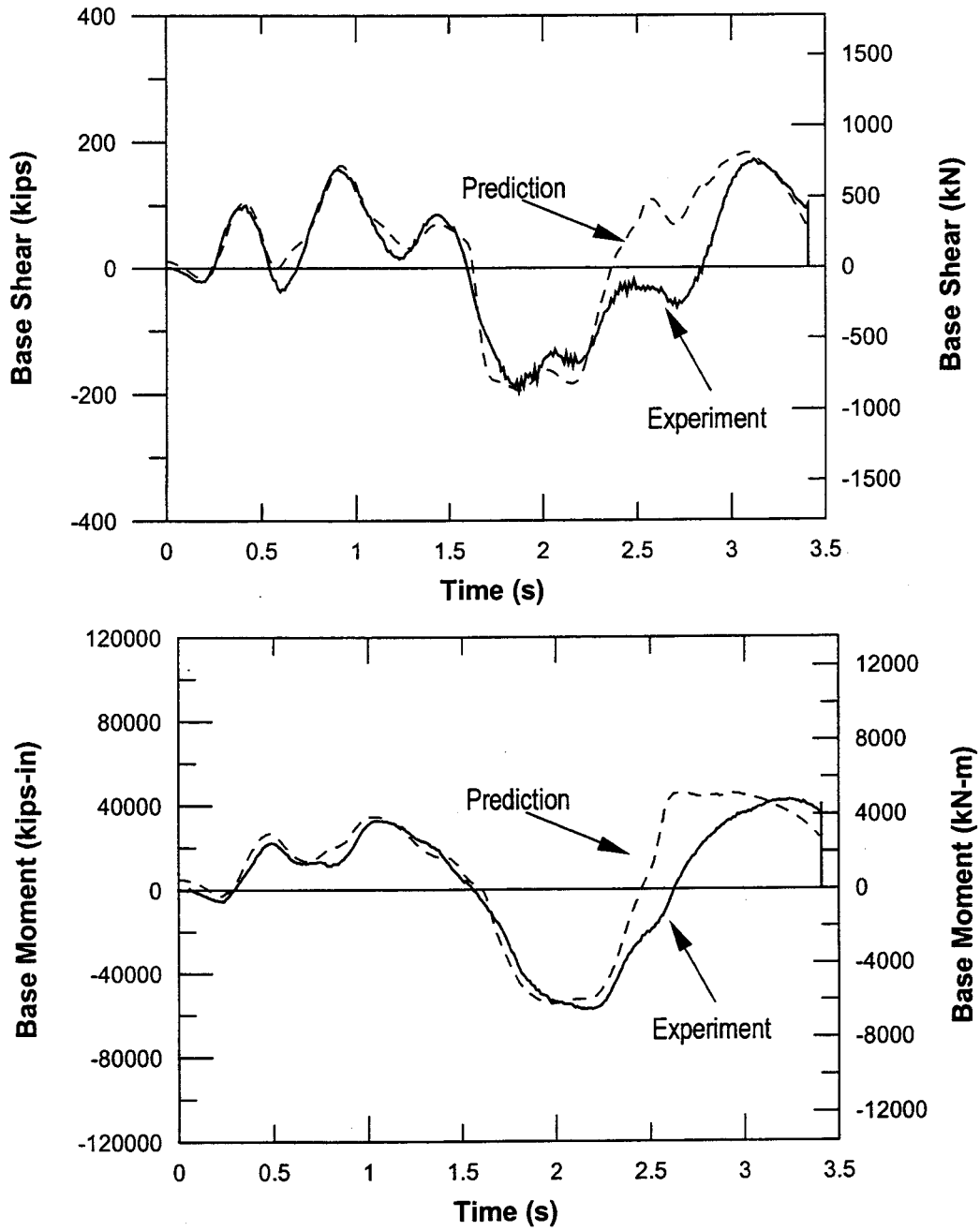


Figure 5.32 – Experimental-analytical comparison  
PT frame response at EQ-III level

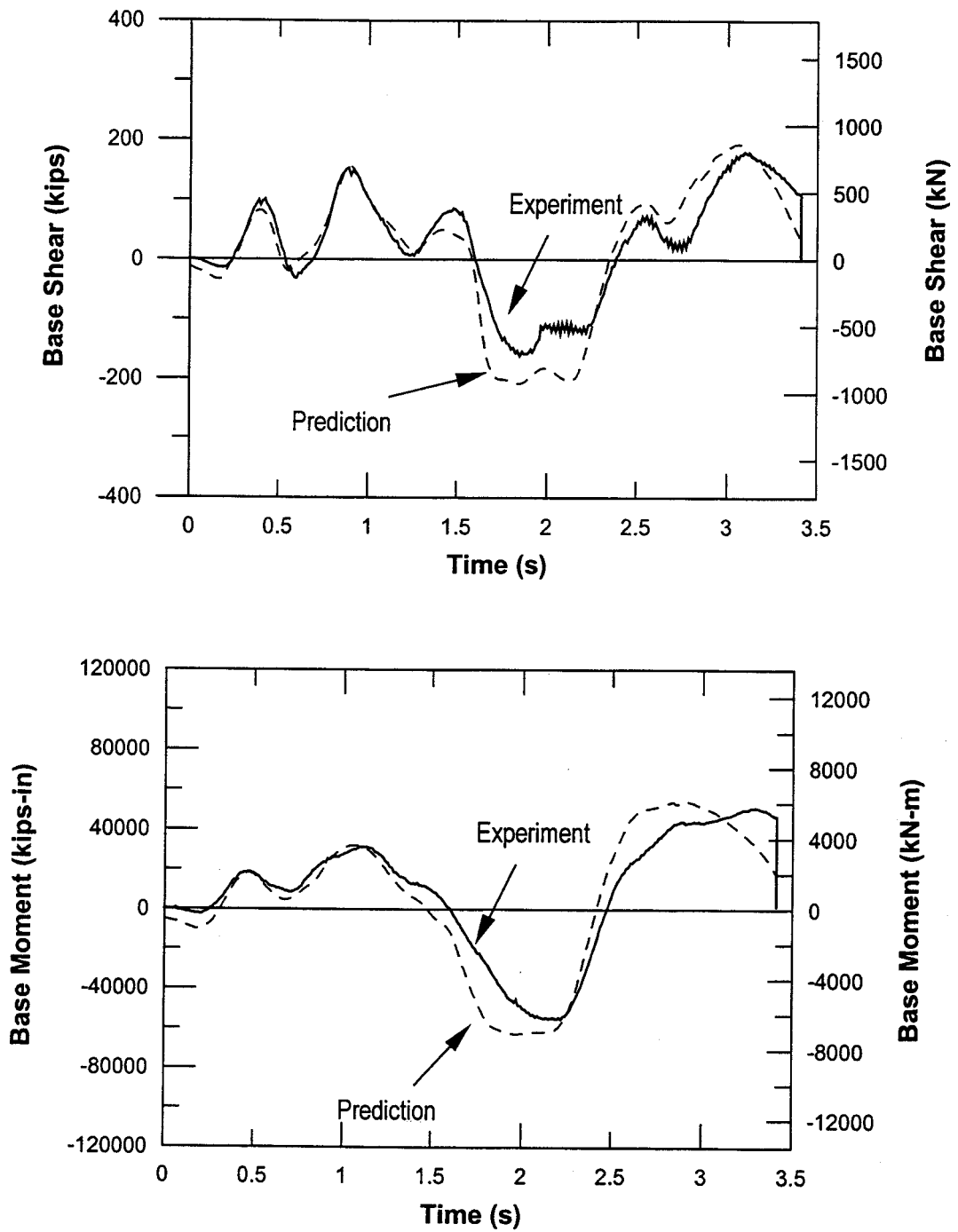


Figure 5.33 – Experimental-analytical comparison  
TCY frame response at EQ-III level

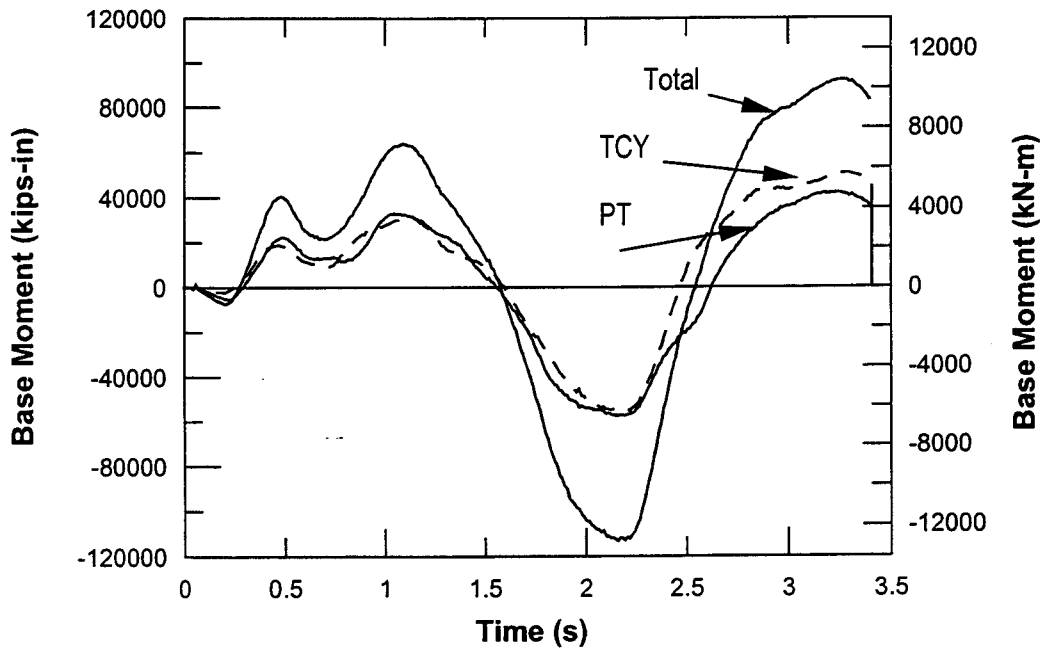
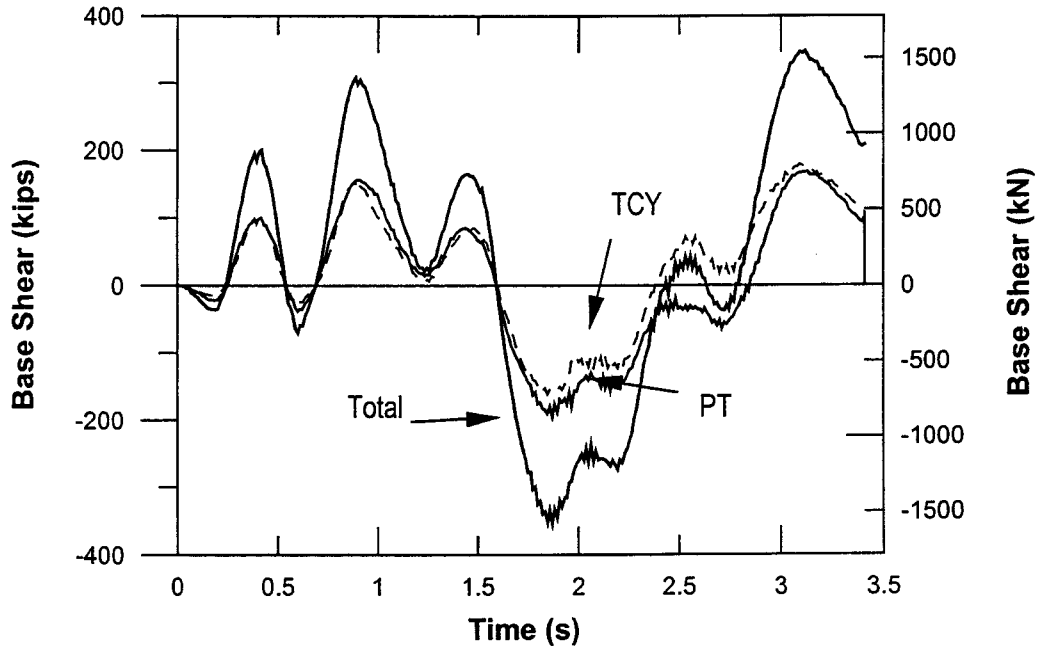


Figure 5.34 – Experimental-results  
PT and TCY frame contributions at EQ-II level

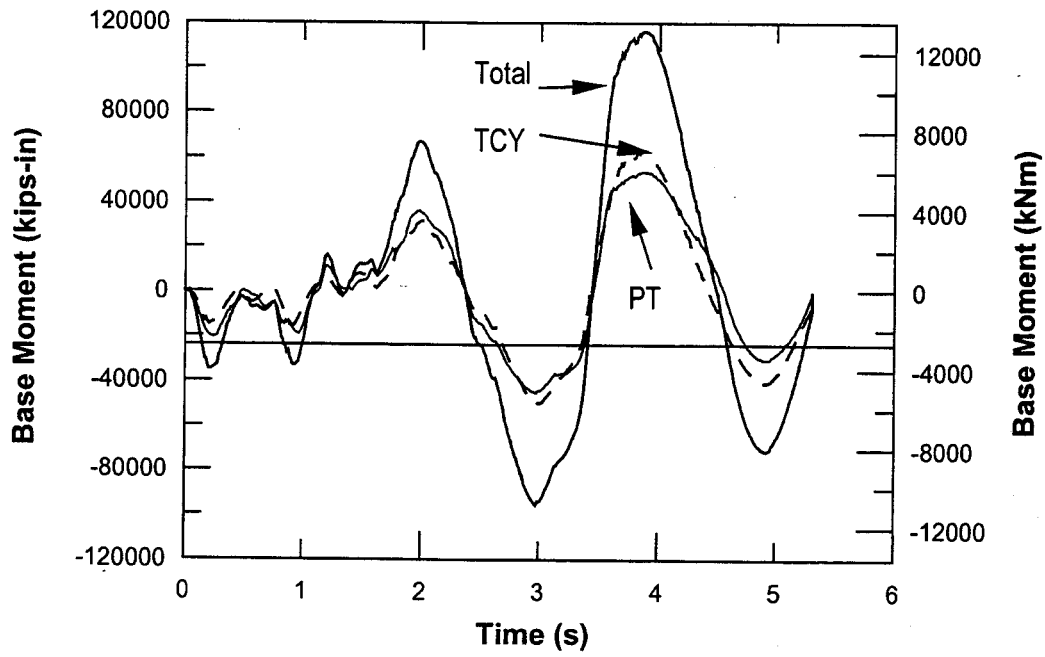
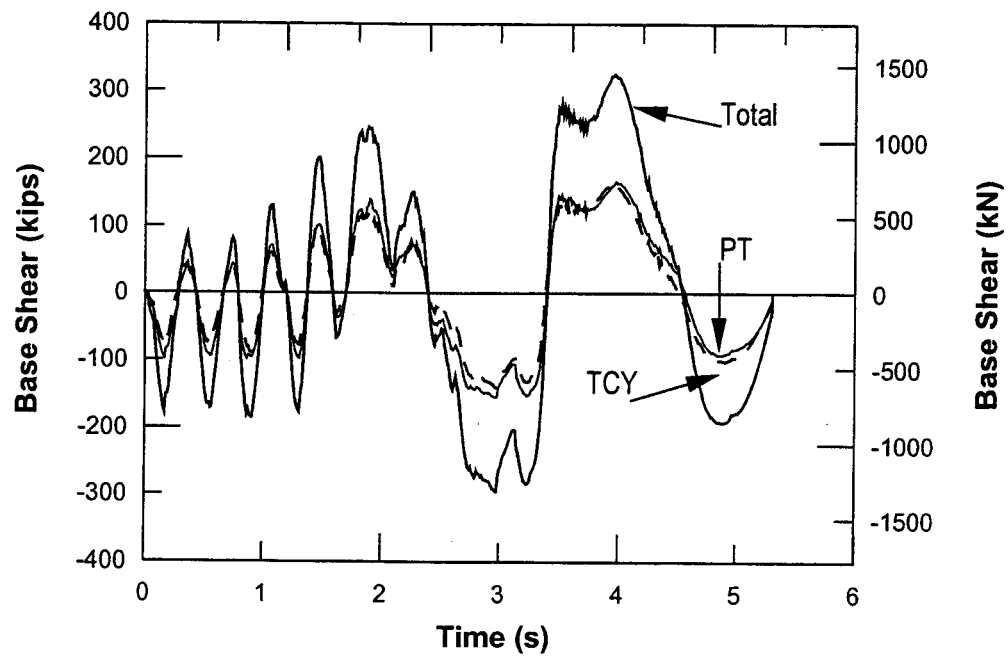


Figure 5.35 – Experimental-results  
PT and TCY frame contributions at EQ-III level

When analyzing the experimental/predicted contribution of the response of the two frame, the agreement is particularly satisfactory in the prestressed frame, while the unexpected damaging of the TCY-Gap connections affected the efficiency of the TCY frame in terms of strength, stiffness, and energy-dissipation capability, as can be clearly noted from (Figs. 5.33-5.34), where the different contribution of the two frames can be seen.

The accuracy of the model in the prediction of the response is thus reduced due to the occurrence of such localized damage, which, as anticipated, could be avoided with minor interventions at the design stage. Therefore, any experimental/analytical comparison has more significance for the EQ-II level of excitation, rather than for EQ-III and subsequent tests. Considering the simplicity of the structural model, the agreement between experiment and prediction is extremely satisfactory.

### **5.3.1. Validation of the Displacement-Based Design (DBD) Method**

The experimental results have confirmed the validity and reliability of the DBD procedure, whose intrinsic merits in the design of precast concrete structures have been previously underlined in paragraph 4.3.

The design drift level of 2% was closely attained in the pseudo-dynamic test under the EQ-III design level earthquake with an average experimental drift of 2.2%.

Although a difference of 10% in the estimation of the displacement of a real M.D.O.F. is already satisfactory, the effects of some discrepancies in the design phase should be taken into account:

- the overestimation of the equivalent viscous damping  $\xi=20\%$  in the design phase when compared to the real test-building behavior. The higher displacements obtained (experimental drift 2.2% vs design drift 2%) is a direct consequence of this.
- the overdesign of the connections. As previously discussed, an overstrength of almost 25% on the whole building base shear was predicted (336.6 kips, 1497 kN) with respect to the DBD ideal value (267.2 kips, 1188 kN). This was confirmed by the test, which presented a base shear envelope at EQ-III level significantly higher (347 kips, 1543 kN) than the design value, but extremely close to the predicted value.

It is reasonable to assume that a reduction of such differences with the ideal parameters coming from the DBD procedure could have led to an even better agreement with the results.

Furthermore, the basic assumption of a linear distribution of the maximum displacement envelope during the dynamic response was validated even if, as predicted by the model, a parabolic shape was observed at higher levels caused by the slight overstrength of the higher floors connections.

### 5.3.1.1. DBD Back-Calculations

Recalling the procedure described in the flow-chart of Figure 4.11, it is clear that fundamental assumptions in the DBD method are:

- 1) the structural deformed shape
- 2) the equivalent viscous damping of the S.D.O.F. substitute structure

An interesting “a posteriori” validation of the procedure can be performed correcting the erroneous initial assumptions and observing the corresponding variation on the Base Shear Design Value. The significant overstrength, analytically predicted and experimentally observed, should be captured.

Table 5.1 – DBD Procedure : original and back-calculations

		Displacement Shape	Average Drift (%)	Damping Ratio (%)	Base Shear	
					(kips)	(kN)
<b>Experimental</b>	EQ-III level	<b>experimental</b>	<b>2.2</b>	<b>13.3</b>	<b>347</b>	<b>1543</b>
<b>DBD</b>	Original Design	linear	2 (target)	20	267	1188
	Back validation	as experimental	2.2	13	322	1432
<i>linear</i>		<b>2.2</b>	<b>13</b>	<b>352</b>	<b>1566</b>	

Imposing the experimentally recorded (under the EQ-III level accelerogram) deformed-shape envelope and the average damping ratio value  $\xi=13.3\%$  as evaluated from the subsequent quasi-static test (top floor displacement close to 10 inch, 254 mm), the corresponding DBD Base Shear would be 322 kips (1432 kN), much closer to the experimental value. On the other hand, excellent agreement would derive from assuming a simple linear deformed shape distribution (as in the DBD procedure) with an average drift of 2.2% (as experimentally recorded) and an

approximate damping value of  $\xi=13\%$ : the design base shear would have been 352 kips (1565 kN).

The latter considerations are summarized in Table 5.1.

### Considerations

In Figure 5.36 the expected (design value) Base Shear ( $V_b$ ) derived with the BDB method is reported (normalized) for different levels of damping ratio ( $\xi$ ). The nature of the displacement spectra adopted (from SEAOC Bluebook) imposes that the relationship between the two parameters is governed by a multiple of the displacement reduction factor  $\eta$  squared.

In fact,

$$V_b = K_{eff} \cdot \Delta_d,$$

where:

$$K_{eff} = 4\pi^2 \frac{m_e}{T_{eff}^2} \quad T_{eff} = \frac{T_q}{\Delta_q} \frac{\Delta_d}{\sqrt{\left(\frac{7}{2+\xi}\right)}} \quad \eta = \sqrt{\left(\frac{7}{2+\xi}\right)}$$

Thus,

$$\Rightarrow V_b = const_1 \cdot f(\eta)$$

$$\Rightarrow V_b \propto \eta^2$$

$$\Rightarrow V_b \propto \left(\frac{7}{2+\xi}\right)$$

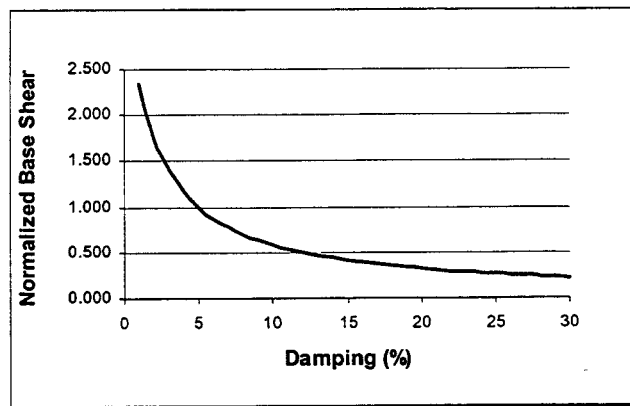


Figure 5.36 – Base Shear-Damping ratio relationship

Fortunately, in the damping range of interest, an overestimation of the damping level at the design phase, leads to a relatively less significant underestimation of the necessary design base shear. For example, maintaining the target design drift at 2%, the experimentally observed Base Shear value (347 kips, 1543 kN) can be obtained if a damping ratio  $\xi=15\%$ , instead of the assumed  $\xi=20\%$ , is estimated: an overestimation close to 33% on the damping capabilities of the

structure would have produced in this case an underestimation of 22% of the necessary strength of the structure at that target displacement (267 kips vs. 347 kips).

It should be underlined, however, that, when approaching smaller level of damping, as typical of precast ductile connections with unbonded tendons, such differences become more significant and less conservative. An erroneous overestimation of the damping in the design phase can produce dangerous underestimation of the design base shear and, consequently, higher displacements (damage) than expected under seismic action.

This undesirable effect is naturally reduced in the case of precast concrete ductile connections without unbonded tendons, which more reflect the behavior of cast-in-place reinforced concrete. A range of higher dissipation capability is in fact guaranteed.

Based on these considerations, the importance of a simple but accurate analytical procedure to predict the behavior of connections utilizing "unbonded" concepts is even more emphasized. On the other hand, the slight (though not significant) overdesign of the structure, which typically characterizes the design phase and other different sources of overstrength, can favorably balance the effects of a possible erroneous overestimation of the structural damping, limiting the structural response displacements to values extremely close to the target design assumptions, as in the case of the PRESSS Test-Building response. But, obviously, a conservative design procedure cannot count on the possible positive effects of similar structural uncertainties such as the material overstrength.

## CHAPTER 6

### CONCLUSIONS

#### 6.1. Brief Summary of the Research Results

Recent developments in the research of precast concrete structures for seismic areas have resulted in the experimental validation of the seismic efficiency of different innovative categories of beam-column ductile connections for frame systems, conceived as alternatives to the traditional approach of “emulating” of cast-in-place reinforced concrete.

The basic scheme of such connections is the adoption of “unbonding” concepts, in the form of unbonded post-tensioned tendons, partially ungrouted mild steel, or a combination of the above. In these cases, a simple analytical description of the behavior of the connection, in the common form of a moment-curvature (or rotation) curve, is seriously complicated by the fact that the strain compatibility in the section, a typical assumption in section analysis, is violated.

Alternative approaches, at different levels of complexity have been developed in the past and proposed in literature:

- calibration of the hysteretic parameters on experimental results
- section analysis with discrete (trilinear) idealization of the moment-rotation behavior
- finite element analysis with use of fiber elements

In the work herein described, a critical review of the past research has been given and a simple and rigorous step-by-step general procedure for a section analysis in presence of strain incompatibility has been proposed, as a valid approach to describe the response of precast frame ductile connections.

Based on the concept of member strain compatibility, an analogy with equivalent cast-in-place connections (named monolithic beam analogy) has been introduced, to provide an additional condition on the global member behavior (displacement) necessary to develop a complete moment-rotation curve of the section.

The analytical general procedure has been validated with the experimental tests on hybrid beam-column subassemblies conducted at National Institute of Standard and Technology (NIST). Based on the former validation, the four different ductile connections adopted in the 5-story PRESSS building test (Pretensioned, Hybrid, TCY and TCY-Gap) have been modeled and included in a finite element model for the prediction of the response of the building test under simulated earthquake loading at different levels.

Analytical predictions as well as preliminary comparisons with the experimental global behavior in the frame direction have been presented, indicating a very good agreement with the results of the pseudodynamic tests, in terms of base shear, base moment, and floor displacement time-histories. The noted general underestimation of the displacement peaks in the prediction is explained by an inherent overestimation of the damping in the analytical model, mostly due to the characteristic of the hysteretic scheme adopted. Furthermore, the unexpected damage occurred to the TCY-Gap connection concurred in progressively reducing, at increasing levels of excitations, the accuracy of the model in the prediction of the response.

In general, the simplicity of the proposed procedure and its validity in predicting the moment-rotation behavior of precast frame ductile connections make it a valuable analysis tool.

## **6.2. Further Investigations and Possible Applications**

If based on the aforementioned analytical approach the modeling of precast frame systems with ductile connections can be conceptually simplified (while still reliable), extensive numerical investigations on the seismic response of these systems can be carried out.

In particular, the effect of alternative design strategies, in terms of connection typologies or design methods (Force-Based-Design or Displacement Based Design), on the structural seismic performance can be compared in order to develop a flexible and rational design procedure for precast frame systems, with possible suggestions for code provisions.

For this purpose, critical design structural parameters as the force or displacement reduction factors ( $R$  and  $\eta$  respectively) and equivalent viscous damping ratio  $\xi$ , can be evaluated depending on the different connections adopted.

The analytical procedure presented herein has been conceived as a general method for a section analysis in presence of restraints of local strain in-compatibility, such as the presence of unbonded tendons/bars, ungrouted mild steel over a short length (with possible combination of the above) or similar restraints. Although applied to the particular case of beam-column precast connections in this study, its conceptual nature suggests the possibility to extend it, with adequate modifications to the basic scheme, to any other similar case of segmental constructions (i.e. segmental bridges) where precast/prestressed elements are tied together with unbonded post-tensioning techniques.

Furthermore, the range of applicability of the proposed approach, based on the monolithic beam analogy concept, is not limited to precast concrete but more generally applicable to the section analysis of ordinary cast-in-place reinforced concrete.

Finally, the validity of the approach is not exclusively related to seismic considerations but can be extended to static analyses under vertical loads, based on a limit state approach, where the definition of a moment curvature (rotation) curve of the critical section is required.

## REFERENCES

- Bychenkov, Y., (1978), "Aseismic Structures with Precast Members", *Proceedings of the FIP 8th Congress*, London, pp. 70-90
- Brewer, L., "Analysis of the Effect of Hysteretic Relationships in Beam-Column Connections on the Earthquake response of Precast Concrete Frame Systems", M.S. thesis, University of Texas at Austin.
- Carr, A., J., (1998), "Ruaumoko Program for Inelastic Dynamic Analysis – Users Manual", Department of Civil Engineering, University of Canterbury, Christchurch, New Zealand.
- Cheok, G.S. and Lew, H., (1990), "Performance of 1/3-Scale Model Precast Concrete Beam-Column Connections Subjected to Cyclic Inelastic Loads" – NISTIR 4433, National Institute of Standards and Technology, NIST, Gaithersburg, MD
- Cheok, G.S. and Lew, H., (1991), "Performance of 1/3-Scale Model Precast Concrete Beam-Column Connections Subjected to Cyclic Inelastic Loads" – Report No. 2 NISTIR 4589, National Institute of Standards and Technology, NIST, Gaithersburg, MD
- Cheok, G.S. and Lew, H., (1993), "Model Precast Concrete Beam-Column Connections Subjected to Cyclic Loading", *PCI Journal*, Precast/Prestressed Concrete Institute, Vol.38, No.4, pp.80-92
- Cheok, G.S. and Stone, W.C., (1994), "Performance of 1/3-Scale Model Precast Concrete Beam-Column Connections Subjected to Cyclic Inelastic Loads" – Report No. 4 NISTIR 5436, National Institute of Standards and Technology, NIST, Gaithersburg., MD
- Cheok, G.S., Stone, W.C. and Kunnath, S. K., (1998), "Seismic Response of Precast Concrete Frames with Hybrid Connections", *ACI Structural Journal*, Vol. 95, No.5, pp.527-539.

- Conley, J.R., Priestley, M.J.N., Sritharan, S., (1999), "Wall Direction Modeling of the Five-Story PRESSS Precast Test Building", Report SSSRP 99/19, University of California, San Diego, CA.
- El-Sheikh, M., Sause, R., Pessiki, S., Lu, L.-W., Kurama, Y., (1998), "Seismic Analysis, Behavior and Design of Unbonded Post-Tensioned Precast Concrete Frames", PRESSS Report No. 98/04, LU Report No. EQ-97-02, Lehigh University, Bethlehem, Pennsylvania
- Igarashi, A., Seible, F., Hegemeir, G and Priestley, M.J.N, (1994), "The U.S. TCCMAR Full-Scale Five-Story Masonry Research Building Test, Part III – Seismic Load Simulation", *Structural Systems Research Project*, University of California, San Diego, SSRP Report No. 94/03.
- MacRae, G., and Priestley, M.J.N., (1994), "Precast Post-tensioned UngROUTED Concrete Beam-Column Subassemblage Tests", Structural System Research Report, SSRP 94/10, University of California at San Diego, La Jolla, CA, 124 pp.
- Mander, J.B., Priestley, M.J.N., and Park, R., (1988) "Theoretical Stress-Strain Model for Confined Concrete", *Journal of the Structural Division, ASCE*, Vol. 114, No. 8,, pp.1804-1826
- Nakaki, S.D., Stanton, J.F., and Sritharan, S., (1999), "An Overview of the PRESSS Five-Story Precast Test Building", *PCI Journal*, Vol.44, No.2, pp.26-39.
- Palmieri, L., (1996) , "Evaluation of Ductile Connections for Precast Frame Systems", Ph.D. Dissertation, University of Minnesota.
- Palmieri, L., Saqan, E., French, C and Kreger, M., (1997) , "Ductile Connections for Precast Concrete Frame Systems", Paper No. SP162-13, *Metu A. Sozen Symposium*, ACI SP 162, American Concrete Institute, Farmington Hills, MI, pp.313-355.

- Pampanin S., Priestley, M.J.N., Sritharan, S., (1999), "Frame Direction Modeling of the Five-Story PRESSS Precast Test Building", Report SSSRP 99/20, University of California, San Diego, CA.
- PBSE Ad-Hoc Committee of Structural Engineers Association of California, APPENDIX G, (1988) – Tentative Performance Based Seismic Engineering Guidelines, *SEAOC Bluebook*.
- Park, R., (1990), "Precast Concrete in Seismic-Resisting Building Frames in New Zealand", *Concrete International*, Vol.12, No.11, pp.43-57
- Popovics, S., (1973), "A numerical Approach to the Complete Stress-Strain Curves for Concrete", *Cement and Concrete Research*, Vol.3, No.5, pp.583-599.
- Priestley, M.J.N., (1991), "Overview of the PRESSS Research Program", *PCI Journal*, Vol.36, No. 4, pp.50-57
- Priestley, M.J.N., (Editor), (1992), Third Meeting of the U.S. Japan Joint Technical Coordinating Committee on Precast Seismic Structural Systems (JTCC-PRESSS), Report No. 92/05.
- Priestley, M.J.N. and Tao, J.R., (1993), "Seismic response of Precast Prestressed Concrete Frames With Partially Debonded Tendons", *PCI Journal*, Vol. 38, No.1, pp.58-67.
- Priestley, M.J.N. and MacRae, G., (1994), "Precast Post-Tensioned UngROUTED Concrete Beam-Column Subassemblage Tests"; *Structural Systems Research Project*, University of California, San Diego, Report No. SSRP-94/10.
- Priestley, M.J.N., et al. (1995), "Northridge Earthquake of January 17, 1994 Reconnaissance Report- vol.2", *Earthquake Spectra*, Supplement C to Volume 11.
- Priestley, M.J.N., (1996), "Seismic Design Philosophy for Precast Concrete Frames ", *Structural Engineering International*, Vol. 6, No.1, pp.25-31.
- Priestley, M.J.N., (1996), "The PRESSS Program –Current Status and Proposed Plans for Phase III", *PCI Journal*, Vol 41, No.2, pp.22-40.

- Priestley, M.J.N. (1998), "Displacement Based Approaches to Rational Limit States Design of New Structures", Keynote Lecture *Eleventh European Conference on Earthquake Engineering*, Paris.
- Priestley, M.J.N., Sritharan, S., Conley, J.R. and Pampanin, S., (1999), "Preliminary Results and Conclusions From the PRESSS Five-Story Precast Concrete test Building", *PCI Journal*, Vol.44, No.6, pp.42-67
- Restrepo, J. I., Park, R. and Buchanan, A. H., (1992), "Tests on Precast Concrete Resisting Frame Components Typical of New Zealand". *Proceedings of the 10<sup>th</sup> World Conference on Earthquake Engineering*, Madrid, vol.8, pp.4395-4402.
- Restrepo, J. I., (1993), "Seismic Behaviour of Connections Between Precast Concrete Elements", Ph.D. Dissertation, Department of Civil Engineering, University of Canterbury, Christchurch, New Zealand
- SHAPE, (1988), Earth Mechanics Computer Program, Fountain Valley, California
- Sagan, E., I., (1996) "Evaluation of Ductile Beam-Column Connections for Use in Seismic-Resistant Precast Frames", Ph.D. Dissertation, University of Texas at Austin.
- Shibata, A., and Sozen, M., (1976) "Substitute Structure Method for Seismic Design in Reinforced Concrete", *Journal of Structural Division, ASCE*, Vol. 102, No. 6.
- Sritharan, S., Priestley, M.J.N., Seible, F. and Igarashi, A., (2000.), "A Five Story Precast Concrete Test Building for Seismic Conditions – an Overview", *Proceedings of the Twelfth World Conference on Earthquake Engineering*, Auckland, New Zealand, Paper No. 1299.
- Stanton, J.F., Stone, W.C., and Cheok, G.S., (1997), "A Hybrid Reinforced Precast Frame for Seismic Regions", *PCI Journal*, Vol. 42, No.2, pp.20-32

Stanton, J.F., Collins, R.H., Galusha, J.G., Sugata, M., Nakaki, S.D., (2000), "A Five Story Precast Concrete Test Building for Seismic Conditions – Design Details", *Proceedings of the Twelfth World Conference on Earthquake Engineering*, Auckland, New Zealand, Paper No. 1297.

Stone, W.C., Cheok, G. S. and Stanton, J. F., (1995), "Performance of Hybrid Moment-Resisting Precast Beam-Column Connections Subjected to Cyclic Loading", *ACI Structural Journal*, Vol.92, No.2, pp.229-249

Takeda, T., Sozen, M., and Nielsen, N., (1970) "Reinforced Concrete Response to Simulated Earthquake", *Journal of Structural Division, ASCE*, Vol.96, No.12

Uniform Building Code, (1997), *International Conference of Building Officials*, Whittier, CA.

**APPENDIX A**

**PHOTO DOCUMENTATION**



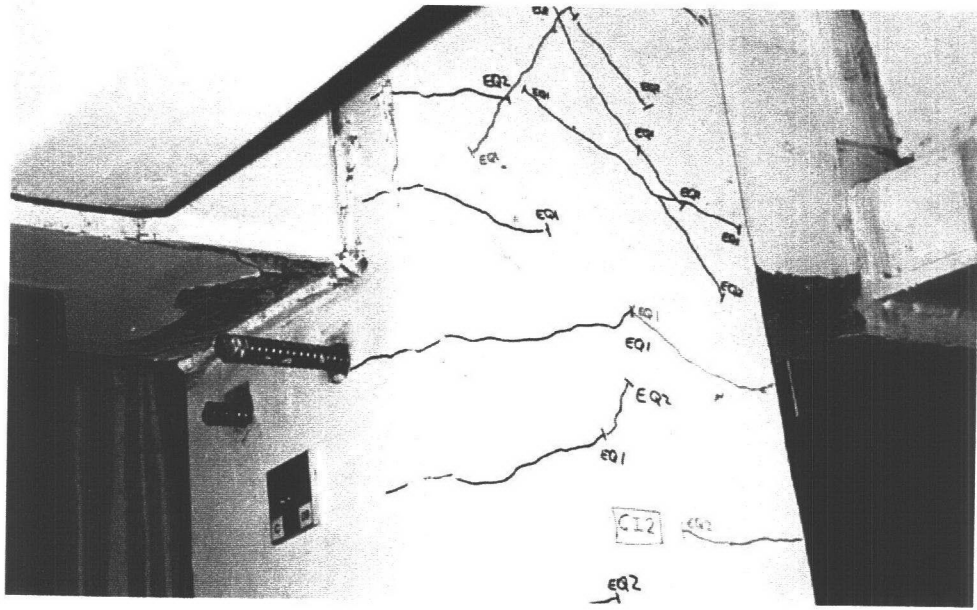


Figure. A.2 – TCY-Gap connections EQ2 Excitation (average drift 1.7 % )

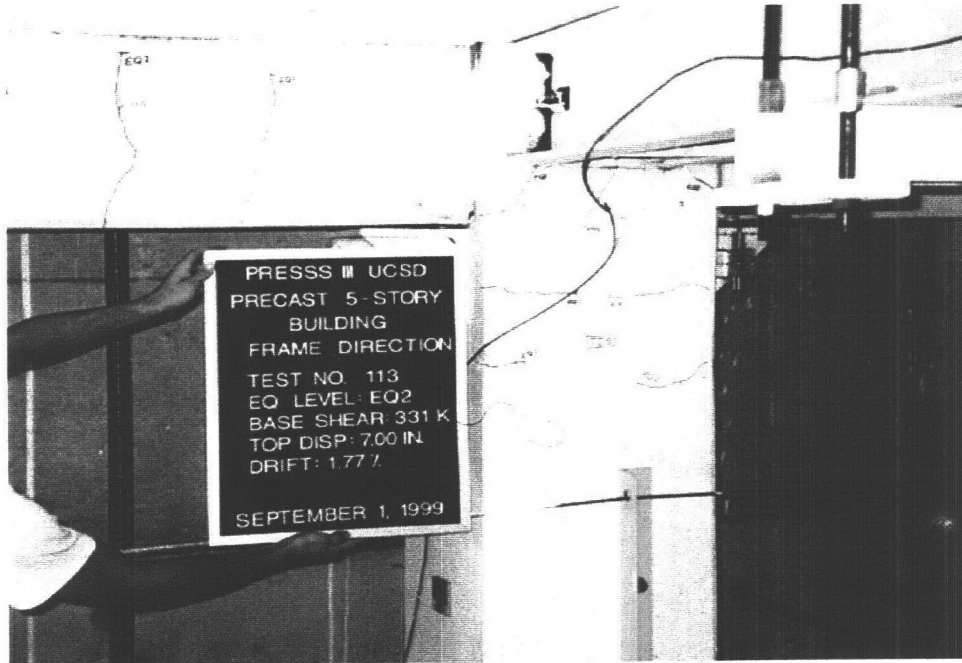


Figure. A.3 – TCY connection EQ II Excitation (average drift 1.7 % )

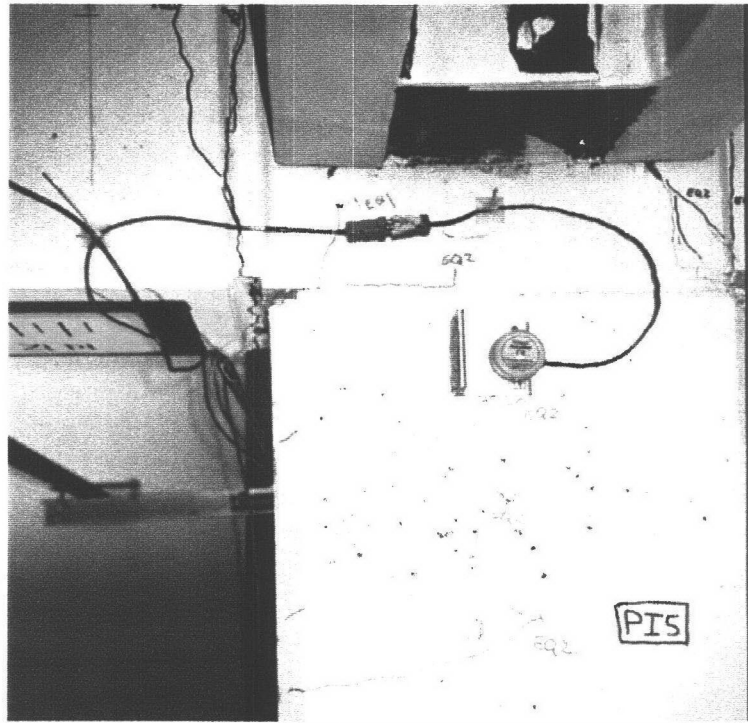


Figure. A.4 – Pretensioned connections EQ2 Excitation (average drift 1.7 % )

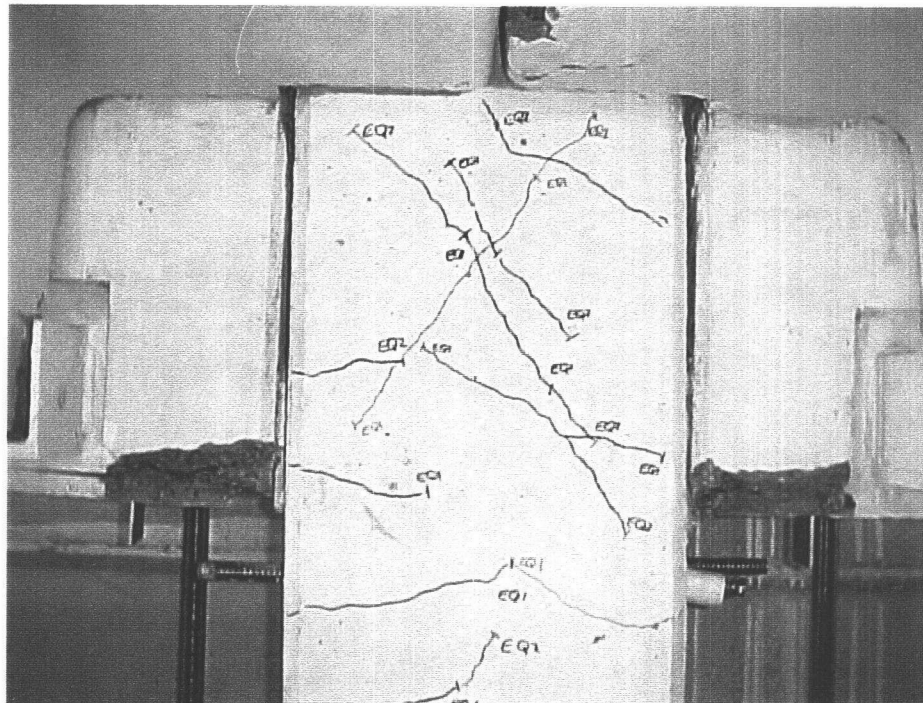
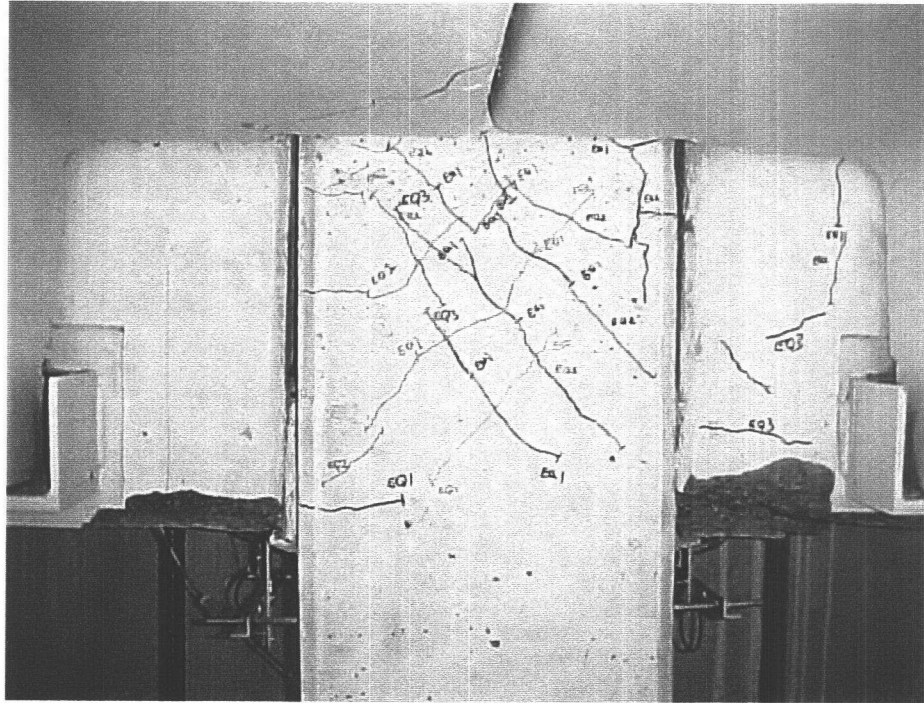


Figure. A.6 – TCY-Gap connections EQ3 Excitation (average drift 2.2 %)

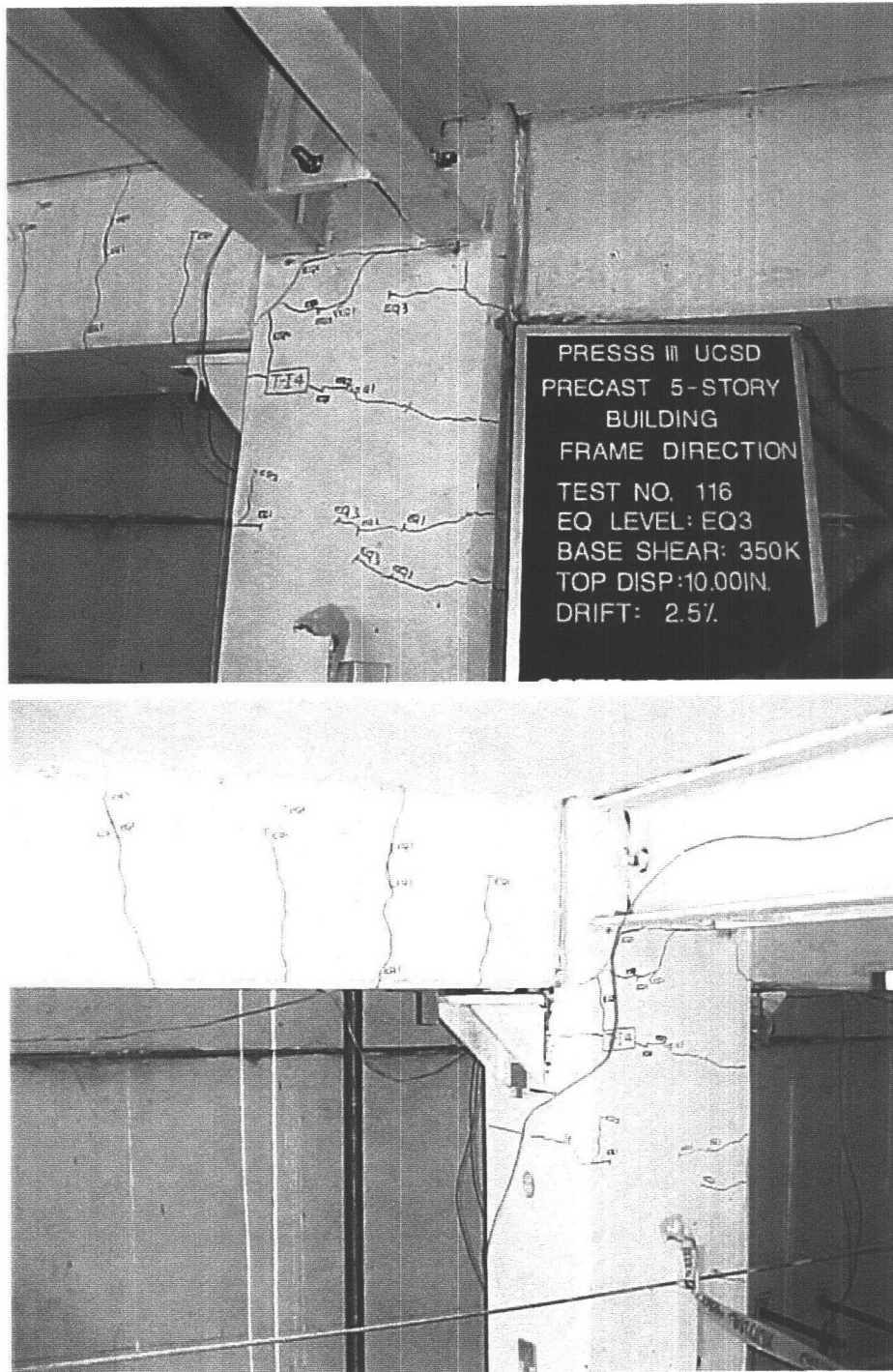


Figure. A.7 – TCY connections EQ3 Excitation (average drift 2.2 %)

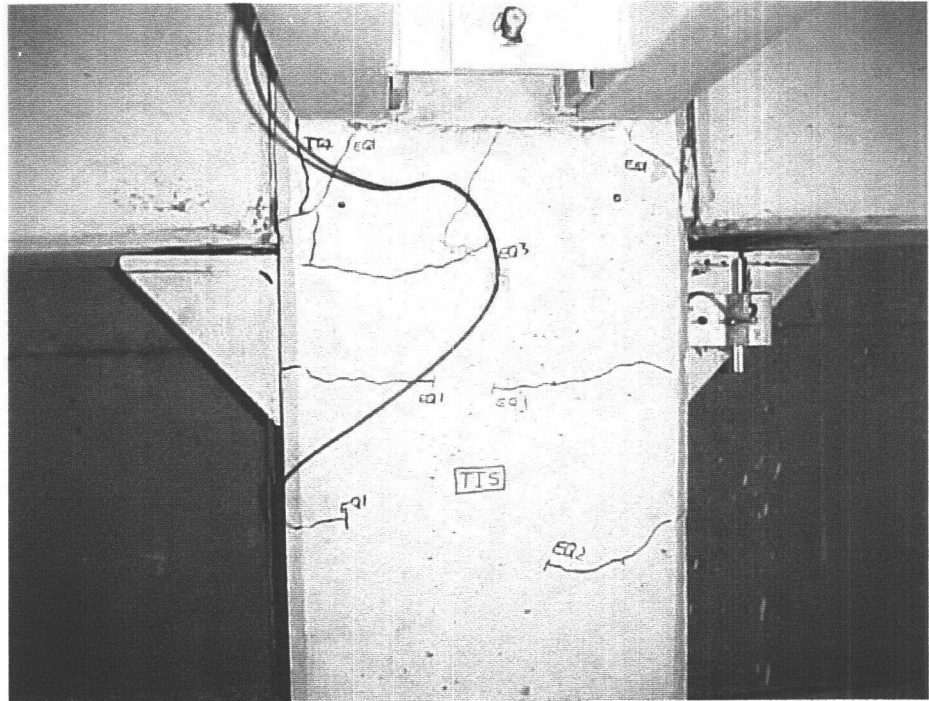


Figure. A.8 – TCY connections EQ3 Excitation (average drift 2.2 %)

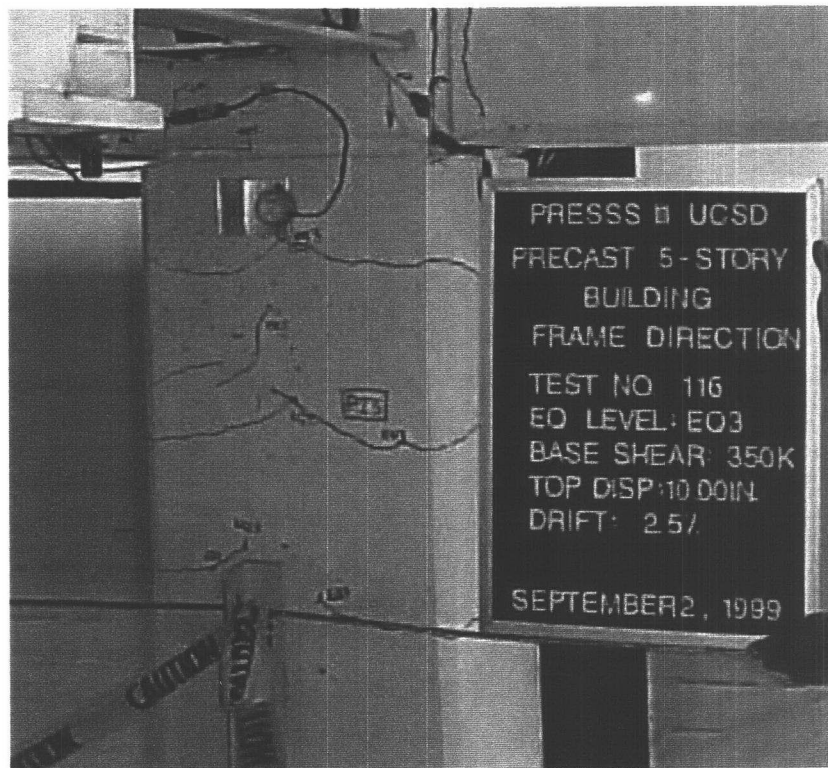
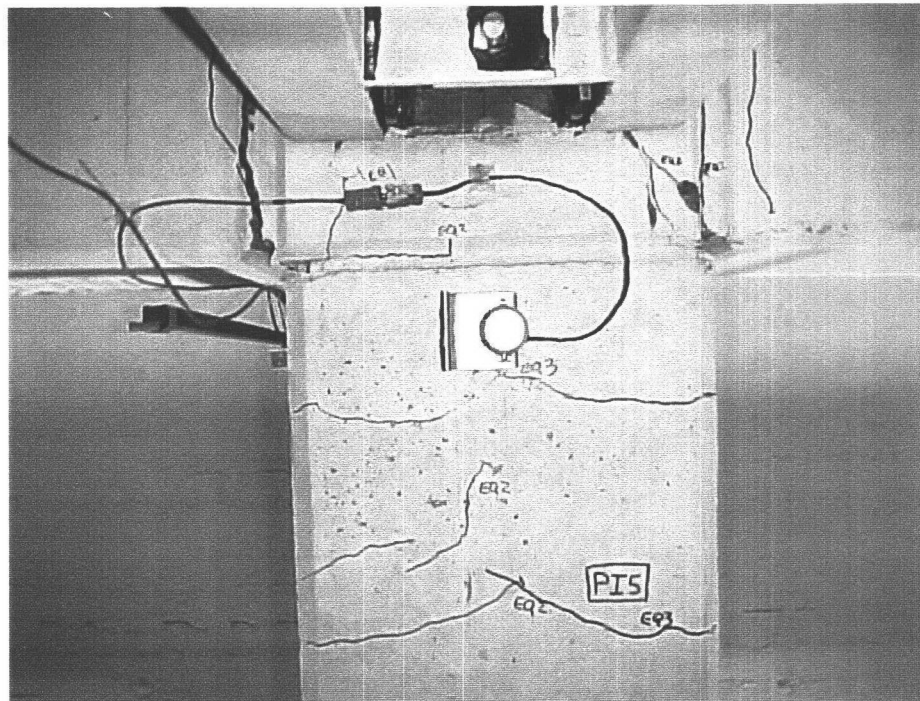


Figure A.9 – Pretensioned connections EQ3 Excitation(average drift 2.2 %)

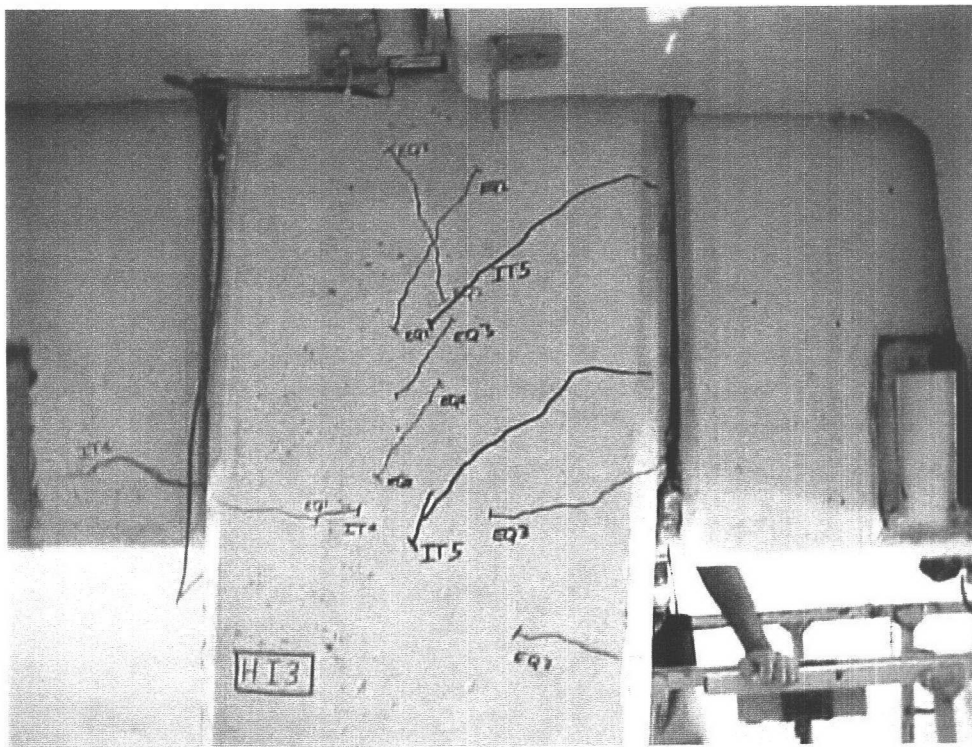
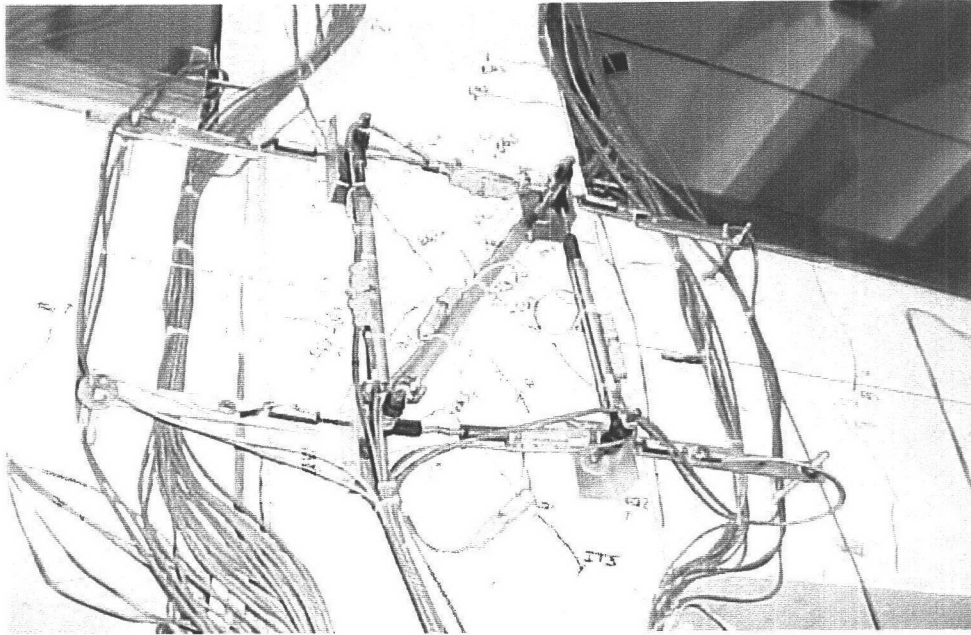


Figure. A.10 – Hybrid connections End of Test(average drift 4.5 %)

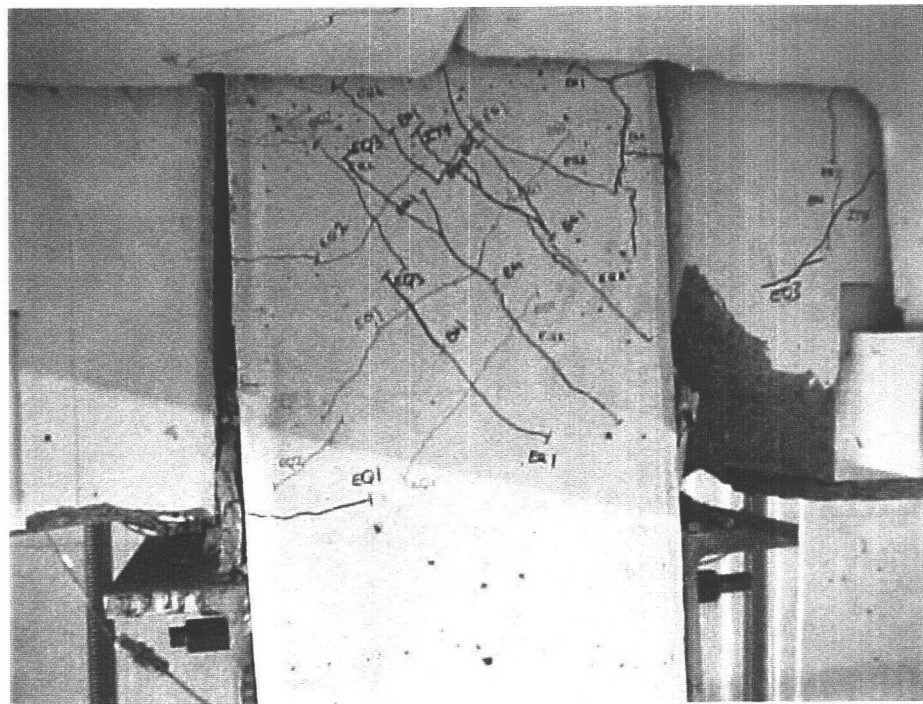
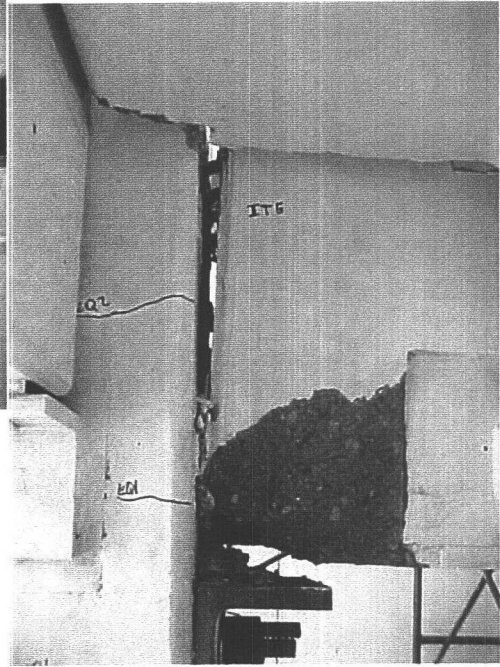
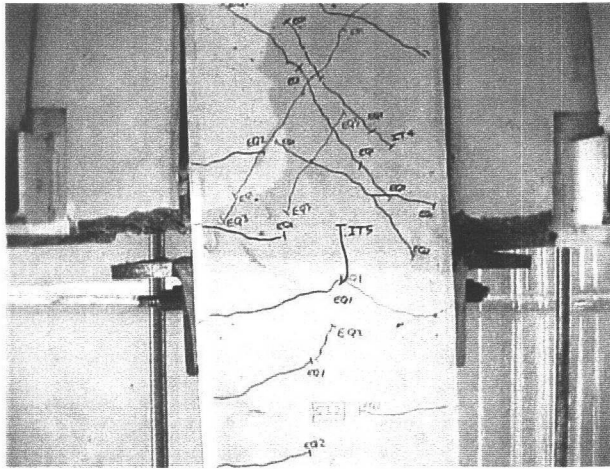


Figure. A.11 – TCY-Gap connection End of Test (average drift 4.5 %)

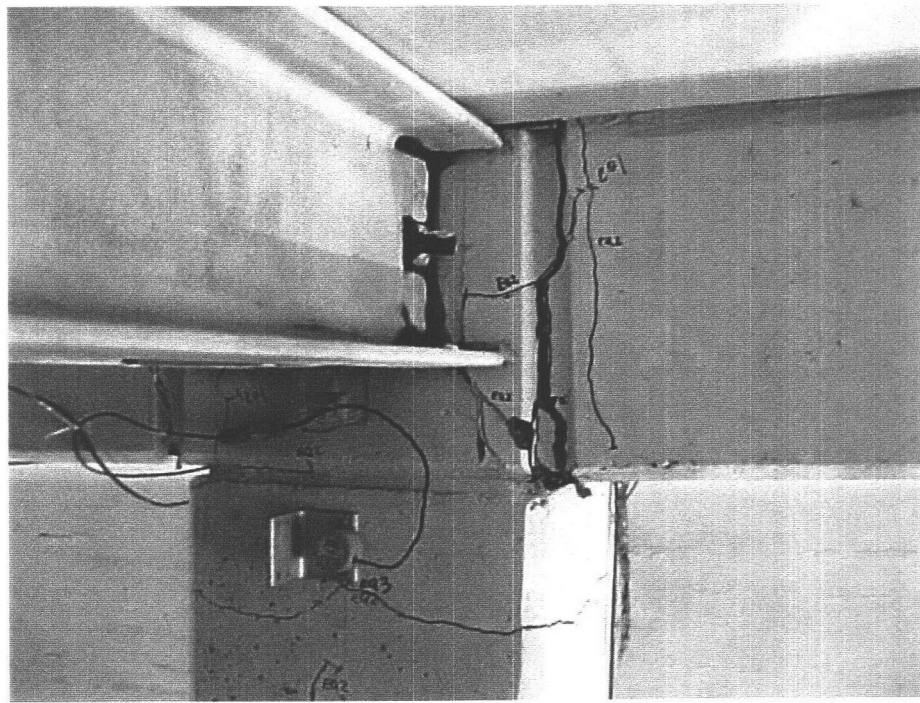
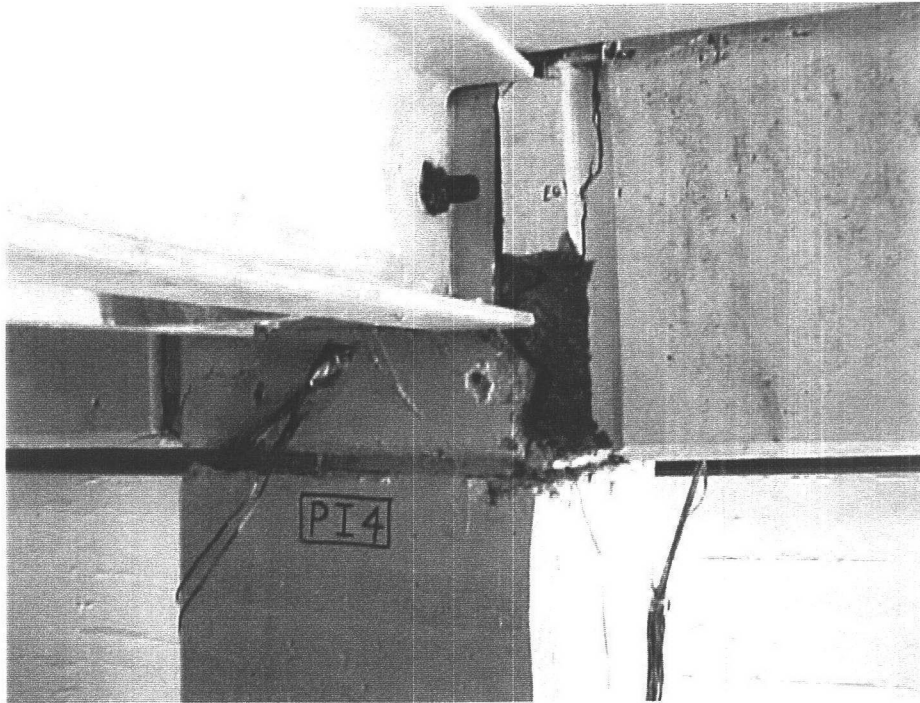


Figure. A.12 – Pretensioned connections – End of Test (average drift 4.5 %)

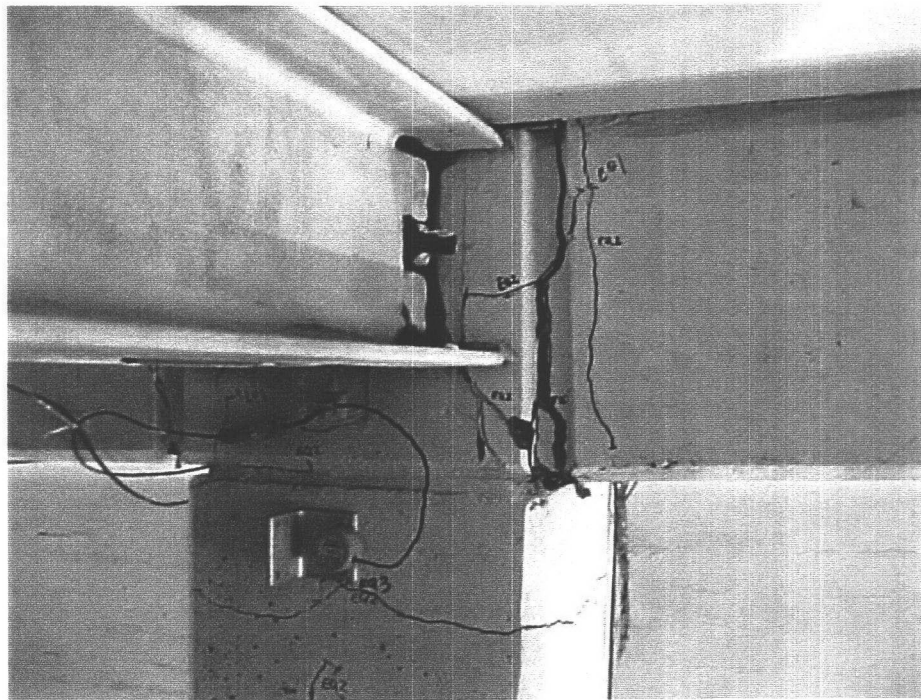
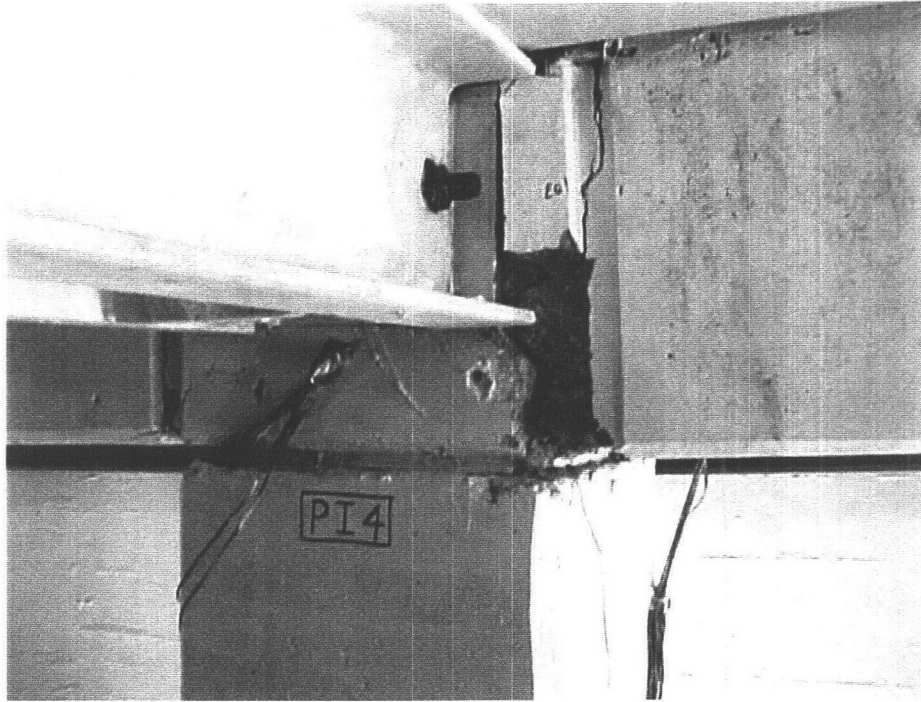


Figure. A.12 – Pretensioned connections – End of Test (average drift 4.5 %)

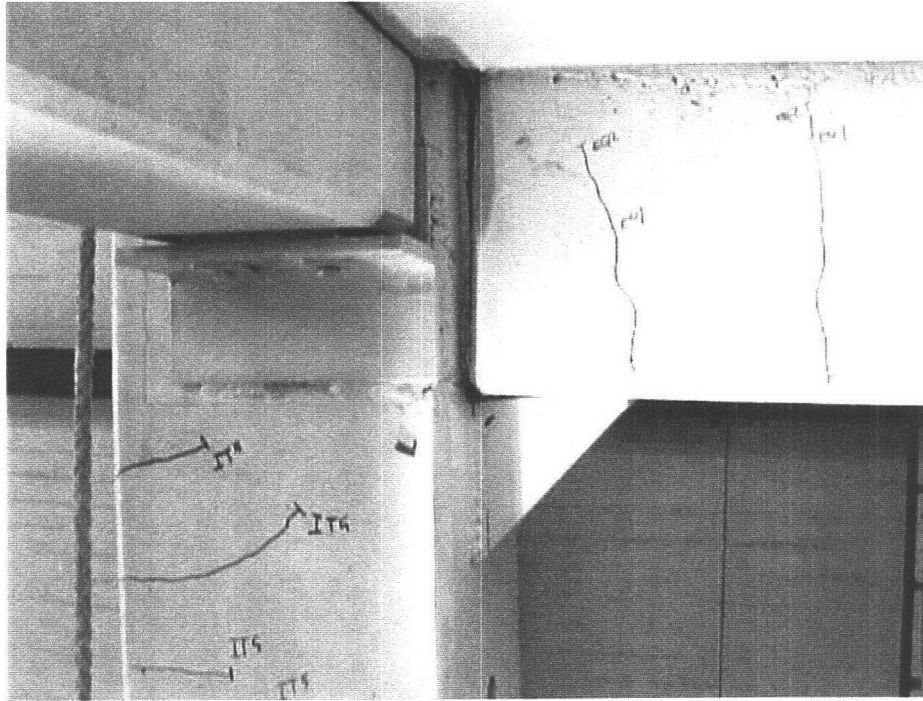
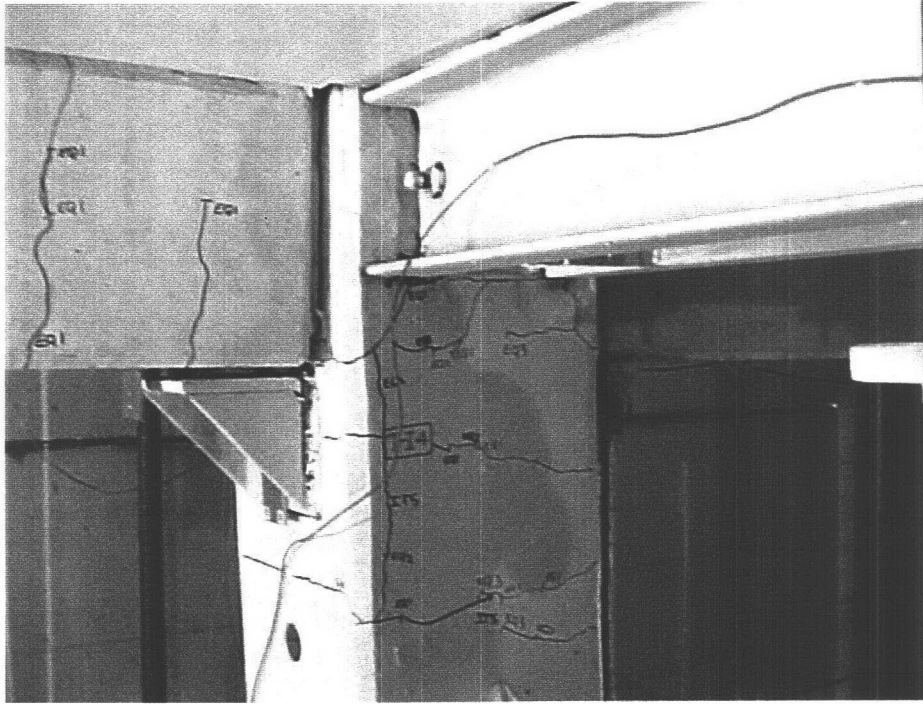


Figure A.13 – TCY connections – End of Test (average drift 4.5 %)

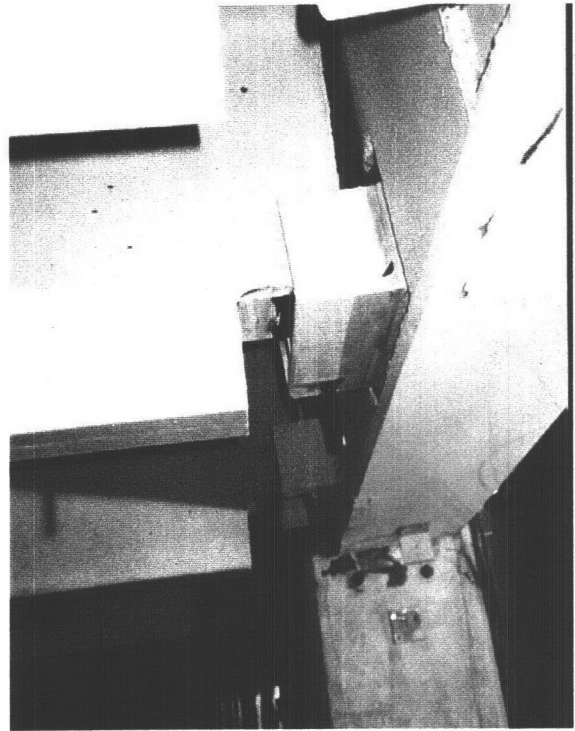
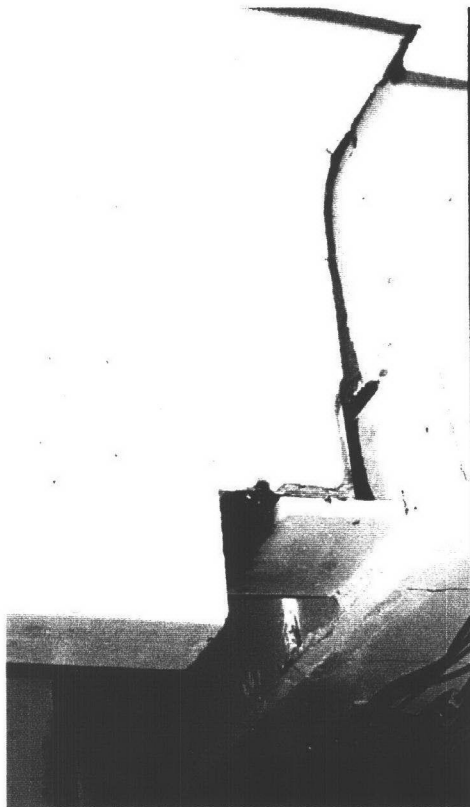


Figure. A.14 – Torsional rotation in hybrid beams: welding intervention (EQ-III level)

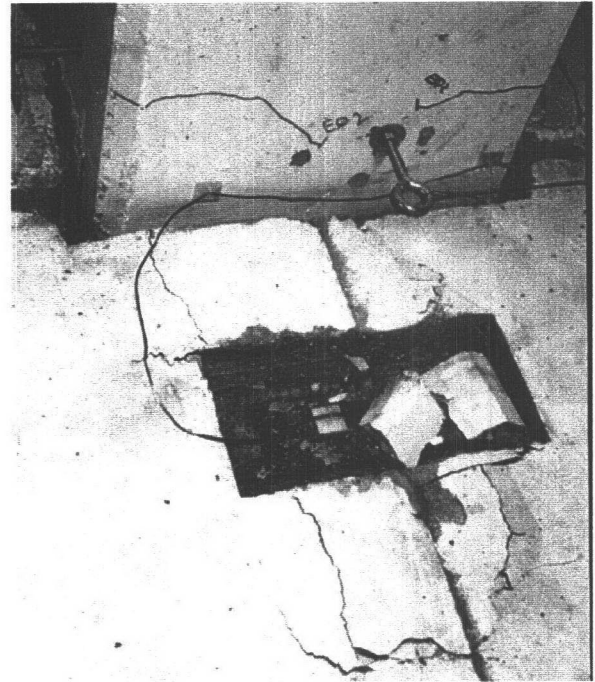


Figure. A.15 – Floor damage (EQ-III level)

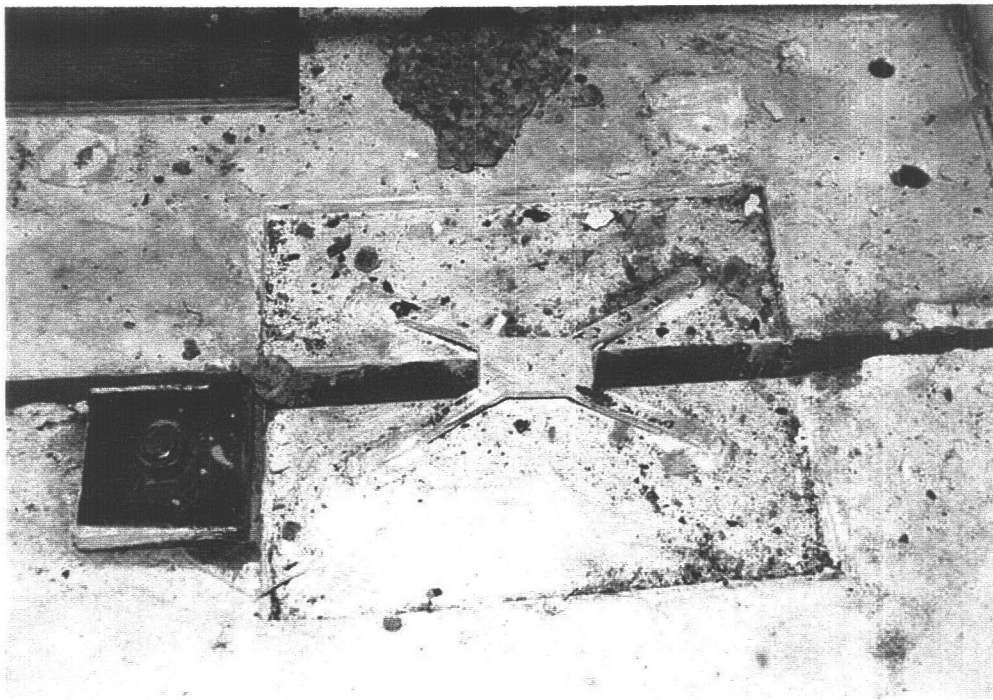
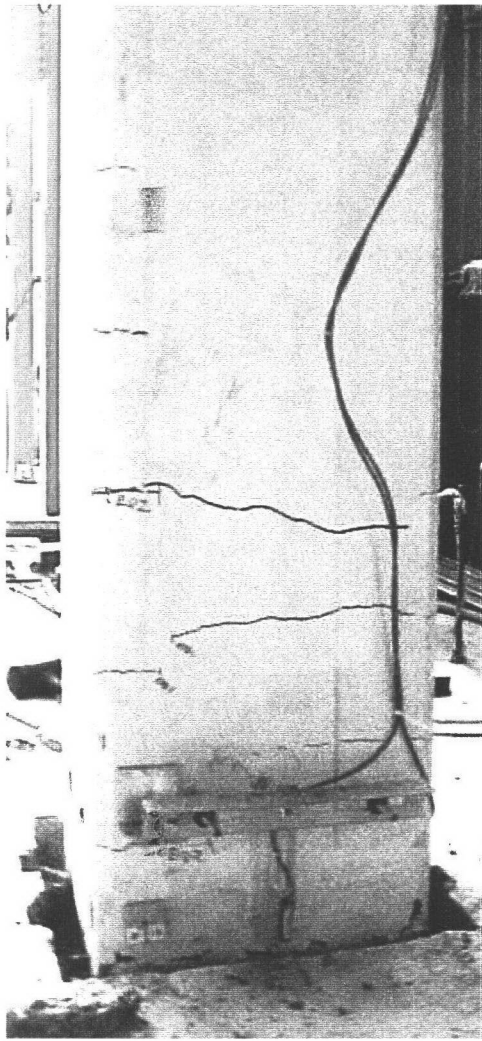
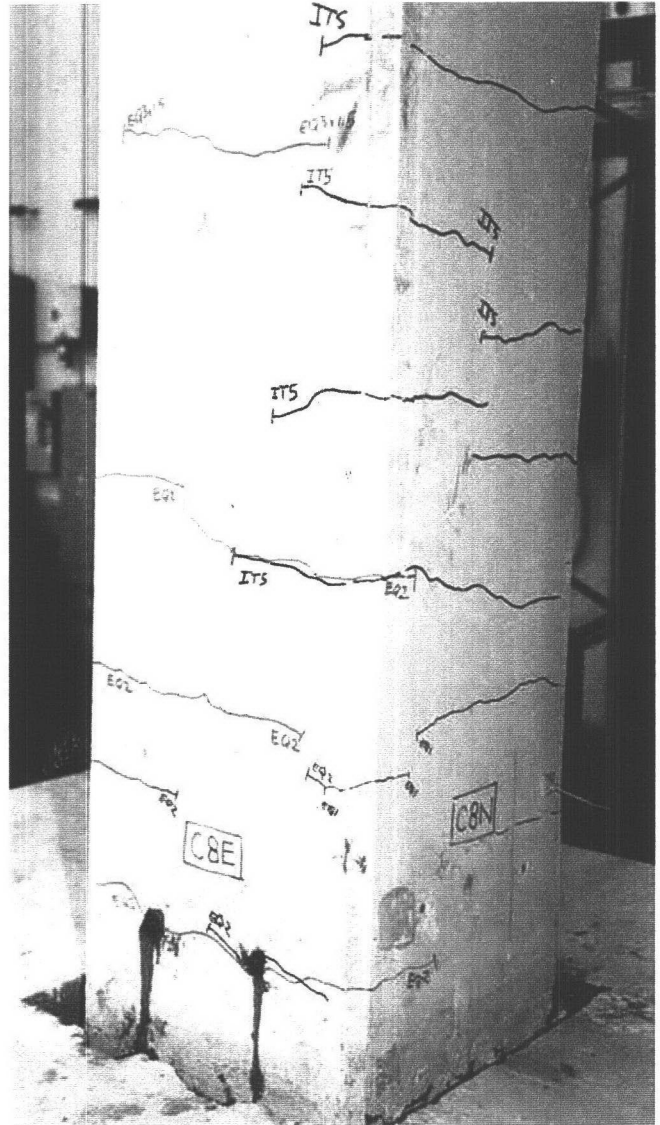


Figure. A.16 – Welded X-plate (EQ-III level)



a) ) EQ-II level



b) End of Test

Figure. A.17 – Seismic columns base- connection to the foundation:

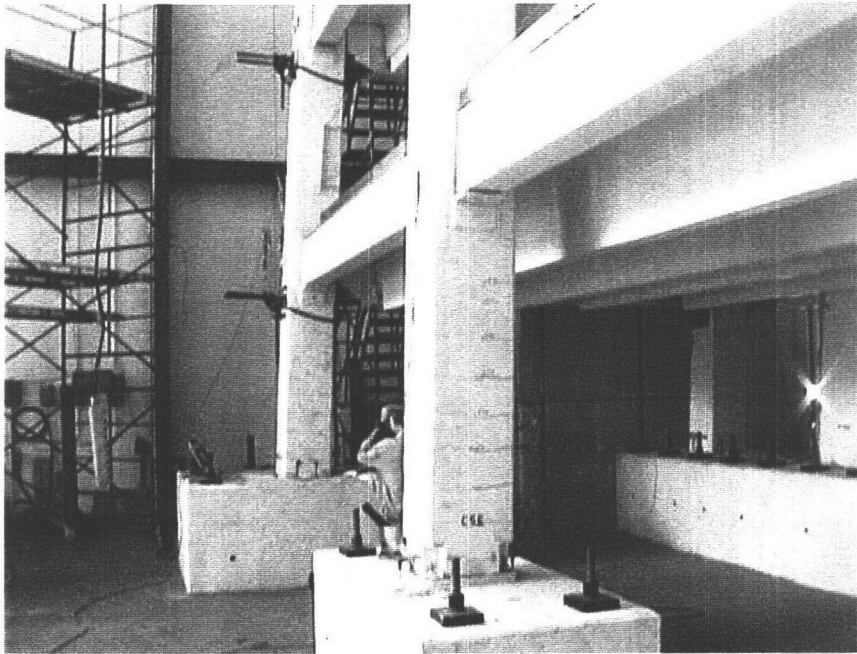


Figure A.18 – Gravity column and first floor slab (End of Test)

